PERFORMANCE OF FRP–ENCASED STEEL–CONCRETE COMPOSITE COLUMNS

PERFORMANCE OF FRP–ENCASED STEEL–CONCRETE COMPOSITE COLUMNS

By

KIAN KARIMI

B.Sc., M.Sc., P.Eng.

A Thesis

Submitted to the School of Graduate studies

In Partial Fulfillment of the requirements

for the Degree

Doctor of Philosophy

McMaster University

April 2011

DOCTOR OF PHILOSOPHY (2011) McMaster University

(Civil Engineering) Hamilton, Ontario

TITLE: Performance of FRP–encased Steel–Concrete Composite Columns

AUTHOR: Kian Karimi

B.Sc. (Shiraz University)

M.Sc. (Sharif University of Technology)

ADVISORS: Dr. Michael J. Tait

Dr. Wael W. El-Dakhakhni

NUMBER OF PAGES: xviii, 195

Abstract

The thesis summarizes the experimental and analytical results of studies on the behavior of two FRP-encased steel-concrete composite columns under axial loading. Composite columns have been conventionally constructed using steel and concrete. This study utilizes FRP in combination with steel and concrete to manufacture composite columns with enhanced behavior. The first type of column is a concrete-encased steel column wrapped with epoxy-saturated glass and carbon fiber reinforced polymer (GFRP and CFRP) sheets in the transverse direction. The second type of composite column utilizes a GFRP tube that surrounds a steel I section column, which is subsequently filled with concrete.

To the best of the author's knowledge, columns comprising FRP, steel and concrete in the shape of the proposed composite systems has not been reported on in the literature. This study includes two major phases. In the first phase, behavior of stub columns is investigated where stability effects are ignored and failure is governed by the loss of cross-sectional strength. In the second phase, influence of stability on the behavior of the proposed composite columns is studied by testing specimens with various slenderness ratios.

To investigate the cross-sectional strength, a total of nine short (500 mm in height) composite column specimens were constructed and tested under axial compression. Five specimens were wrapped with FRP sheets and the remaining four were constructed using a GFRP tube. Experimental results showed significant enhancement in the behavior of the composite columns which was achieved due to confinement and composite action between the constituent materials. The compressive strength of the confined concrete core in the composite specimens constructed using FRP sheets and GFRP tube increased by a factor of 2.4 and 1.8, respectively. An analytical model was developed to predict cross-sectional behavior of the proposed composited column.

With the primary objective of investigating the influence of slenderness on the behavior of the composite columns, ten additional column specimens, ranging between 1,000 mm and 3,000 mm in height, were tested. Five specimens were constructed using FRP sheets and five constructed using the GFRP tube technique. It was found that the compressive strength of the confined concrete core in the longest tubular composite specimen was reduced to approximately 60% of that of the corresponding short specimen. No confinement was achieved in the longest FRP wrapped composite column specimen.

Three bare steel columns, ranging between 500 mm and 3,000 mm in height, were also tested to facilitate comparison with the composite columns in terms of increased axial capacity, as well as stiffness and energy dissipation characteristics of the columns. The compressive strength, elastic axial stiffness and ultimate axial strain of the bare steel columns increased by a factor of up to 10, 6 and 3, respectively, in the composite columns constructed utilizing the concrete-filled GFRP tube. These factors were reduced to 5.2, 2.5 and 2.6, respectively, in the concrete-encased steel columns wrapped with FRP jackets.

Finally, an analytical model was developed to establish the capacity curves for the proposed composite columns accounting for slenderness effects. A simple design equation to predict the compressive strength of the tubular composite columns was proposed based on the capacity curve generated from the analytical model. Compressive capacity of the composite columns predicted using the proposed design equation showed favorable agreement with the experimental results.

To my parents, SORAYA and JALAL

And to my brother, ASHKAN

Acknowledgements

I am extremely grateful to my research advisors, Dr. Michael J. Tait and Dr. Wael W. El-Dakhakhni, for their encouragement, continuous support, excellent guidance and the opportunity that they provided me to mature as a researcher. I would also like to extend my sincere gratitude to the members of my supervisory committee, Dr. John C. Wilson and Dr. Stephen C. Veldhuis, for their interest in my research and their valuable guidance throughout the development of this research work.

I wish to extend my appreciation and gratitude to all the technical staff working at the Applied Dynamics Laboratory (ADL), in particular Mr. David Perrett and Mr. Kent Wheeler for their advice and unparalleled assistance during the experimental phases of this thesis. The help I received from Mr. Peter Koudys is also much appreciated.

The following organizations are gratefully acknowledged for their financial support towards this study: the McMaster University Center for Effective Design of Structures funded through Ontario Research and Development Challenge Fund (ORDCF) of the Ministry of Research and Innovation, the Natural Sciences and Engineering Research Council of Canada (NSERC), Walters Inc. for their support in the construction of the test setup and Fyfe Co. LLC for donating the FRP materials.

Finally and most importantly, I am indebted to my family for their continuous encouragement, support and confidence in me. This thesis is dedicated to my parents, *Soraya* and *Jalal*, for their endless sacrifice and love and to my brother, *Ashkan*.

Publication List

This thesis consists of the following papers:

Paper I

Karimi, K., El-Dakhakhni, W. W., and Tait, M. J. (2010). "Performance enhancement of steel columns using concrete–filled composite jackets." *ASCE Journal of Performance of Constructed Facilities*, DOI: 10.1061/(ASCE)CF.1943-5509.0000162.

Paper II

Karimi, K., Tait, M. J., and El-Dakhakhni, W. W. (2010). "Testing and modeling of a novel FRP–encased steel–concrete composite column." *Journal of Composite Structures*, DOI: 10.1016/j.compstruct.2010.11.017.

Paper III

Karimi, K., El-Dakhakhni, W. W., and Tait, M. J. "Slenderness effects on the behavior of steel–concrete composite columns wrapped with FRP jackets." Submitted for publication on December 2010, *ASCE Journal of Performance of Constructed Facilities*.

Paper IV

Karimi, K., Tait, M. J., and El-Dakhakhni, W. W. "Influence of slenderness on the behavior of a FRP–encased steel–concrete composite column." Submitted for publication on October 2010, *ASCE Journal of Composites for Construction*.

Paper V

Karimi, K., Tait, M. J., and El-Dakhakhni, W. W. "Analytical modeling and design of a novel FRP–encased steel–concrete composite column with various slenderness ratios." Submitted for publication on January 2011, *Engineering Structures*.

Co-Authorship

This thesis has been prepared in accordance with the regulations for a "Sandwich" thesis format or as a compilation of papers stipulated by the Faculty of Graduate Studies at McMaster University and has been co-authored.

Chapter 2: Performance Enhancement of Steel Columns Using Concrete–filled Composite Jackets

By: K. Karimi, W. W. El-Dakhakhni, and M. J. Tait

Construction of the short composite column specimens wrapped with FRP sheets, testing of the short steel and composite column specimens, analysis of experimental data and development of the analytical model was conducted by K. Karimi under supervision of Dr. M.J. Tait and Dr. W.W. El-Dakhakhni. The paper was written by K. Karimi and edited by Dr. W.W. El-Dakhakhni and Dr. M.J. Tait.

Chapter 3: Testing and Modeling of a novel FRP–encased Steel–Concrete Composite Column

By: K. Karimi, M. J. Tait, and W. W. El-Dakhakhni

Construction of the short composite column specimens encased in the GFRP tube, preparation of the test setup, testing of the short steel and composite column specimens, analysis of experimental data and development of the analytical model was conducted by K. Karimi under supervision of Dr. M.J. Tait and Dr. W.W. El-Dakhakhni. The paper was written by K. Karimi and edited by Dr. M.J. Tait and Dr. W.W. El-Dakhakhni.

Chapter 4: Slenderness Effects on the Behavior of Steel–Concrete Composite Columns Wrapped with FRP Jackets

By: K. Karimi, W. W. El-Dakhakhni, and M. J. Tait

Fabrication of the long composite column specimens wrapped with FRP sheets, testing and data analysis was conducted by K. Karimi under supervision of Dr. M.J. Tait and Dr. W.W. El-Dakhakhni. The paper was written by K. Karimi and edited by Dr. W.W. El-Dakhakhni and Dr. M.J. Tait.

Chapter 5: Influence of Slenderness on the Behavior of a FRP–encased Steel–Concrete Composite Column

By: K. Karimi, M. J. Tait, and W. W. El-Dakhakhni

Fabrication of the long composite column specimens encased in the GFRP tube, preparation of the test setup, testing of the long steel and composite column specimens and data analysis was conducted by K. Karimi under supervision of Dr. M.J. Tait and Dr. W.W. El-Dakhakhni. The paper was written by K. Karimi and edited by Dr. M.J. Tait and Dr. W.W. El-Dakhakhni.

Chapter 6: Analytical Modeling and Design of a Novel FRP–encased Steel–Concrete Composite Column with Various Slenderness Ratios

By: K. Karimi, M. J. Tait, and W. W. El-Dakhakhni

The analytical model and design guidelines were proposed by K. Karimi in consultation with Dr. W.W. El-Dakhakhni and Dr. M.J. Tait. The paper was written by K. Karimi and edited by Dr. M.J. Tait and Dr. W.W. El-Dakhakhni.

Table of Contents

List of Tables

List of Figures

Chapter 1: Outline of Study

1.1. Introduction

Composite columns have been widely used in high-rise buildings, highway bridges and offshore structure due to their load carrying capacity and energy dissipation characteristics. Conventional composite columns consist of steel and concrete and are typically classified as concrete-filled steel tubular (CFST) columns or concrete-encased steel (CES) columns.

Fiber reinforced polymers (FRP), considered as a relatively new construction material, have been increasingly utilized in new construction as well as for the retrofit of existing structures. The FRP consists of fiber reinforcements embedded in an epoxy matrix. The initial higher cost of FRP compared to conventional construction materials is offset by significant savings in labor and overall project life cycle costs due to their superior properties which include high strength-to-weight ratio, durability and ease of application.

FRP has been combined with concrete to create composite columns in different forms such as FRP wraps for retrofit purposes or as concrete-filled FRP tubes in new construction. In these composite columns, FRP provides confinement to the concrete resulting in enhanced compressive strength and energy dissipation capacity and protects the concrete from weathering. As a result, FRP wrapping has been extensively utilized for strengthening bridge piers.

Two novel composite columns consisting of steel, concrete and FRP were proposed and investigated experimentally and analytically in this dissertation. The proposed composite systems can also be applied as a retrofit technique in strengthening existing steel columns.

1.2. Significance of Research

Review of the literature shows that substantial research effort has primarily focused on utilizing FRP in structural members and developing corresponding design guidelines for concrete structures. In addition, limited studies on the application of FRP to steel structures have mainly focused on retrofitting corroded members.

In an effort to integrate advantages of various construction materials and to extend the application of FRP in strengthening steel columns, two novel composite columns are proposed in this research. The proposed composite columns consist of a steel column encased in concrete and wrapped with FRP sheets or surrounded by a concrete-filled FRP tube. FRP provides confinement to the concrete resulting in enhanced compressive behavior. It is also expected to enhance the long-term durability of the column. The steel column replaces the vertical reinforcement in conventional reinforced concrete (RC) column and provides additional shear capacity in addition to enhancing column ductility. Furthermore, concrete enhances the lateral stability of the embedded steel column.

The majority of studies on the behavior of composite columns reported on in the literature have focused on cross-sectional behavior of the columns by testing and analytical modeling of short composite columns. In this research, testing and analytical modeling of the behavior of the proposed composite columns are investigated over a wide range of slenderness ratios.

1.3. Research Objectives

The main objectives of this research were to:

- Conduct an experimental program to investigate the cross-sectional and the overall compressive behavior of the proposed composite columns by testing columns with various slenderness ratios;

- Develop an analytical model to predict the behavior of the proposed composite columns accounting for slenderness influence;
- Evaluate the efficiency of the proposed composite systems as retrofit techniques in enhancing the compressive strength, axial stiffness and energy dissipation capacity of steel columns and investigate the effect of slenderness ratio on the enhanced compressive behavior of the retrofitted columns;
- Examine and compare the confinement efficiency of the proposed rectangular composite columns wrapped with the FRP sheets and the circular composite columns encased in FRP tubes; and
- Investigate the influence of column diameter, FRP thickness, number of FRP wraps, corner radius, FRP axial stiffness, steel-to-concrete ratio and concrete shrinkage on the compressive behavior of the proposed composite columns.

1.4. Scope

This thesis consists of five main chapters. Chapters 2 and 3 of this thesis focus on the cross-sectional behavior of FRP-encased steel-concrete composite columns. Chapters 4 and 5 investigate the effect of slenderness on the behavior of composite columns. An analytical to predict the behavior of FRP-encased steel-concrete composite columns is developed and evaluated in Chapter 6.

A total of 22 column specimens were tested in the experimental program, 19 were composite columns and 3 were steel columns. The steel columns were tested for comparative purposes in order to investigate the potential of utilizing the proposed composite systems for retrofit applications. The column specimen heights ranged between 500 mm and 3000 mm, covering a wide range of slenderness ratios, and were tested under axial loading.

Analytical predictions of the compressive behavior of the composite columns were determined utilizing column stability relationships and cross-sectional strength based on

an FRP-confined concrete model and were verified and, when needed, calibrated using experimental results. To meet the research objectives, the research program was divided into the following phases:

- Design and construction of the column specimens (five short composite columns wrapped with FRP sheets, four short composite columns encased in FRP tubes, five composite columns wrapped with FRP sheets ranging between 1,000 mm and 3,000 mm in height, five composite columns encased in FRP tube ranging between 1,000 mm and 3,000 mm in height and three control steel columns ranging between 500 mm and 3,000 mm in height);
- Testing the column specimens under axial loading
- Analysis of test results;
- Development of an analytical tool to simulate compressive behavior of the proposed composite columns with various slenderness ratios based on the Euler buckling equation and available FRP-confined concrete models; and
- Performing a parametric study and developing related design guidelines for the application of the two proposed composite systems in new construction or retrofit of existing steel columns.

1.5. Summary

1.5.1. Chapter 2: Performance Enhancement of Steel Columns using Concrete-filled Composite Jackets

Currently, a significant numbers of bridges worldwide require strengthening due to deterioration and/or increased traffic loads. In this paper, a novel technique for strengthening steel columns and bridge piers, using a composite jacket, is proposed and assessed. The proposed retrofit technique involves wrapping the steel columns with epoxy saturated FRP sheets and subsequently filling the voids between the steel and the composite jacket with concrete. A total of seven short column specimens with a height of 500 mm were tested. Two were bare steel columns tested for comparative purposes and

the remaining five were composite columns. The varying parameters were the number of FRP wraps and the corner radius of the columns.

The column specimens were tested under axial load. The boundary conditions were simulated as fixed-pin, which enabled the tested column specimens to reach their cross-sectional capacity. Experimental results showed significant enhancement in behavior of the composite columns compared to the bare steel columns. The compressive strength, ultimate axial strain and elastic axial stiffness of the composite columns were increased by a maximum factor of 3, 6 and 3, respectively, compared to the control steel columns. Increasing the number of FRP wraps and the corner radius of the cross-section enhanced the compressive strength and ultimate axial strain of the composite columns while their effects were negligible on the elastic axial stiffness. Failure of the composite column specimens was initiated by rupture of the FRP jacket followed by crushing and spalling of the concrete.

A design-oriented analytical model was also developed to predict the behavior of the proposed short composite columns. In this model, the steel was assumed as an elastic-perfectly plastic material and the concrete was modeled using a stress-strain relationship proposed by Lam and Teng (2003) for confined concrete. Lateral confining pressure was evaluated in the two orthogonal column cross section directions based on equilibrium equations and compatibility of deformations between the constituent materials and an average value for the confining pressure was established. The equations for evaluating the compressive strength and ultimate axial strain of the confined concrete from Lam and Teng's (2003) model were calibrated using the test results. A technique to estimate the ultimate axial strain based on an energy balance approach was also developed, which resulted in conservative predictions compared to the calibrated Lam and Teng (2003) expression. The analytical model predictions were found to be in good agreement with the experimental results. Maximum variations between the analytical and test results were observed in the composite column specimen with the maximum number of FRP wraps.

1.5.2. Chapter 3: Testing and Modeling of a Novel FRP-encased Steel-Concrete Composite Column

A novel composite column consisting of a FRP tube, steel and concrete was proposed. The composite column specimens were constructed by placing a FRP tube around a steel column and filling the void between the steel and tube with concrete. A total of seven short column specimens were tested under axial load. The boundary conditions were simulated as pin-pin. Three specimens were bare steel columns tested for comparative purposes in applying the proposed composite system as a retrofit technique.

Results from the experiments showed that the compressive strength, axial stiffness and ultimate axial strain of the composite columns were a maximum of 6, 4 and 2 times greater, respectively, than those of the steel columns. The enhancement in the compressive strength and ultimate axial strain indicated the enhanced energy dissipation capacity of the composite columns associated with the area under the axial load versus axial displacement relationship. The compressive strength of the concrete was increased by a maximum factor of 1.8 in the composite columns. Adding the shrinkage reducing agent to the concrete mix resulted in approximately a 20% increase in compressive strength of the confined concrete. Failure of the composite columns was initiated by a sudden rupture of the FRP tube followed by crushing of the concrete.

An analytical model was developed to predict the behavior of the proposed composite columns. The confinement was assumed uniform and the lateral confining pressure was evaluated considering equilibrium of the FRP tube. In the proposed composite columns, the FRP tube was assumed to be under a bi-axial state of stress and the lateral tensile stress in the tube at failure was evaluated from the Tsai-Wu failure criteria. The confined concrete core was modeled using the constitutive relationship proposed by Lam and Teng (2003). The analytical predictions showed favorable agreement with the test results although some discrepancy was observed over the inelastic range primarily due to the inability of the model to account for shrinkage effects.

1.5.3. Chapter 4: Slenderness Effects on the Behavior of Steel-Concrete Composite Columns Wrapped with FRP Jackets

In this chapter, the influence of stability on the behavior of the FRP-wrapped steel-concrete columns which were introduced in Chapter 2 is investigated. A total of nine column specimens ranging between 500 mm and 3,000 mm in height were tested under axial load. The boundary conditions were simulated as a pin-pin connection. Six specimens were composite columns and three were steel columns tested for comparison purposes in employing the composite system as a retrofit technique.

Experimental results showed that the compressive strength, elastic stiffness and energy dissipation capacity of the composite columns were increased by a maximum ratio of 5, 2.5 and 14, respectively, compared to the corresponding steel columns. The compressive strength reduced by approximately 60% with an increased height of the composite column from 500 mm to 3,000 mm. Failure of all the composite column specimens occurred due to overall member buckling. Buckling strength relationships were established from the test results.

1.5.4. Chapter 5: Influence of Slenderness on the Behavior of a FRP-encased Steel-Concrete Composite Column

In this chapter, the stability effects on the behavior of the composite columns encased in a FRP tube which were introduced in Chapter 3 is evaluated. A total of nine column specimens with various slenderness ratios were constructed and tested under axial load. The boundary conditions were simulated as pin-pin. Six specimens were composite columns and the remaining three were steel columns tested for comparative purposes in employing the composite system as a retrofit technique. The specimens ranged between 500 mm and 3,000 mm in height.

Experimental results showed enhanced compressive behavior in composite column specimens shorter than 2,000 mm due to confinement and composite action. Negligible

confinement was achieved in composite columns longer than 2,000 mm due to the loss of stability at small axial strain values prior to any significant confinement activation. The compressive strength, elastic stiffness and ultimate axial strain of the tested composite columns were a maximum of 10, 6 and 3 times, respectively, greater than corresponding values for the bare steel columns. The enhancement in compressive strength of the composite columns, compared to the bare steel columns, generally increased with increased column height. The initial eccentricity inherent in the tested column specimens was estimated based on moment-curvature measurements. The buckling strength relationships for the tested column specimens were established from test results.

1.5.5. Chapter 6: Analytical Modeling and Design of a Novel FRP-encased Steel-Concrete Composite Column with Various Slenderness Ratios

An analytical model based on an incremental analysis approach was developed to predict the behavior of the FRP-encased steel-concrete composite columns with various slenderness ratios which were introduced in Chapter 5. In this method the buckling load and the cross-sectional strength of the column at each axial strain increment were evaluated and compared. The cross-sectional strength curves were obtained from the analytical model developed in Chapter 2. In evaluating the buckling load, the modulus of elasticity of the concrete corresponding to each axial strain increment was obtained from the first derivative of the stress-strain relationship of the confined concrete.

In the short composite columns the Euler buckling load was greater than the cross-sectional strength for all the strain increments and failure occurred due to loss of cross-sectional strength. In long composite columns, the two relationships intersected. When the point of intersection was located within the inelastic limit, the composite column was designated to have failed due to inelastic overall buckling and was classified as an intermediate long column. When the stability and the cross-sectional strength relationships intersected in the elastic range, the composite column was designated to have failed due to elastic overall buckling and was classified as a slender column. Since

confinement is activated primarily within the inelastic range (axial strains of greater than 2,000 με), no confinement was achieved in the slender composite columns.

The capacity curves showing the compressive capacity of the composite columns versus the slenderness ratio were established based on the analytical model predictions and showed favorable agreement with the experimental results. The slenderness ratio of the composite columns was evaluated by transforming the composite cross-section to an equivalent concrete cross-section. The slenderness ratios separating the three classes of composite columns (short, intermediate long and slender) were established from the analytical model. A study was conducted using the developed analytical model to investigate the effect of column diameter, FRP tube thickness and axial modulus and the steel-to-concrete ratio on the capacity curve and the value of the critical slenderness ratio separating short and long composite columns. A design equation for the composite columns was proposed from the analytical model.

1.6. Future Research

The experimental program and the analytical approach developed in this dissertation can be extended to consider the following future research:

- Effect of shrinkage on the confinement mechanism can be further studied by testing additional composite specimens with and without adding shrinkage reducing agents to the concrete mix. The proposed analytical model may be further developed to include shrinkage effects.

- In employing the proposed composite system utilizing FRP tubes in retrofitting existing steel columns, a solid FRP tube cannot be placed around the column as it will interfere with other structural members connected to the top and bottom of the column. Therefore, split FRP tubes bonded together may be utilized in retrofit applications. The feasibility of this retrofit technique can be investigated by testing additional composite column specimens constructed using split FRP tubes.

- The developed design equation for FRP-encased steel concrete composite columns should be calibrated with a comprehensive database of tests on composite columns with various slenderness ratios.

- The effect of the residual stresses in the steel column and the out-of-straightness of the columns may also be implemented into the developed analytical model.

Chapter 2: Performance Enhancement of Steel Columns using Concrete-filled Composite Jackets

2.1. Summary

This paper studies the cross sectional behavior of steel columns strengthened with fiber reinforced polymers (FRPs). The composite column is constructed by wrapping the steel I section column with epoxy-saturated glass and carbon FRP (GFRP and CFRP) sheets in the transverse direction and subsequently filling the voids between the FRP and the steel with concrete. Experimental tests are performed on stub columns under axial compression including 1 to 3 CFRP wraps. A corner treatment technique, to avoid stress concentration at the corners and improve confinement efficiency, is also investigated. A simplified analytical model is developed to predict the axial behavior of the composite columns. Experimental results showed significant enhancement in the behavior of the composite columns primarily due to the confinement mechanism imposed by the FRP jacket and concrete. Increasing the corner radius results in higher compressive strength of the confined concrete and ultimate axial strain of the composite columns. Good agreement between the analytically-developed axial load-displacement relationships and the test data indicates that the model can closely simulate the cross section behavior of the composite columns.

Keywords: analytical techniques, composite columns, concrete, confinement, fiber reinforced polymer, sheets, steel columns

2.2. Introduction

The current and future performance of a significant number of bridges worldwide is uncertain due to deterioration and corrosion, increased traffic volume and seismic loads exceeding the original design loads (Kratky 2004). The performance of approximately 90,000 bridges in the United States and Canada is questionable while over 80,000 bridges are no longer in use due to structural deficiency (Loud and Kliger 2001). Steel bridges

comprise almost half of these deficient bridges. The United States Department of Transportation has raised concern about the numerous deficient steel bridges (Shaat et al. 2004) in the country and has allocated specific funding for bridge rehabilitation projects. Strengthening and upgrading are cost-efficient alternatives to restore structural performance of these facilities instead of demolition and reconstruction which is usually more costly.

Fiber reinforced polymers (FRPs) have been widely applied in strengthening and repair of structures. These materials are composed of fiber reinforcement embedded in an epoxy matrix. Although FRP is more costly than common constructional materials, the ease of application of FRP systems leads to significant savings in labor costs and construction time which offset the material's higher initial cost. In addition, the excellent durability of FRP eliminates long-term maintenance costs.

FRP composites were initially utilized in concrete structures for both internal and external reinforcement in concrete beams and slabs as well as confining wet-lay-up wraps in concrete columns. The number of reported studies on the application of FRP for the repair of structural steel members is considerably fewer than concrete members. Furthermore, these materials have been primarily applied to steel beams and girders in the form of bonded sheets or plates to increase the shear or flexural capacity. Applications of FRP in strengthening steel columns have been limited to steel hollow section columns (Zhao and Zhang 2007). Short columns were wrapped with transverse FRP sheets to prevent outwards local buckling of the steel section (Shaat and Fam 2006; Teng and Hu 2007; Tao et al. 2007). In long columns, longitudinal FRP sheets were bonded to the steel columns to prevent overall buckling about the weak axis (Shaat and Fam 2006).

This paper focuses on studying cross sectional behavior of steel columns strengthened using wet-lay-up FRP sheets. The columns are wrapped with epoxy saturated FRP sheets with the fibers oriented in the circumferential direction. The resulting voids between the

FRP and steel are filled with concrete. This type of composite column can be considered a steel column partially encased in concrete and wrapped with FRP. Typical concrete encased steel columns consist of an I-shaped steel section with concrete cast around the entire section. In this study, the additional FRP jacket is expected to enhance the axial behavior of the composite column by providing confinement to the concrete cores and preventing outward lateral buckling of the steel flanges. The main objectives of this strengthening technique are to increase the axial capacity, stiffness and energy dissipation capacity of the columns. In the composite columns, both concrete and steel contribute in carrying the axial load. As a result, appropriate detailing is necessary to ensure transfer of the additional gravity loads from the girders to the steel column and to the concrete cores.

As shown in Fig. 2.1, conventional composite columns can be classified into 5 groups with steel and concrete as their constituent materials. These 5 categories are: partially encased composite columns (PEC) (Chicoine et al. 2003), fully encased composite columns (FEC), concrete-filled steel tubes (CFST), concrete-filled double skin tubular columns (CFDST) and steel tubes filled with steel-reinforced concrete. The main advantage of a partially encased composite column (PEC) over a fully encased column (FEC) is that the PEC column only requires formwork on two sides. Another type of composite column is the concrete-filled steel tubular column (CFST) shown in Fig. 2.1(c). This column type utilizes the steel tube to confine the concrete and the concrete prevents inward buckling of the steel resulting in improved axial behavior. Disadvantages of this type of construction include the exposed steel leading to lower fire resistance compared to an encased-steel column, the limited number of steel tube cross-sectional sizes and additional fabrication requirements for the fixed beam-to-column connections in circular CFT columns (Prickett and Driver 2006). A new form of the CFT columns is the concrete-filled double skin steel tube (CFDST) depicted in Fig. 2.1(d) consisting of two concentric steel tubes with concrete cast between them. These columns are lighter than CFT columns and possess higher bending stiffness and better cyclic behavior (Tao and Han 2006). The most recent type of the steel-concrete composite column incorporates advantages of both concrete-filled steel tubes (CFST) and concrete-encased steel

columns. These columns are formed by inserting a steel section into a concrete-filled steel tube as shown in Fig. 2.1(e) (Wang et al. 2004).

The proposed composite columns in this study integrate most of the advantages of the conventional concrete-steel composite columns including prevention of local buckling and lateral confinement of the concrete. Furthermore, the FRP wraps act as a stay-in-place formwork for the concrete, the FRP jacket protects the steel against corrosion and the concrete against weathering.

In this study, the cross sectional behavior of the proposed composite columns is evaluated through a set of experimental tests on stub columns. The varying parameters among the tests are the number of CFRP wraps and the corner radius. A corner treatment technique to avoid stress concentration at corners of the specimens and to enhance confinement efficiency is introduced. Some research studies have indicated that no confinement is provided in rectangular columns with zero corner radius (Mirmiran et al. 1998; Wu et al. 2006b) while most of the published studies suggest certain level of confinement in columns with sharp edges (Rochette and Labossi`ere 2000; Yang et al. 2004; Wang and Wu 2008; Chaallal et al. 2003a). This issue is investigated for the particular composite columns proposed in this paper.

An analytical model is developed to predict the axial behavior of the composite columns. The model utilizes equilibrium and compatibility conditions between the constituent materials.

2.3. Experimental Work

A total of seven column specimens were tested in the experimental program, two were used as control specimens and five columns were wrapped with one to three CFRP layers. All of the strengthened specimens were first wrapped with a single glass FRP (GFRP) layer to prevent galvanic corrosion, which can occur when steel and carbon fibers are in direct contact (Shaat and Fam 2006). The selected steel columns were 500 mm long

W150×14, which ensured the yield capacity of the cross section was attained prior to local or overall buckling (CSA 2009).

The following steps outline the construction procedure of the composite specimens: All rust on the steel surface was removed using a wire brush and acetone; FRP sheets were cut to appropriate size; a two component epoxy was uniformly blended with a mix ratio of 100:42 by volume using a low speed mixer at 400-600 RPM; the FRP sheets were saturated in the epoxy; the saturated GFRP sheets were wrapped around the column followed by additional CFRP wraps; 200mm overlap in the FRP jacket was used to prevent any debonding prior to the FRP reaching its ultimate strength; the specimens were cured at room temperature for a minimum of 48 hours prior to pouring the concrete; the specimens were filled with concrete and cured for a minimum of 28 days prior to testing.

In two of the specimens, a corner treatment technique was applied to increase the corner radius of the specimens. In this technique, round steel bars with 12.7 mm diameter were welded to the steel flanges at the corners prior to applying FRP wraps. Fig. 2.2 shows schematics view *and c*ross sectional dimensions of the composite specimens.

2.3.1. Material Properties

The carbon and glass fiber sheets were uni-directional fabrics made of carbon and glass fibers with additional stabilizing aramid and glass cross fibers, respectively. Dry fiber sheets were impregnated with the epoxy resin on-site forming a wet lay-up system prior to being applied to the specimens. Material properties of these products are presented in Table 2.1. Average yield and ultimate tensile strength values of 411 MPa and 526 MPa, respectively, were obtained for the steel column from tensile coupon tests. Yeild strength of the steel bars was 350 MPa. The 28-day average compressive strength of concrete cylinders was 44.0 MPa.

2.3.2. Test Matrix, Setup and Instrumentation

The test matrix is presented in Table 2.2 where the letters "C" and "S" in the identification code denote control specimen and composite specimen, respectively. The following digit indicates the specimen number in each group (control/composite) and the last digit following the hyphen indicates the number of applied CFRP wraps. The letter "C" at the end denoted specimens with corner treatment.

The specimens were tested under pure axial loading using a 2,500 kN actuator with the load applied under displacement control at a rate of 0.2 mm/min. Four displacement transducers (DTs) were mounted at each side of the specimen to measure the axial shortening during the tests. Strain gauges were also installed at mid-height of the specimens in longitudinal direction to measure axial strains to evaluate elastic stiffness of the specimens. Fig. 2.3 shows the instrumentation and test setup.

2.3.3. Test Results

The axial load-displacement behavior of the tested specimens is shown in Fig. 2.4(a) and 4(b) for the specimens without and with corner treatment, respectively. Axial displacements are plotted based on the DTs readings over the entire length of the specimens. In order to highlight the confinement and the composite action between the three constituent materials in enhancing axial behavior of the composite columns, separate contributions of the steel column and the unconfined concrete are superimposed and denoted as "Steel+Unconfined concrete" in Fig. 2.4. The axial capacity of the column corresponding to any level of displacement is evaluated as:

$$F = A_c\sigma_c + A_s\sigma_s \tag{2.1}$$

where, A_c and A_s are the total cross sectional area of the concrete cores and the steel, respectively, and σ_c and σ_s are the compressive stress in the concrete and the steel, respectively.

In developing "Steel+Unconfined concrete" diagram, axial behavior of the steel is obtained from the control specimen tests and the compressive behavior of the concrete is calculated based on the concrete model proposed by Popovics (1973). In this model, the compressive stress of concrete f_c as a function the concrete strain is given by:

$$f_c = \frac{f'_{co} x r}{r - 1 + x^r} \tag{2.2}$$

where, f'_{co} is the compressive strength of unconfined concrete and

$$x = \frac{\varepsilon_c}{\varepsilon_{co}} \tag{2.3}$$

where, ε_c is the compressive strain of concrete and ε_{co} is the corresponding strain at peak strength of unconfined concrete commonly taken as 0.002 and

$$r = \frac{E_c}{E_c - E_{\text{sec}}} \tag{2.4}$$

where E_c and E_{sec} are the tangent and secant modulus, respectively, given by:

$$E_c = 5{,}000\sqrt{f'_{co}} \text{ MPa} \tag{2.5}$$

$$E_{\text{sec}} = \frac{f'_{co}}{\varepsilon_{co}} \tag{2.6}$$

Comparing the axial load-displacement diagrams of the composite columns and the "Steel+Unconfined concrete" in Fig. 2.4 shows the effect of the FRP confinement and the composite action on the axial behavior of the composite columns, which is a significant enhancement in the peak strength and ultimate displacement. It is also observed that

increasing the number of CFRP wraps increases the ultimate capacity of the composite columns while its effect is less considerable on the ultimate displacement (a measure of the energy dissipation capacity) and insignificant on the elastic axial stiffness (slope of the initial linear branch in the load-displacement diagrams in Fig. 2.4) since confinement was passive rather than active (Andrawes et al. 2010; Krstulovic-Opara and Thiedeman 2000). Mirmiran and Shahawy (1997) and Chaallal et al. (2003b) have reported similar findings on the effect of the number of FRP wraps on axial stiffness of FRP-confined concrete columns.

The increased peak strength, elastic stiffness and corresponding strain to peak strength of the composite specimens are evaluated with respect to the control specimens and presented in Table 2.3 along with the compressive strength of the confined concrete cores (f'_{cc}) for each tested specimen. The ultimate strength of the composite columns was approximately 2 to 3 times greater than the ultimate strength of the steel columns. This was primarily due to the compressive strength of the confined concrete, which was approximately doubled by increasing the number of CFRP wraps from 1 (Column S1-1) to 3 wraps (Column S3-3). The strain corresponding to the peak strength of the composite columns was increased by a ratio of 3 to 6 compared to the control steel columns. Elastic axial stiffness of the composite columns was approximately 3 times greater than that of the steel columns.

Increasing the corner radius of the composite specimens enhanced the compressive strength of the confined concrete by a ratio of approximately 1.3. The ultimate axial strains achieved in the specimens with corner treatment were also considerably higher compared to the specimens with similar number of CFRP wrap without corner treatment.

Photographs of the failed specimens are presented in Fig. 2.5. Failure of the bare steel columns was associated with steel yielding over the entire cross section followed by local buckling of the steel flanges and web as shown in Fig. 2.5(a). Failure of the composite columns initiated by rupture of the FRP jacket at the corners as shown in Fig. 2.5. Local

buckling of the steel flanges and web and crushed concrete were observed after removal of the FRP jacket as shown in Fig. 2.5(c). No debonding along the CFRP overlap length occurred, indicating adequacy of the developed overlap length.

2.3.4. Enhancement Factors

To evaluate the performance of the proposed composite columns, enhancement factors are introduced and evaluated. These parameters were originally proposed by Yang et al. (2008) to evaluate the axial behavior of concrete-filled steel tubes and were found to be correlated. The factors have been modified to accommodate the proposed composite scheme. They include composite action index (*C.A.I.*), confinement ratio (*C.R.*), and ductility index (*D.I.*).

The level of composite action between the constituent materials in enhancing axial capacity of the composite specimens is assessed by the *C.A.I.* defined as:

$$C.A.I. = \frac{A_s f_y + A_c f_{cc}^{'}}{A_s f_y + A_c f_{co}^{'}} \tag{2.7}$$

The degree of confinement is expressed in terms of the *C.R.* defined as:

$$C.R. = \frac{A_{FRP}\sigma_{h,rup\,FRP}}{A_c f_{co}^{'}} = \frac{(A_{GFRP}E_{GFRP} + A_{CFRP}E_{CFRP})\varepsilon_{h,rup\,CFRP}}{A_c f_{co}^{'}} \tag{2.8}$$

where, A_{FRP} and $\sigma_{h,rup\ FRP}$ are the cross sectional area and actual hoop stress in the FRP jacket at rupture, respectively. $\varepsilon_{h,rup\ CFRP}$ is the actual hoop strain at CFRP rupture taken as 0.6 of the CFRP material ultimate tensile strain and E_{CFRP} and E_{GFRP} are the tensile modulus of the CFRP and GFRP wraps in hoop direction, respectively. Due to the larger ultimate tensile strain of the GFRP wraps ($\varepsilon_{u\ GFRP}$=0.022) compared to the CFRP ($\varepsilon_{u\ CFRP}$=0.012) failure will be initiated by rupture of the CFRP layers.

Ductility of the composite specimens is expressed in terms of the ductility index (*D.I.*) defined as (Woods et al. 2007):

$$D.I. = \frac{\varepsilon_u}{\varepsilon_y} \tag{2.9}$$

where, ε_u and ε_y are the ultimate and yield axial strain, respectively.

The above factors are evaluated from the experimental data and presented in Table 2.4. It can be observed that higher confinement (*C.R.* factor) results in increased composite interaction between the constituent materials (higher *C.A.I.* value) and subsequently leads to a more pronounced enhancement in the compressive strength of the column. Higher *C.R.* values were obtained for the specimens with corner treatment compared to the specimens without corner treatment and with similar number of CFRP wraps.

Ductility of the composite columns was a maximum of 6 times greater compared to the control steel columns. The ductility index increased with the number of CFRP wraps.

2.4. Analytical Investigation

In this section, an analytical model is developed to predict the axial behavior of the composite columns. This design-oriented model can be employed to estimate the enhancement in load bearing capacity and stiffness of the composite columns. The model assumes, that at the onset of failure, the steel has yielded over its entire cross section and the concrete has reached its peak confined strength. The axial load-displacement diagrams are obtained using Eq. (2.1).

Steel is assumed to be an elastic-perfectly plastic material as represented in Fig. 2.6(a). The experimental test results carried out in this research show a strain hardening branch in the axial load-displacement relationship of the composite specimens indicating a high

level of concrete confinement (Wu et al. 2006a). A majority of the existing confined concrete models in the literature assume a strain softening branch after the peak stress, which only applies to a low level of confinement.

In this paper, the axial stress-strain relationship for concrete under high confinement proposed by Lam and Teng (2003a) is adopted in consistency with the shape of the axial-load displacement diagrams from the tested specimens (Fig. 2.6(b)). This model assumes a parabolic stress-strain behavior up to a specified strain limit ε_t. In this region the confinement effect is not sufficiently developed and as such, the concrete follows a stress-strain relationship similar to that of the unconfined concrete. After reaching the strain limit ε_t the confinement action results in a linear stress-strain behavior. The described stress-strain relationship is expressed as (Lam and Teng 2003a):

$$\sigma_c = \begin{cases} E_c\varepsilon_c - \dfrac{(E_c - E_2)^2}{4f_{co}^{'}}\varepsilon_c^2 & (0 \le \varepsilon_c \le \varepsilon_t) \\ f_{co}^{'} + E_2\varepsilon_c & (\varepsilon_t \le \varepsilon_c \le \varepsilon_{cu}) \end{cases} \tag{2.10}$$

where, ε_{cu} and E_2 are the ultimate axial strain of the confined concrete and the slope of the linear second portion of the curve, respectively.

The axial strain at the transition point, ε_t, and E_2 are estimated by (Lam and Teng 2003a):

$$\varepsilon_t = \frac{2f_{co}^{'}}{E_c - E_2} \tag{2.11}$$

$$E_2 = \frac{f_{cc}^{'} - f_{co}^{'}}{\varepsilon_{cu}} \tag{2.12}$$

In the proposed composite columns the concrete is under a tri-axial state of stress. The two necessary parameters in establishing the axial behavior of the confined concrete, based on Eq. (2.10), are its ultimate axial strength and strain (f'_{cc} and ε_{cu}).

2.4.1. Ultimate Strength of the Confined Concrete

Several confined concrete models (Samaan et al. 1998; Saafi et al. 1999; Lam and Teng 2003a) evaluate the compressive strength by calibrating an expression originally proposed by Richart et al. (1928) as:

$$f'_{cc} = f'_{co} + k_1 f_L \tag{2.13}$$

where, f_L is the lateral confining pressure and k_1 is the confinement factor. A linear relationship similar to Eq. (2.13) between f_L and the compressive strength of the confined concrete, f'_{cc}, is assumed in this paper.

Eq. (2.13) is developed for a circular confined concrete column under uniform confinement. However, in confined rectangular or square concrete columns, the confining pressure is non-uniform and unequal in the two orthogonal directions. Therefore, an average representative value of the confining pressure must be established.

In the rectangular columns, confinement is mainly developed at the corners of the section whereas, the FRP sheets along the sides provide negligible confinement. This results in non-uniform pressure distribution along the sides with its maximum value at the corners. In most of the analytical confined concrete models, the lateral pressure profile along each side of the section is assumed as a parabolic or triangular distribution with its maximum and minimum values occurring at the corners and the middle of each side, respectively (Mokari and Moghadam 2008; Braga et al. 2006).

In design-oriented confined concrete models, the confining pressure profile is commonly approximated by a uniform distribution for simplicity. To account for non-uniformity of lateral pressure and less significant confinement along the sides, it is postulated that a reduced area of the concrete is efficiently confined. In the parabolic distribution, the efficiently confined concrete core is surrounded by four parabolas forming a 45° slope with the sides of the cross section at the corners (Wang and Restrepo 2001; Lam and Teng 2003b; Harajli 2006; Wu et al. 2007). Inside these parabolic zones, the confinement effect is negligible. An effective lateral confining pressure is defined as:

$$f_L' = k_e f_L \tag{2.14}$$

where, k_e is the confinement effectiveness coefficient. This coefficient was first proposed by Mander et al. (1988) as:

$$k_e = \frac{A_e}{A_c} \tag{2.15}$$

where, A_e is the area of the effectively confined concrete.

A similar approach to estimate the lateral confinement over the concrete cores is employed in this paper. Fig. 2.7 shows the confining mechanism where, t_s and w_s are the flange and web thickness of the steel column, t_{CFRP} and t_{GFRP} are the thickness of the carbon and glass FRP jacket, a and b are the shorter and longer dimensions of the steel cross section, $f_{L1,C}$ and $f_{L2,C}$ are the lateral confining pressures in two orthogonal directions 1 and 2 and $\sigma_{u,CFRP}$ and $\sigma_{u,GFRP}$ are the ultimate tensile strength of the carbon and glass FRP jackets, respectively. Equilibrium of the FRP jacket along axis 1 (Fig. 2.7(c)) requires that:

$$f_{L1,C} = \frac{2\varepsilon_{h,rup\,CFRP}\left(E_{CFRP}t_{CFRP} + E_{GFRP}t_{GFRP}\right)}{b - 2t_s} \tag{2.16}$$

Fig. 2.8 shows half of the steel section flange acting as a cantilever plate under two uniform pressures applied by the concrete core ($f_{L2,C}$) and the FRP sheets ($f_{L2,FRP}$). Postulating uniform distribution of $f_{L2,FRP}$ is an approximation for simplicity of the analytical model, although it is predicted to be a non-uniform pressure with its largest values at the middle and tip of the steel flanges to resist expansion of the steel web and out of plane deflection of the tip of the flange as the concrete expands under axial loading.

A unit width strip of the flange is presented in Fig. 2.8(b). The maximum tip deflection of the flange can be evaluated by applying beam theory as:

$$\Delta_{\max,Flange} = \frac{\left(f_{L2,C} - f_{L2,FRP}\right)\times 1\times\left(\frac{a - w_s}{2}\right)^4}{8E_s\left(\frac{1}{12}\times 1\times t_s^3\right)} \tag{2.17}$$

where, E_s is the elastic modulus of steel.

Compatibility of deformations at the corner of the column requires that the calculated deflection of the steel flange tip be equal to half the elongation of the FRP strips attached to the concrete surface parallel to the steel web calculated as:

$$\Delta_{\max,Flange} = \frac{1}{2}\varepsilon_{h,rup\,CFRP}\times b \tag{2.18}$$

Substituting Eq. (2.17) into Eq. (2.18) results in the following expression for the lateral confining pressure on the concrete core along axis 2 i.e. ($f_{L2,C}$):

$$f_{L2,C} = f_{L2,FRP} + \varepsilon_{h,rup\,CFRP} \times E_s \times \frac{bt_s^3}{3\left(\frac{a - w_s}{2}\right)^4} \tag{2.19}$$

The uniform pressure applied by the FRP jacket over the tip of the steel flange can be evaluated by considering equilibrium of a FRP strip with a unit width shown in Fig. 2.8(c) calculated as:

$$f_{L2,FRP} = \frac{\varepsilon_{h,rup\,CFRP}\left(E_{CFRP}t_{CFRP} + E_{GFRP}t_{GFRP}\right)}{a} \tag{2.20}$$

The assumption that the steel flanges act as cantilever plates under the transverse pressures applied by the concrete cores and resisted by the FRP jacket complies with the observed failure of the tested specimens where the steel flange has deflected outwards as shown in Fig. 2.9.

A parabolic confinement mechanism is assumed based on the axial stress contours obtained from finite element analysis of the proposed composite columns by Karimi et al. (2009). The parabolic mechanism is commonly assumed for concrete confined in square or rectangular sections as previously described. For the particular composite columns in this study, the unconfined parabolic zones are assumed to form only along the FRP jacket due to the higher rigidity of the steel flanges and web comparing to the FRP. Fig. 2.10(a) and 2.10(b) shows the parabolic confinement mechanism forming inside the composite specimens without and with corner treatment, respectively. Assuming a parabolic confinement mechanism, the confinement effectiveness coefficient, k_e, introduced in Eq. (2.15) is expressed as:

$$k_e = 1 - \frac{b - 2t_s}{3(a - w_s)} \tag{2.21}$$

for the specimens without corner treatment and:

$$k_e = 1 - \frac{\frac{1}{6}(b - 2R_c)^2}{\frac{1}{2}(a - w_s)(b - 2t_s) + \left(R_c + \sqrt{2R_c t_s - t_s^2}\right)b - \left(2 + \frac{3\pi}{2}\right)R_c^2} \tag{2.22}$$

for the specimens with round steel bars at the corners where, R_c is the radius of the steel bars. Evaluating Eq. (2.21) and (2.22) for the given cross-sectional dimensions resulted in values of 0.52 and 0.62 for k_e in specimens without and with corner treatment, respectively.

The effective lateral confining pressures along the two orthogonal axes 1 and 2 in Fig. 2.7(b) are determined as:

$$f'_{L1,C} = k_e f_{L1,C} \tag{2.23}$$

$$f'_{L2,C} = k_e f_{L2,C} \tag{2.24}$$

Due to the non-uniformity of the lateral confinement resulting from the cross-section shape, an average effective confining pressure is introduced based on the corresponding pressures on the two perpendicular sides of the concrete cores as:

$$f'_{L,avg} = \frac{f'_{L1,C}(b - 2t_s) + f'_{L2,C}\left(\frac{a - w_s}{2}\right)}{D} \tag{2.25}$$

where, D is diameter of equivalent circular concrete cores shown in Fig. 2.7 given by:

$$D = \sqrt{(b-2t_s)^2 + \left(\frac{a-w_s}{2}\right)^2} \tag{2.26}$$

A linear regression was carried out between the strength enhancement (f'_{cc}- f'_{co}) and the lateral confining pressure (f_L) evaluated from Eq. (2.25) for the tested specimens and the confinement factor, k_1, in Eq. (2.13) was found to be 2.9 from the best fit. This value is similar to the proposed k_1 value (k_1=3.3) in the confined concrete model developed by Lam and Teng (2003a).

2.4.2. Ultimate Strain

Since failure of the composite specimens is characterized by rupture of the FRP jacket which subsequently led to crushing of the concrete, the ultimate axial strain of the columns (ε_u) is assumed as the failure strain of the confined concrete cores (ε_{cu}). Two separate approaches are investigated to estimate the ultimate axial strain of the confined concrete cores. The first approach calibrates the expression proposed by Lam and Teng (2003b) to experimental test results while the second approach uses an energy-based method first utilized by Mander et al. (1988) to evaluate the ultimate axial strain of reinforced concrete columns.

2.4.2.1. Lam and Teng's method

Often confined concrete models in the literature assume the maximum lateral confining pressure as the only parameter affecting the ultimate axial strain through the following expression (Richart et al. 1929; Saafi et al. 1999; Spoelstra and Monti 1999; Montoya et al. 2006):

$$\varepsilon_{cu} = \varepsilon_{co}\left(1 + k_2 \frac{f_L}{f'_{co}}\right) \tag{2.27}$$

where, k_2 is the strain enhancement factor.

Lam and Teng (2003a) demonstrated the dependency of the ultimate axial strain of the FRP confined concrete columns (ε_{cu}) on the stiffness of the FRP jacket in addition to the confining pressure. They employed the model proposed by Ottoson (1979) for concrete under a tri-axial state of stress. In this model, concrete is assumed as a non-linear elastic material with its properties being represented by the secant values of the elastic modulus and Poisson's ratio. They suggested the following expression for the normalized ultimate strain of confined concrete:

$$\frac{\varepsilon_{cu}}{\varepsilon_{co}} = \frac{\varepsilon_{h,rup\,FRP}}{\nu_{secu}\varepsilon_{co}} + \frac{1-\nu_{secu}-2\nu_{secu}^2}{\nu_{secu}}\left(\frac{E_{FRP}t_{FRP}}{E_{sec}R}\right)\left(\frac{\varepsilon_{h,rup\,FRP}}{\varepsilon_{co}}\right) + \frac{4(k_1-1)}{\sqrt{3}}\frac{1-\nu_{secu}-2\nu_{secu}^2}{\nu_{secu}}\left(\frac{E_{FRP}t_{FRP}}{E_{sec}R}\right)^2\left(\frac{\varepsilon_{h,rup\,FRP}}{\varepsilon_{co}}\right)^2 \tag{2.28}$$

where, $\varepsilon_{h,rup\,FRP}$ is the actual hoop strain at FRP rupture, ν_{secu} the secant Poisson's ratio of the confined concrete at the ultimate strain, E_{FRP} the tensile modulus of the FRP jacket, t_{FRP} the thickness of the FRP jacket, R radius of the circular column and k_1 is the confinement factor in Eq. (2.13). ε_{co} is commonly taken as 0.002.

Lam and Teng (2003a) highlighted the significant dependence of the secant Poisson's ratio (ν_{secu}) on the confinement stiffness ratio ($E_{frp}t/E_{sec}R$) through analysis of existing test data and proposed ε_{cu} as a function of the confinement stiffness ratio and the strain ratio ($\varepsilon_{h,rup\,FRP}/\varepsilon_{co}$) using the following formula:

$$\frac{\varepsilon_{cu}}{\varepsilon_{co}} = c + k_2\left(\frac{E_{FRP}t_{FRP}}{E_{sec}R}\right)^{\alpha}\left(\frac{\varepsilon_{h,rup\,FRP}}{\varepsilon_{co}}\right)^{\beta} \tag{2.29}$$

where, c is the normalized ultimate strain of the unconfined concrete and k_2 is the strain enhancement factor. The two coefficients α and β were obtained as 1.0 and 1.45 through regression analysis of the experimental data for concrete columns confined by different

types of FRP materials. Eq. (2.29) was developed for circular columns. However, experimental observations showed that the ultimate axial strain increases with the aspect ratio in rectangular confined concrete columns and a shape factor k_s for the strain enhancement was later introduced into Eq. (2.29) (Lam and Teng 2003b).

The factor k_s evaluated for the composite columns in this paper is given by:

$$k_s = \left(\frac{b - 2t_s}{(a - w_s)/2} \right)^{0.5} \times \frac{A_e}{A_c} \tag{2.30}$$

Realizing that:

$$\frac{E_{FRP} \varepsilon_{h,rup\,FRP} t_{FRP}}{R} = f_L \tag{2.31}$$

Substituting E_{sec} and f_L from Eq.s (2.6) and (2.31), respectively, into Eq. (2.29) results in:

$$\frac{\varepsilon_{cu}}{\varepsilon_{co}} = c + k_2 k_s \left(\frac{f_L}{f'_{co}} \right) \left(\frac{\varepsilon_{h,rup\,FRP}}{\varepsilon_{co}} \right)^{0.45} \tag{2.32}$$

The above expression to estimate the ultimate axial strain is calibrated using a least square fit to the test data resulting in values of 5.3 and 13.1 for the parameters c and k_2, respectively.

2.4.2.2. Energy Approach

The second method to predict the ultimate axial strain is based on an energy balance approach proposed by Mander et al. (1988) for reinforced concrete columns. Implementing this method for the composite columns leads to the following energy expression:

$$U_{CFRP} + U_{GFRP} = U_{cc} + U_{sc} - U_{co} \tag{2.33}$$

This formula equates the strain energy restored in the FRP jackets at the point of failure (U_{CFRP}+U_{GFRP}) to the difference between the restored energies in the concrete with and without confinement (U_{cc}-U_{co}), and the additional energy required to yield the steel section in compression (U_{sc}). The strain energy terms in Eq. (2.33) are evaluated by calculating the area under corresponding stress-strain curves for each material as:

$$\begin{aligned} U_{CFRP} &= A_{CFRP} \int_0^{\varepsilon_{h,rupCFRP}} \sigma_{CFRP} d\varepsilon_{CFRP} = 2(a+b) t_{CFRP} \int_0^{\varepsilon_{h,rupCFRP}} E_{CFRP} \varepsilon_{CFRP} d\varepsilon_{CFRP} \\ &= (a+b) t_{CFRP} E_{CFRP} \times \varepsilon_{h,rupCFRP}^2 \end{aligned} \tag{2.34}$$

$$U_{GFRP} = A_{GFRP} \int_0^{\varepsilon_{h,rupCFRP}} \sigma_{GFRP} d\varepsilon_{GFRP} = (a+b) t_{GFRP} E_{GFRP} \times \varepsilon_{h,rupCFRP}^2 \tag{2.35}$$

$$U_{cc} = A_c \int_0^{\varepsilon_{cu}} f_c \, d\varepsilon_c \tag{2.36}$$

$$U_{sc} = A_s \int_0^{\varepsilon_{cu}} f_s \, d\varepsilon_c \tag{2.37}$$

$$U_{co} = A_c \int_0^{\varepsilon_{sp}} f_c \, d\varepsilon_c \tag{2.38}$$

where, f_s is the axial stress in the steel column and ε_{sp} the spalling strain of the unconfined concrete.

Eq. (2.36) can be evaluated based on the assumed stress-strain curve for the confined concrete (see Eq. (2.10)). Substituting Eq. (2.10) into Eq. (2.36), U_{cc} can be expressed as:

$$U_{cc} = A_{cc} \left[\frac{1}{2} E_c \varepsilon_t^2 - \frac{(E_c - E_2)^2}{12} \varepsilon_t^3 + f_{co}^{'} (\varepsilon_{cu} - \varepsilon_t) + \frac{1}{2} E_2 (\varepsilon_{cu}^2 - \varepsilon_t^2) \right] \tag{2.39}$$

Eq. (2.37) for restored strain energy in the steel column can also be evaluated assuming an elastic perfectly plastic model for the steel given by:

$$\int_0^{\varepsilon_{cu}} f_s \, d\varepsilon_s = \frac{1}{2}\varepsilon_{sy} f_{sy} + f_{sy}\left(\varepsilon_{cu} - \varepsilon_{sy}\right) \tag{2.40}$$

where, f_{sy} and ε_{sy} are the yield stress and strain of steel, respectively. The area under the stress-strain curve of unconfined concrete U_{co} in Eq. (2.38) can be approximated by the expression proposed by Mander et al. (1988) as:

$$\int_0^{\varepsilon_{sp}} f_c \, d\varepsilon_c = 0.017\sqrt{f'_{co}} \quad \text{MJ/m}^3 \tag{2.41}$$

The ultimate axial strain for each tested column is obtained based on the energy approach by evaluating Eq.s (2.34), (2.35), (2.39), (2.40) and (2.41) and substituting the values into Eq. (2.33) to solve for ε_{cu}.

Fig. 2.11 shows the ultimate axial strains values for the five tested columns evaluated based on Lam and Teng's calibrated expression and Mander's energy approach in comparison with corresponding experimental results. It is concluded that the energy approach results in a conservative prediction of the ultimate axial strains.

2.5. Comparison of Analytical and Experimental Results

Results obtained from the analytical model are presented in Table 2.5 in terms of peak strength, ultimate strain and strength of the confined concrete cores along with ratio of each parameter evaluated analytically over its experimentally obtained value. From Table 2.5 it can be seen that the analytical model closely estimates the peak strength, ultimate strain and strength of the confined concrete cores in the tested columns with an error of less than 10%, 18% and 21% for each of these parameters, respectively. Fig. 2.12 shows the overall axial force-displacement relationship obtained from the analytical model for each of the five tested composite columns in comparison with the experimental curves. It can be seen that the analytical model predictions are in good agreement with the experimental results for the columns including one and two number of CFRP wraps.

However, greater deviation is found to occur as the number of CFRP layers increases (Column S3-3).

2.6. Parametric Study

The developed analytical model can be used to evaluate influence of the unconfined concrete strength (f'_{co}) and ultimate tensile strength of the CFRP wraps ($\sigma_{u,CFRP}$) on the enhanced compressive behavior of the composite columns. For example, Fig. 2.13(a) and 2.13(b) show effect of f'_{co} on the enhancement in strength and ultimate strain of the composite column S3-3, respectively. $P_{u,Compos.}$ and $P_{u,Cont.}$ in this figure are the compressive strength of the composite column and the control steel column, respectively. $\varepsilon_{u,Compos.}$ and $\varepsilon_{u,Cont.}$ are the ultimate axial strain of the composite and control column, respectively. As can be seen in Fig. 2.13(a), the strength enhancement increases proportionally with f'_{co}. However, Fig 2.13(b) shows that the enhancement in ultimate axial strain of the composite columns decreases by increasing f'_{co}. Therefore, use of a high strength concrete enhances the load carrying capacity of the composite columns, however it reduces the ultimate axial strain which affects the energy dissipation capacity of the column.

Fig. 2.14(a) and 2.14(b) show effect of $\sigma_{u,CFRP}$ on the enhancement in strength and ultimate axial strain of the composite column S3-3, respectively. As an example, by increasing $\sigma_{u,CFRP}$ from its current value (876 MPa) to 1600 MPa, the strength enhancement ratio ($P_{u,Compos}/P_{u,Cont.}$) increases from 2.8 to 3.6 and the ultimate axial strain enhancement ratio ($\varepsilon_{u,Compos.}/\varepsilon_{u,Cont.}$) increases from 5.2 to 9.2.

2.7. Conclusions

A novel composite column was introduced by strengthening steel columns using wet lay-up FRP sheets. The enhanced compressive strength, stiffness and energy dissipation capacity of proposed composite columns was evaluated through experimental work.

The strengthening procedure comprised wrapping the columns with epoxy-saturated FRP sheets and subsequently filling the resulting voids between the steel column and FRP jacket with concrete. The varying parameter among the tests was the number of CFRP wraps and corner radius of the composite columns. Experimental results showed significant enhancement in the strength, elastic axial stiffness and ultimate displacement of the steel columns after strengthening. Confinement was enhanced by increasing the number of CFRP wraps and corner radius of the composite specimens. Failure of the composite columns initiated by rupture of the FRP jacket which subsequently led to crushing of the concrete. Local buckling of the steel flanges and web was observed after removal of the FRP jacket. Experimental results indicated that for the column having three CFRP wraps the compressive strength of the confined concrete cores increased by a factor of 2.4. The corner treatment technique was found efficient in enhancing the compressive strength of the confined concrete by approximately 30%.

An analytical model was developed to evaluate the ultimate strength and ultimate axial strain of the composite columns and predict the corresponding axial load-displacement behavior. The model assumes a region inside each concrete core where the concrete is highly confined between the steel flange and web and a parabolic zone adjacent to the FRP jacket where concrete is not efficiently confined. An average representative value of the non-uniform lateral confining pressure over the concrete cores was then established based on the equilibrium and compatibility equations between the constituent materials. A linear relationship was assumed between the confining pressure and the compressive strength of the concrete, which was calibrated based on the data from the tested columns. A realistic evaluation of the confining pressure is the key to accurately predict the ultimate strength of the columns with non-uniform confinement.

The ultimate axial strain of the composite columns was predicted using two different methods. The first method calibrates an expression that assumes the ultimate axial strain as a function of the confinement stiffness ratio and the maximum lateral confining

pressure. The second approach was based on the strain energy equilibrium equations between the constituent materials at the point of failure. Estimates of the ultimate strain values from the first method were in good agreement with the test results while the energy approach led to underestimated values.

The estimated ultimate strength and strain values for the composite columns were further employed in predicting the corresponding axial load-displacement behavior based on an existing stress-strain relationship for the confined concrete and elastic perfectly plastic behavior for the steel. The predicted load-displacement relationships from the analytical model were in good agreement with the experimental results. The greatest deviations were observed for the specimen with the maximum number of CFRP wraps which indicates limitation of the analytical model for use in highly confined columns.

The analytical model was used to study effect of the concrete strength and ultimate tensile strength of the CFRP wraps on compressive behavior of the composite columns. It was found that although high strength concrete increases the strength of the composite columns it reduces the ultimate axial strain which affects energy dissipation capacity.

This study introduced a simple, cost-effective and reliable technique to enhance axial behavior of steel columns. The presented analytical model could be applied in analyzing cross sectional behavior of such columns and implemented in related design codes.

Appendix 2.1. Notation

The following symbols are used in this paper:

a = shorter dimension of the steel section;

A_c = total cross sectional area of the concrete cores;

A_e = area of the effectively confined concrete;

A_s = cross sectional area of the steel;

A_{CFRP} = cross sectional area of the CFRP jacket;

A_{GFRP} = cross sectional area of the GFRP jacket;

b = longer dimension of the steel section;

c = normalized ultimate strain of the unconfined concrete;

C.A.I. = composite action index;

CFRP = carbon fiber reinforced polymer;

C.R. = confinement ratio;

D.I. = ductility index;

D = diameter of equivalent circular concrete cores;

$\Delta_{max,\ Flange}$ = maximum tip deflection of the flange;

ε_c = compressive strain of concrete;

ε_{co} = corresponding strain at peak strength of the unconfined concrete;

ε_{cu} = ultimate axial strain of the confined concrete;

ε_t = axial strain at the transition point in the stress-strain relationship for the confined concrete;

$\varepsilon_{h,rup\ FRP}$ = actual hoop strain at FRP rupture;

$\varepsilon_{h,rup\ CFRP}$ = actual hoop strain at CFRP rupture;

$\varepsilon_{u,CFRP}$ = ultimate tensile strain of the CFRP wraps;

$\varepsilon_{u,GFRP}$ = ultimate tensile strain of the GFRP wraps;

ε_u = the ultimate axial strain at the point of failure;

$\varepsilon_{85\%}$ = the post failure axial strain at the point where the strength of the column degrades to 85% of its peak value;

$\varepsilon_{u,Compos.}$ = ultimate axial strain of the composite column;

$\varepsilon_{u,Cont.}$ = ultimate axial strain of the control steel column;

ε_{sp} = the spalling strain of the unconfined concrete;

ε_{sy} = yield strain of the steel;

ε_y = the yield axial strain;

E_c = tangent elastic modulus of unconfined concrete;

E_{sec} = secant elastic modulus of unconfined concrete;

E_2 = slope of the linear second portion of the stress-strain relationship for the confined concrete;

E_{FRP} = tensile modulus of the FRP jacket;

E_{CFRP} = tensile modulus of the CFRP wraps in hoop direction;

E_{GFRP} = tensile modulus of the GFRP wraps in hoop direction;

E_s = elastic modulus of steel;

f_c = compressive stress of concrete;

f'_{co} = compressive strength of unconfined concrete;

f'_{cc} = compressive strength of confined concrete;

f_L = lateral confining pressure;

$f_{L1,C}$ = lateral confining pressure in direction 1;

$f_{L2,C}$ = lateral confining pressure in direction 2;

$f_{L2,FRP}$ = uniform pressure applied by the FRP jacket on the steel flanges;

f'_L = effective lateral confining pressure;

$f'_{L1,C}$ = effective lateral confining pressure in direction 1;

$f'_{L2,C}$ = effective lateral confining pressure in direction 2;

f_s = axial stress in the steel column;

f_{sy} = yield stress of the steel;

GFRP = glass fiber reinforced polymer;

k_1 = confinement factor;

k_2 = strain enhancement factor;

k_e = confinement effectiveness coefficient;

k_s = shape factor;

v_{secu} = secant Poisson's ratio of the confined concrete at the ultimate strain;

$P_{u,Compos.}$ = compressive strength of the composite column;

$P_{u,Cont}$ = compressive strength of the control steel column;.

R_c = corner radius (radius of the steel bars placed at the corners);

$\sigma_{h,rup,FRP}$ = actual hoop stress in the FRP jacket at rupture;

$\sigma_{u,CFRP}$ = ultimate tensile strength of the CFRP jacket;

$\sigma_{u,GFRP}$ = ultimate tensile strength of the GFRP jacket;

t_{FRP} = thickness of the FRP jacket

t_{CFRP} = thickness of the CFRP jacket;

t_{GFRP} = thickness of the GFRP jacket;

t_s = flange thickness of the steel column;

U_{cc} = strain energy restored in the confined concrete at failure;

U_{co} = strain energy restored in the unconfined concrete;

U_{CFRP} = strain energy restored in the CFRP jacket at failure;

U_{GFRP} = strain energy restored in the GFRP jacket at failure;

U_{sc} = strain energy required to yield steel in compression;

w_s = web thickness of the steel column;

Appendix 2.2. References

Andrawes, B., Shin, M. and Wierschem, N. (2010). "Active confinement of reinforced concrete bridge columns using shape memory alloys." *J. of Bridge Engineering*, 15(1), 81-89.

Braga, F., Gigliotti, R., and Laterza, M. (2006). "Analytical stress-strain relationship for concrete confined by steel stirrups and/or FRP jackets." *J. Struct. Eng. ASCE*, 132(9), 1402-1416.

Chaallal, O., Hassan, M. and Shahawy, M. (2003a). "Confinement model for axially loaded short rectangular columns strengthened with fiber-reinforced polymer wrapping." *ACI Struct. J.*, 100(2), 215–221.

Chaallal, O., Shahawy, M., and Hassan, M. (2003b). "Performance of axially loaded short rectangular columns strengthened with carbon fiber-reinforced polymer wrapping." *J. Compos. Constr.*, 7(3), 200-208.

Chicoine, T., Massicotte, B. and Tremblay, R. (2003). "Long-term behavior and strength of partially encased composite columns made with built-up steel shapes." *J. Struct. Eng. ASCE*, 129(2), 141-150.

CSA. (2009). "Limit states design of steel structures. Standard CAN/ CSA S16-09." Canadian Standards Association, Mississauga, Ont.

Harajli, M. H. (2006). "Axial stress–strain relationship for FRP confined circular and rectangular concrete columns." *Cem. Concr. Compos.*, 28, 938–948.

Karimi, K., Tait, M. J., and El-Dakhakhni, W. W. (2009). "A novel retrofit technique for strengthening steel column using FRP." *Proc., CSCE 2009 Annual General Conference*, St. John's, Newfoundland, Canada.

Kratky, R. J. (2004). "Assessment of performance of vital long-span bridges in the United States." *American Society of Civil Engineers*, 1-32.

Krstulovic-Opara, N., and Thiedeman, P. D. (2000). "Active confinement of concrete members with Self-stressing composites." *ACI Mater. J.*, 97(3), 297-308.

Lam, L., and Teng, J. G. (2003a). "Design-oriented Stress-strain Models for FRP-confined Concrete." *Constr. Build. Mater.*, 17, 471-489.

Lam, L. and Teng, J. G. (2003b). "Design-oriented stress-strain model for FRP-confined concrete in rectangular columns." *J. Reinf. Plast. Compos.*, 22(13), 1149-1186.

Loud, S., and Kliger, H. (2001). "Infrastructure Composites Report – 2001." *Composites Worldwide*, Solana Beach, California.

Mander, J.B., Priestley, M. J. N., and Park, R. (1988). "Theoretical stress–strain model for confined concrete." *J. of Struct. Eng. ASCE*, 114(8), 1804–26.

Mirmiran, A., and Shahawy, M. (1997). "Behavior of concrete columns confined by fiber composites." *J. Struct. Eng. ASCE*, 123(5), 583-590.

Mirmiran, A., Shahawy, M., Samaan, M. and El Echary, H. (1998). "Effect of column parameters on FRP-confined concrete." *J. Compos. Constr.*, 2(4), 175–85.

Mokari, J., and Moghadam, A. S. (2008). "Experimental and theoretical study of reinforced concrete columns with poor confinement retrofitted by thermal post tension steel jacketing", *Journal of Applied Sciences*, 8(24), 4579-4586.

Montoya, E., Vecchio, F. J., and Sheikh, S. A. (2006). "Compression field modeling of confined concrete: constitutive models." *J. Mater. Civ. Eng.*, 18(4), 510-517.

Ottoson, NS. (1979). "Constititive model for short-term loading of concrete." *J. Eng. Mech. Div.*, 105(1), 127-141.

Popovics, S. (1973). "A numerical approach to the complete stress-strain curves for concrete", *J. Cem. Concr. Res.*, 3(5), 583-599.

Prickett, B. S., and Driver, R. G. (2006). "Behavior of partially encased composite columns made with high performance concrete." Report No. 262, Dept. of Civil & Environmental Engineering, University of Alberta.

Richart, F.E., Brandtzaeg, A., and Brown, R.L. (1928). "A study of the failure of concrete under combined compressive stresses." Bulletin no. 185, Engineering Experimental Station, University of Illinois, Champaign.

Richart, F. E., Brandtzaeg, A., and Brown, R. L. (1929). "The failure of plain and spirally reinforced concrete in compression," Bulletin no. 190, Engineering Experimental Station, University of Illinois, Champaign.

Rochette, P., and Labossi`ere, P. (2000). "Axial testing of rectangular column models confined with composites." *J. Compos. Constr.*, 4(3):129–136.

Samaan, M., Mirmiran, A., and Shahawy, M. (1998). "Model of concrete confined by fiber composites." *J. Struct. Eng. ASCE,* 124(9), 1025–1031.

Saafi, M., Toutanji, H. A. and Li, Z. (1999). "Behavior of concrete columns confined with fiber reinforced polymer tubes." *ACI Mater. J.*, 96(4), 500-510.

Shaat, A, Schnerch, D, Fam, A, and Rizkalla, S. (2004). "Retrofit of steel structures using Fiber-Reinforced Polymers (FRP): State-of-the-art." *Transportation research board (TRB) annual meeting*, CD-ROM (04-4063).

Shaat, A., and Fam, A. (2006). "Axial loading tests on short and long hollow structural steel columns retrofitted using carbon fibre reinforced polymers." *Can. J. Civil Eng.*, 33, 458–470.

Spoelstra, M. R., and Monti, G. (1999). "FRP confined concrete model." *J. Compos. Constr.*, 3(3), 143-150.

Tao, Z., and Han, L. H. (2006). "Behavior of concrete-filled double skin rectangular steel tubular beam-columns." *J. of Constr. Steel Res.*, 62, 631-646.

Tao, Z., Han, L. H., and Zhuang, J. P. (2007). "Axial loading behavior of CFRP strengthened concrete-filled steel tubular stub columns." *Advances in Structural Engineering,* 10(1), 37-46.

Teng, J. G. and Hu, Y. M. (2007). "Behavior of FRP-jacketed circular steel tubes and cylindrical shells under axial compression." *J. Constr. Build. Mater.,* 21: 827–838.

Wang, Y. C., and Restrepo, J. I. (2001). "Investigation of concentrically loaded reinforced concrete columns confined with glass fiber-reinforced polymer jackets." *ACI Struct. J.*, 98(3), 377-385.

Wang, Q., Zhao, D., and Guan, P. (2004). "Experimental study on the strength and ductility of steel tubular columns filled with steel-reinforced concrete." *J. Eng. Struct.*, 26, 907-915.

Wang, L. M. and Wu, Y. F. (2008). "Effect of corner radius on the performance of CFRP-confined square concrete columns: Test." *J. Eng. Struct.*, 30(2), 493-505.

Woods, J. M., Kiousis, P. D., Ehsani, M. R., Saadatmanesh, H., and Fritz, W. (2007). "Bending ductility of rectangular high strength concrete columns." *J. Eng. Struct.*, 29, 1783-1790.

Wu, G., Lu, Z.T., and Wu, Z. S. (2006a). "Strength and ductility of concrete cylinders confined with FRP composites." *J. Constr. Build. Mater.*, 20, 134–48.

Wu, Y. F., Tao, L. and Oehlers, D. J. (2006b). "Fundamental principles that govern retrofitting of reinforced concrete columns by steel and FRP jacketing." *Advances in Structural Engineering*, 9(4), 507–533.

Wu, G., Wu, Z. S., and Lu, Z. T. (2007). "Design-oriented stress-strain model for concrete prisms confined with FRP composites." *J. Constr. Build. Mater.*, 21, 1107-1121.

Yang, X. B., Wei, J., Nanni, A. and Dharani L. R. (2004). "Shape effect on the performance of carbon fiber reinforced polymer wraps." J. *J. Compos. Constr.,* 8(5), 444–451.

Yang, H., Lam, D., and Gardner, L. (2008). "Testing and analysis of concrete-filled elliptical hollow sections." *J. Eng. Struct.*, 30(12), 3771-3781.

Zhao, X. L. and Zhang, L. (2007) "State-of-the-art review on FRP strengthened steel structures." *J. Eng. Struct.*, 29: 1808-1823.

Table 2.1. Material properties of the CFRP and GFRP composite laminates and epoxy

	Tensile Strength (MPa)	Tensile Modulus (GPa)	Ultimate Elongation (%)	Thickness (mm)
CFRP compsite laminate	876	72.4	1.2	1.0
GFRP compsite laminate	575	26.1	2.2	1.3
Saturant Epoxy	72.4	3.18	5.0	---

Table 2.2. Test matrix

Test No.	ID.	Number of GFRP layers	Number of CFRP layers	Corner Treatment
1	C1-0	0	0	No
2	C2-0	0	0	No
3	S1-1	1	1	No
4	S2-2	1	2	No
5	S3-3	1	3	No
6	S4-1C	1	1	Yes
7	S5-2C	1	2	Yes

Table 2.3. Experimental results

Specimen ID	Peak Strength		Elastic Stiffness		Strain at the Peak Strength (ε_u)		f'_{cc}
	(kN)	Increase (Ratio)	kN/mm	Increase (Ratio)	(%)	Increase (Ratio)	(MPa)
Avg. (C1-0,C2-0)	720	N/A	724	N/A	0.47	N/A	N/A
S1-1	1,444	2.01	2,046	2.83	1.62	3.44	54.6
S2-2	1,650	2.29	2,017	2.79	1.98	4.26	70.1
S3-3	2,129	2.96	2,111	2.91	2.04	4.39	106.2
S4-1C	1,883	2.62	2,354	3.25	1.94	4.13	70.2
S5-2C	2,319	3.22	2,336	3.23	3.02	6.43	96.5

Table 2.4. Summary of the experimentally evaluated proposed indices for assessing enhanced behavior of the composite columns

	C.A.I	C.R.	D.I.
Avg. (C1-0,C2-0)	N/A	N/A	2.35
S1-1	1.11	0.66	8.1
S2-2	1.27	1.10	9.9
S3-3	1.63	1.55	10.2
S4-1C	1.13	0.86	9.7
S5-2C	1.40	1.44	15.1

Table 2.5. Analytical model predictions

Specimen ID	Peak Strength		Strain at the Peak Strength		$f_{cc}^{'}$	
	(kN)	Ana./Exp.	(%)	Ana./Exp.	(MPa)	Ana./Exp.
S1-1	1,595	1.10	1.63	0.89	66.4	1.21
S2-2	1,800	1.09	2.02	1.02	81.9	1.16
S3-3	1,976	0.93	2.41	1.18	97.0	0.91
S4-1C	2,078	1.10	2.04	1.05	71.9	1.02
S5-2C	2,400	1.03	2.70	0.89	90.8	0.94

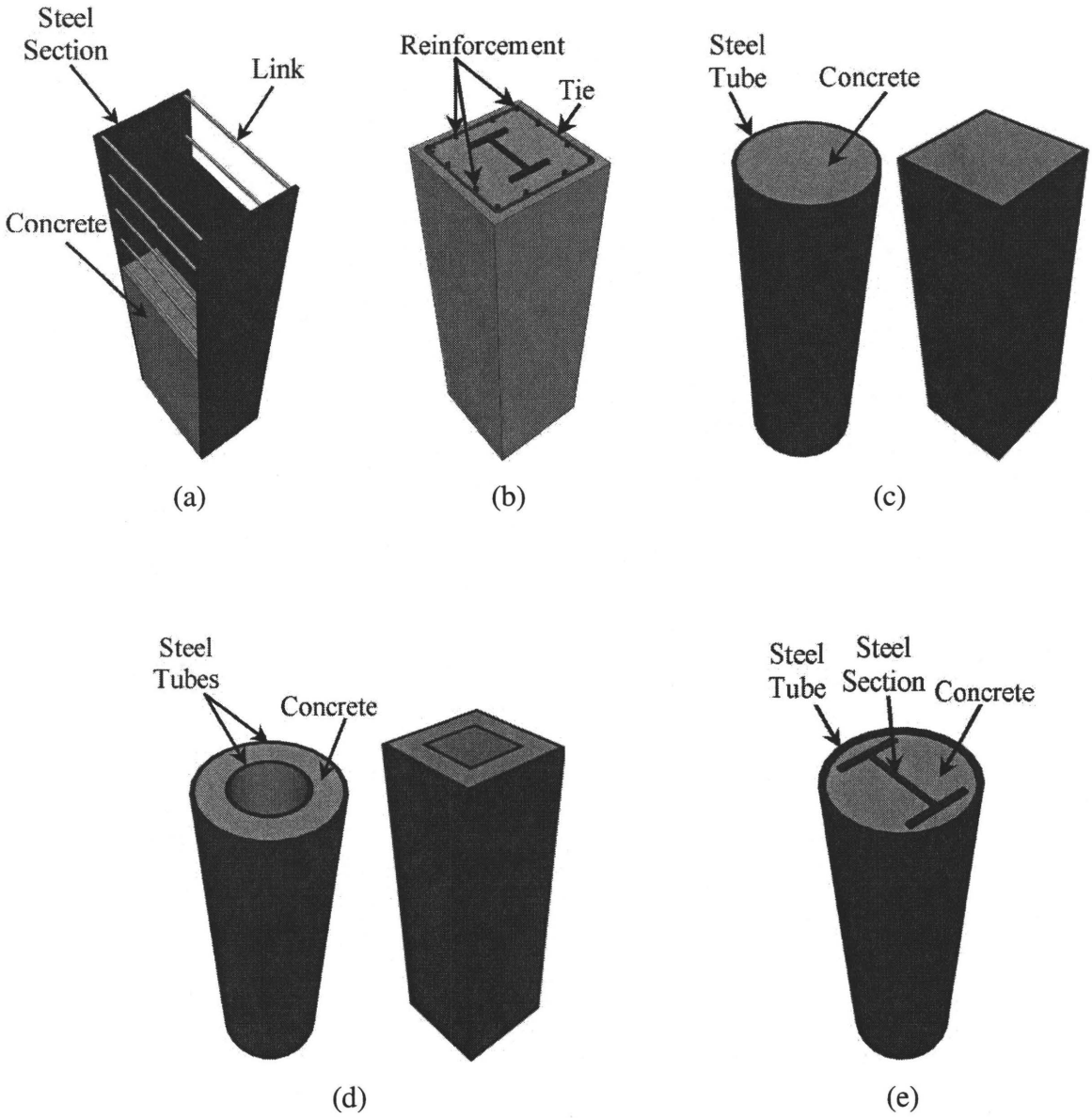

Figure 2.1. Conventional composite columns (a) partially encased (b) fully encased (c) concrete filled steel tubular columns (d) concrete filled double skin tubular columns (e) steel tubular columns filled with steel-reinforced concrete

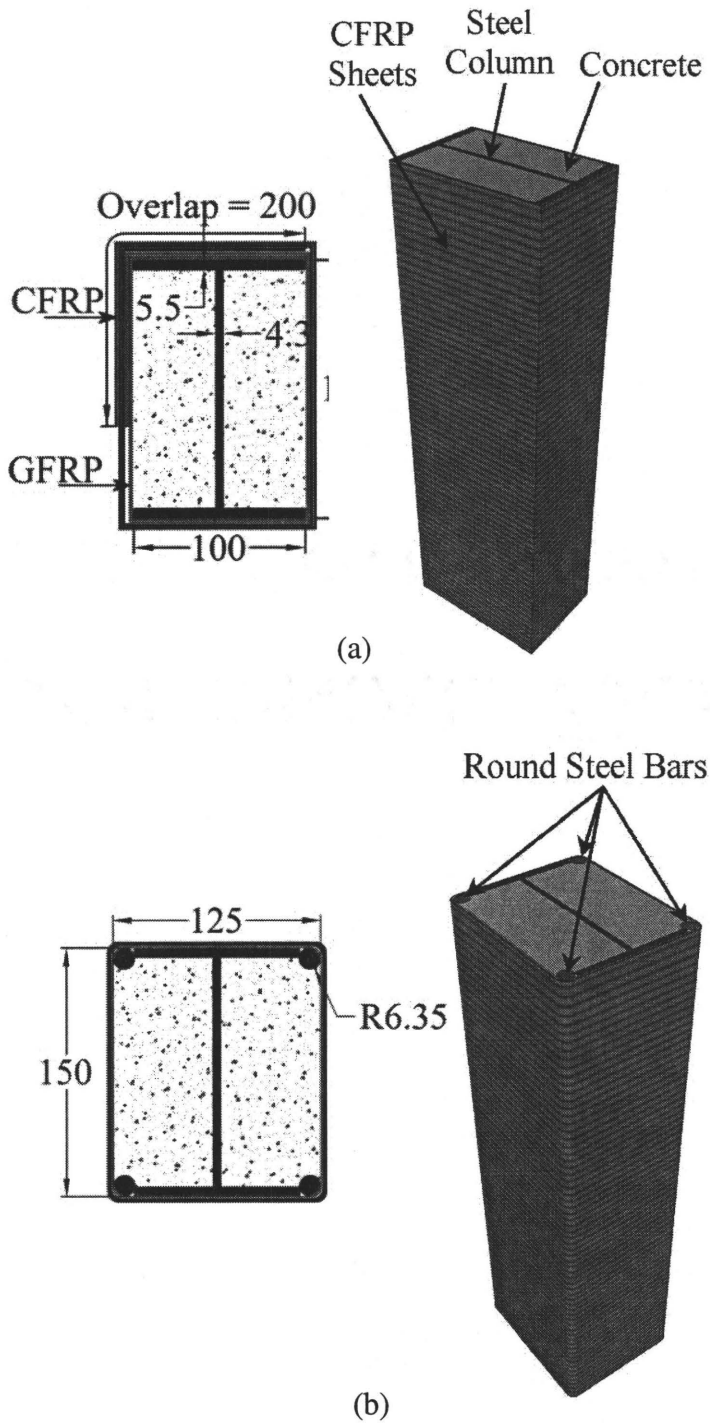

Figure 2.2. Proposed composite columns (a) without corner treatment (b) with round steel bars at the corners

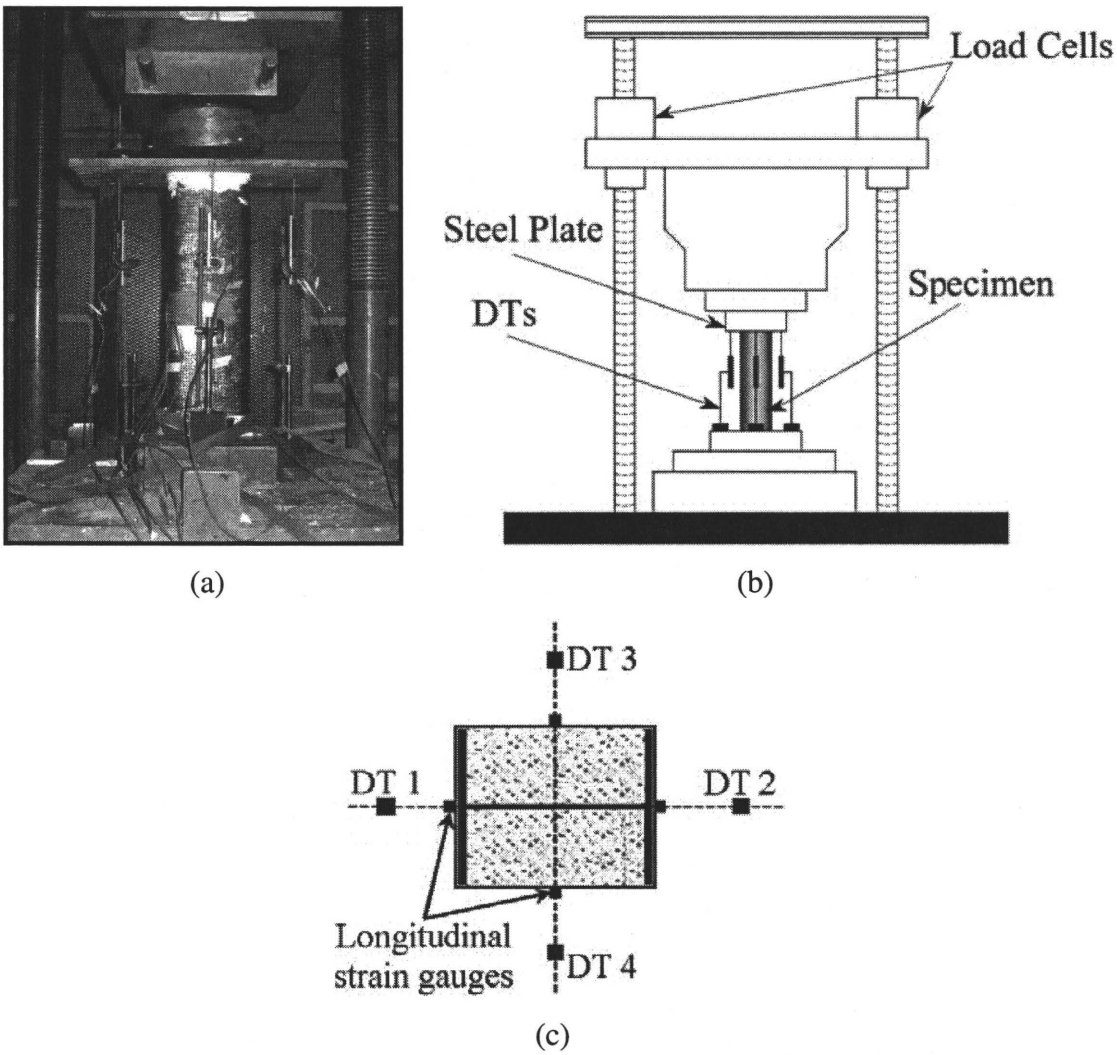

Figure 2.3. Test setup (a) 2,500 kN compression test machine (b) schematic view of the test setup (c) instrumentation layout

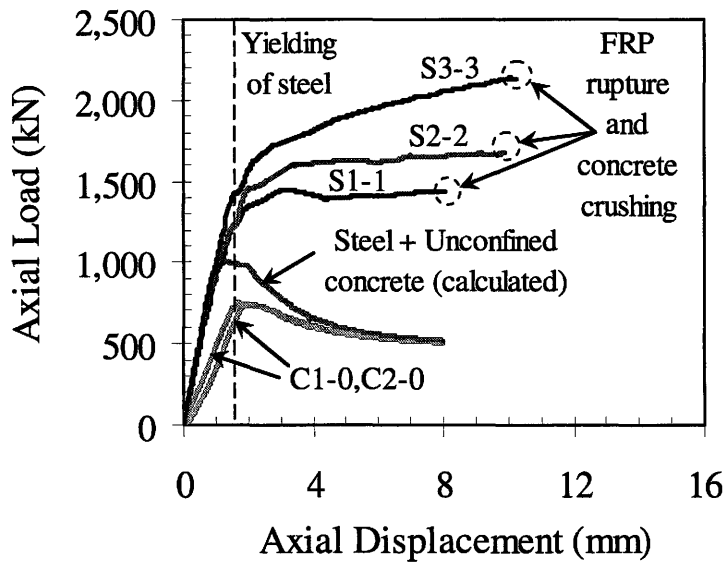

(a)

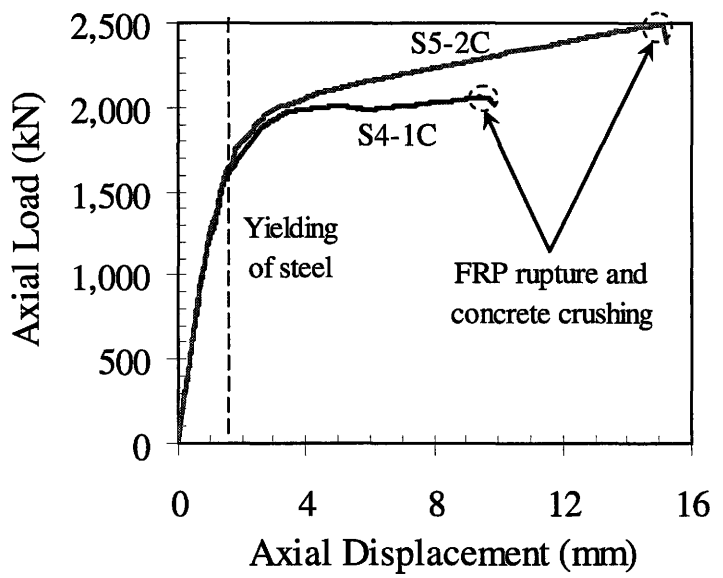

(b)

Figure 2.4. Axial load-displacement diagrams from the tests (a) specimens without corner treatment (b) specimens with corner treatment

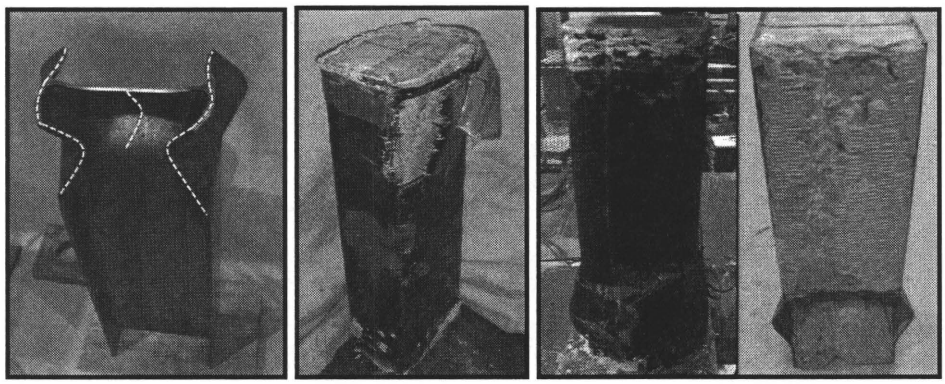

(a) C1-0 (b) S1-1 (c) S2-2

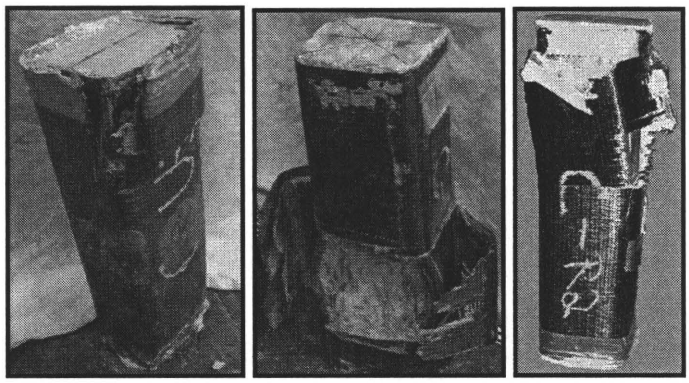

(d) S3-3 (e) S4-1C (f) S5-2C

Figure 2.5. Failure mode of the tested short columns

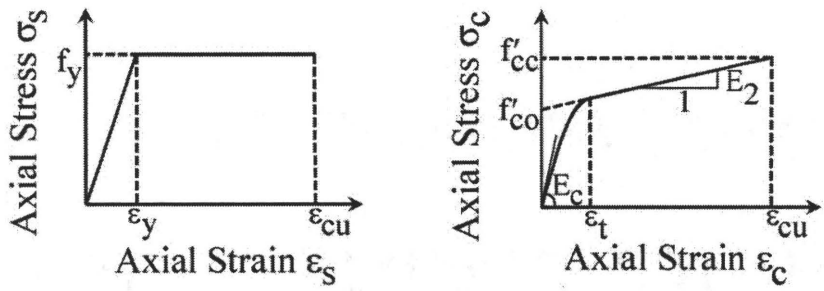

(a) (b)

Figure 2.6. The stress-strain relationship for (a) steel (b) confined concrete

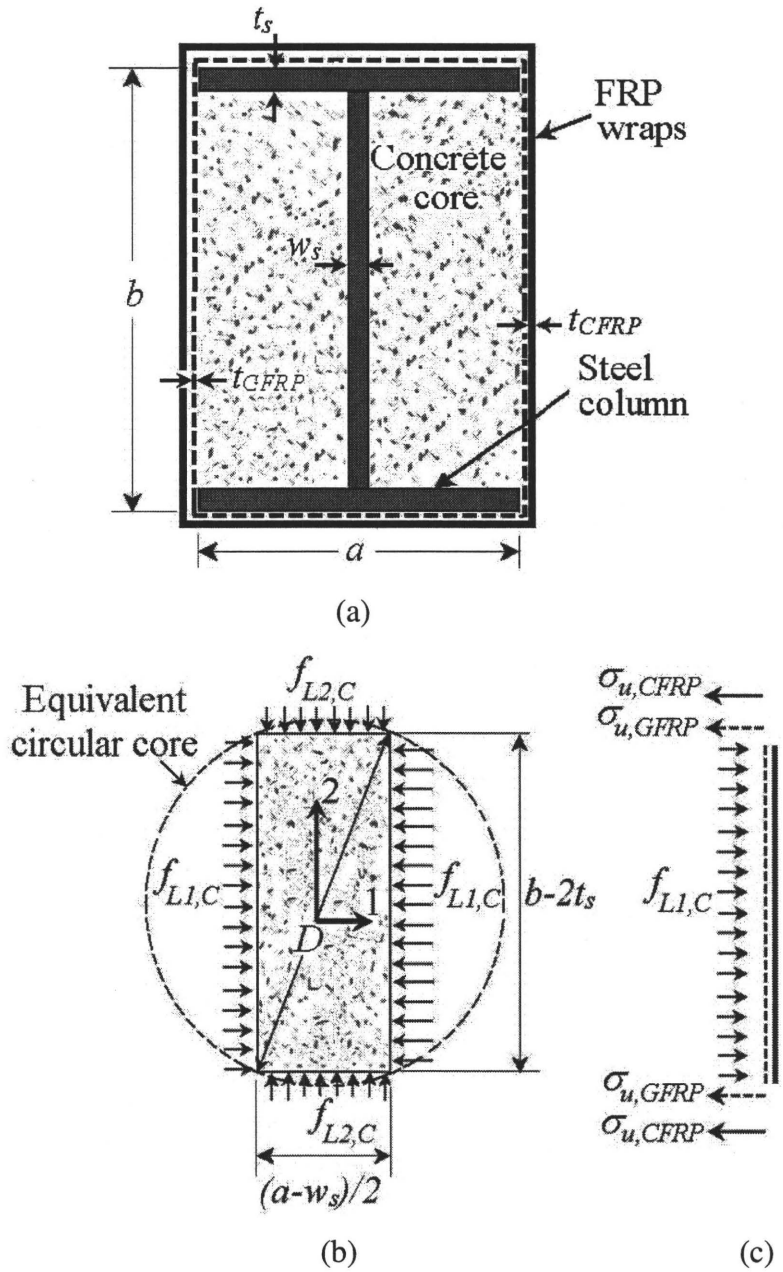

Figure 2.7. Confining mechanism in the proposed composite columns (a) composite cross section (b) concrete core under confinement (c) free body diagram of the FRP jacket in direction 1

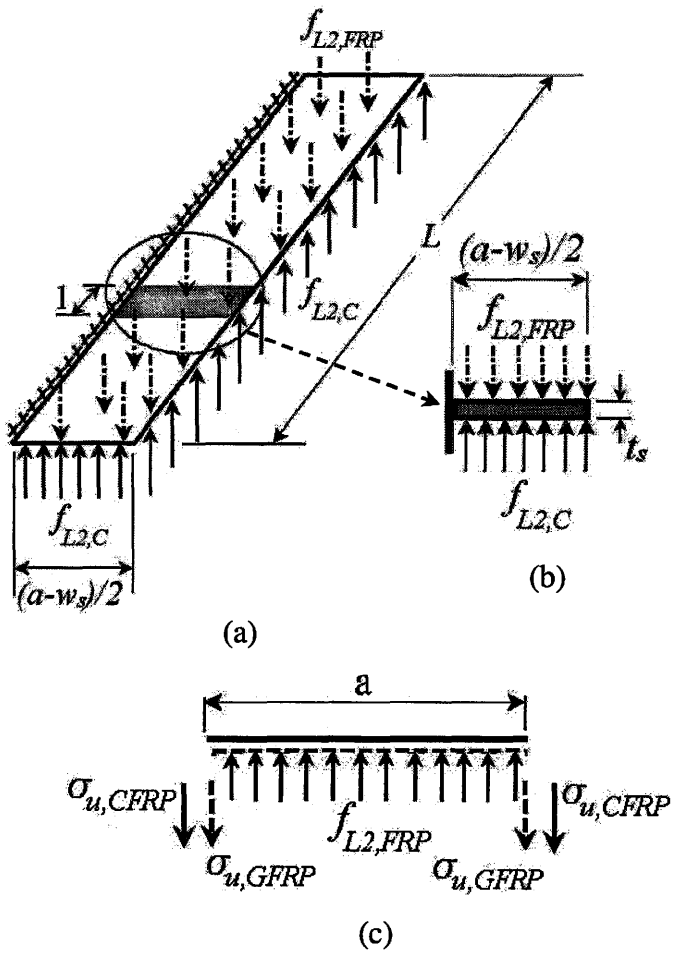

Figure 2.8. (a) Free body diagram of the steel flange (b) a strip of the steel flange with a unit width acting as a cantilever beam (c) free body diagram of a FRP strip with a unit width bonded to the concrete surface

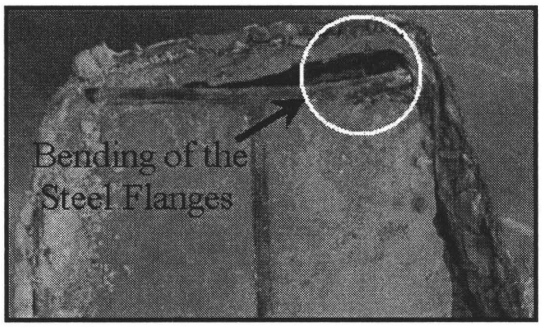

Figure 2.9. Steel flange acting as a cantilever plate under lateral pressures applied by the concrete core and the FRP jacket

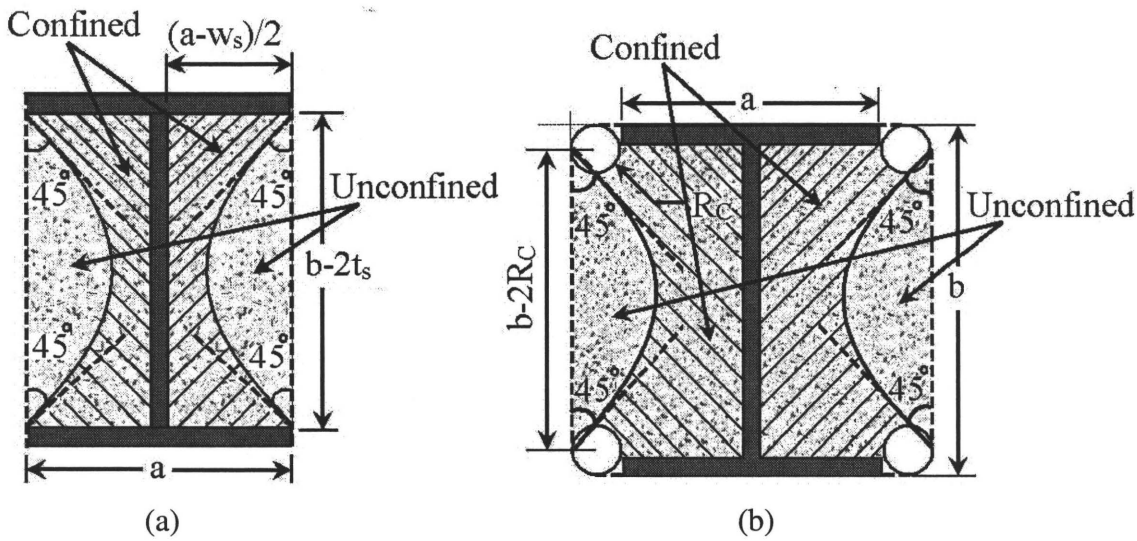

Figure 2.10. Assumed confined and unconfined regions of concrete in the analytical model (a) specimens without corner treatment (b) specimens with corner treatment

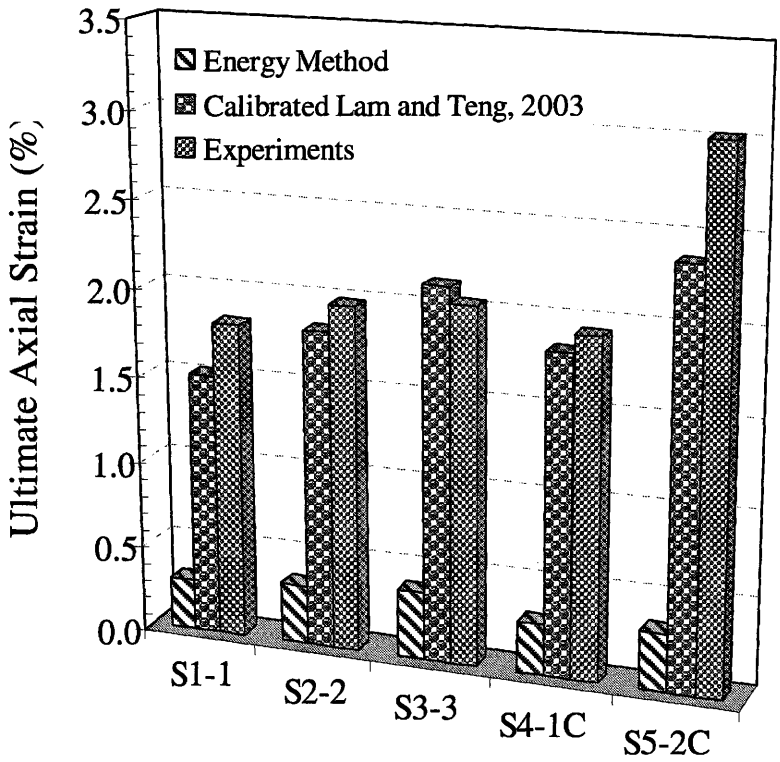

Figure 2.11. Ultimate axial strain values from the analytical model and test results

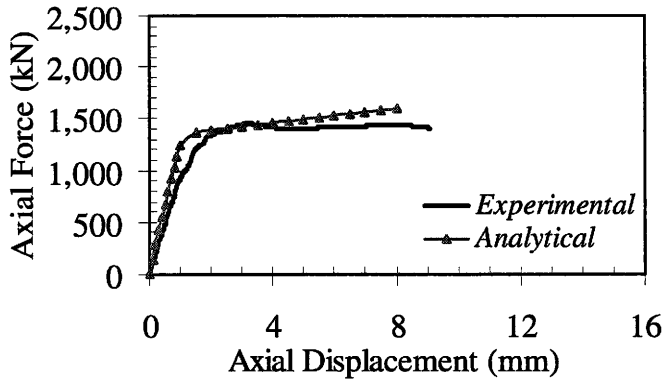

(a) S1-1

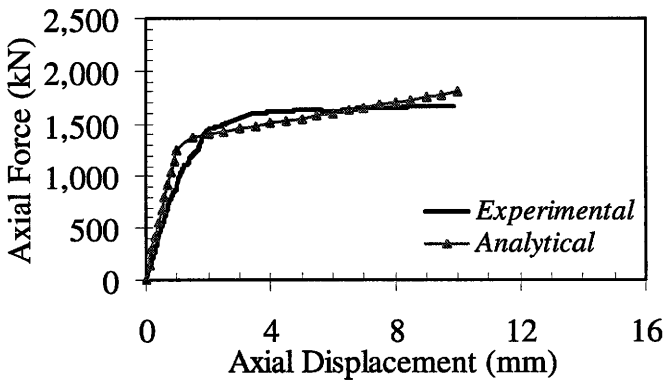

(b) S2-2

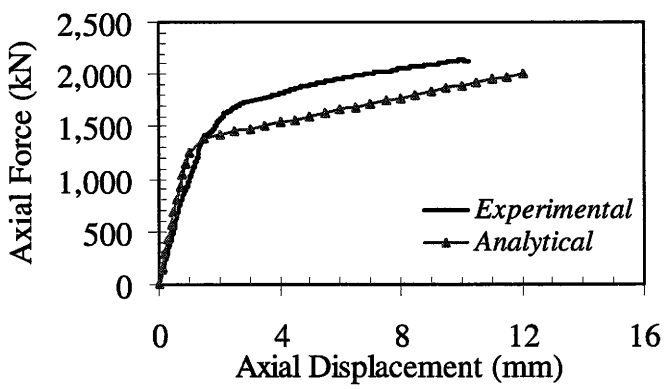

(c) S3-3

Figure 2.12. Analytically predicted axial load-displacement diagrams of the composite columns in comparison with the test results

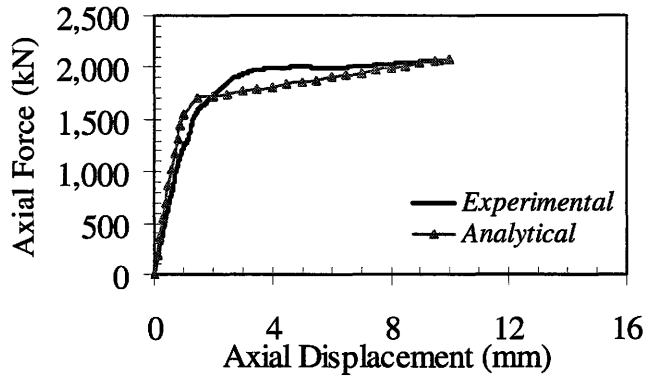

(d) S3-3

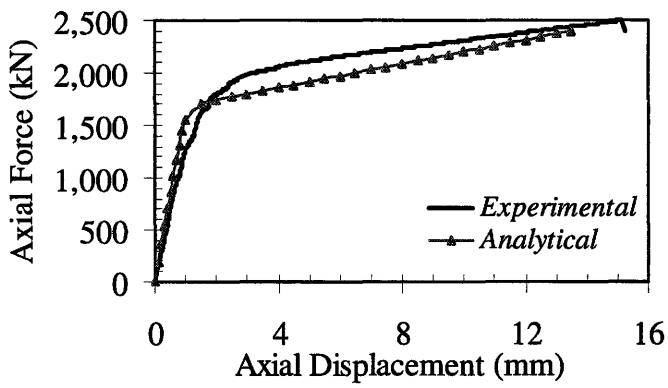

(e) S5-2C

Figure.2.12. Continued

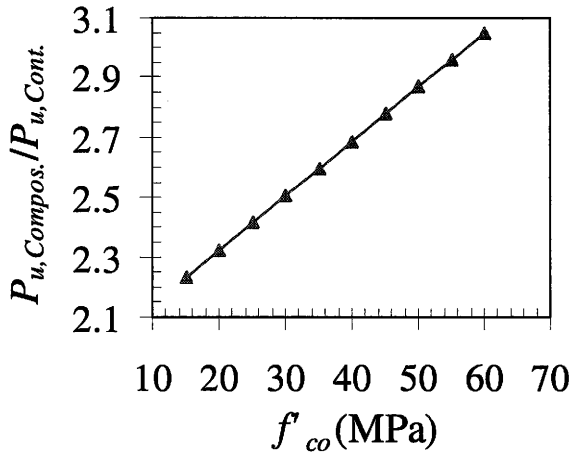

(a)

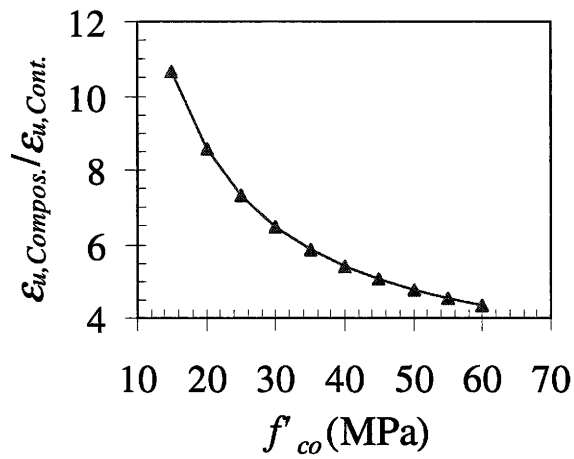

(b)

Figure 2.13. Influence of the unconfined concrete strength on behavior of the composite column S3-3 (a) strength enhancement versus f'_{co} (b) ultimate axial strain enhancement versus f'_{co}

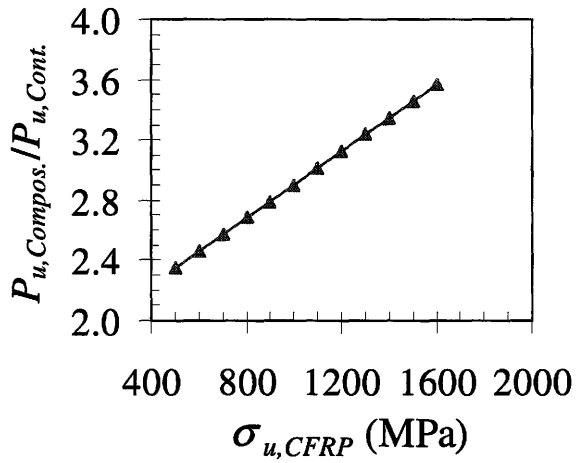

(a)

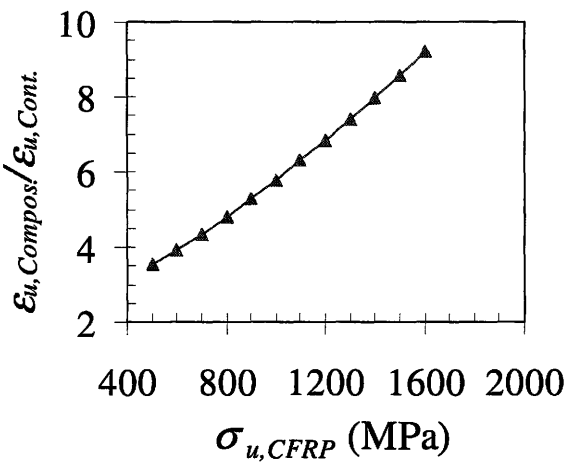

(b)

Figure 2.14. Influence of the ultimate tensile strength of the CFRP wraps on behavior of the composite column S3-3 (a) strength enhancement versus $\sigma_{u,CFRP}$ (b) ultimate axial strain enhancement versus $\sigma_{u,CFRP}$

Chapter 3: Testing and Modeling of a Novel FRP-encased Steel-Concrete Composite Column

3.1. Summary

A composite column consisting of steel, concrete and fiber reinforced polymer (FRP) is presented and assessed through experimental testing and analytical modeling. The composite column utilizes a glass FRP (GFRP) composite tube that surrounds a steel I-section, which is subsequently filled with concrete. The GFRP tube acts as a stay-in-place form in addition to providing confinement to the concrete. This study investigates the behavior of the proposed composite columns under axial loading. A total of seven specimens were tested. The influence of concrete shrinkage on the compressive behavior of the composite columns was also investigated. Significant confinement and composite action resulted in enhanced compressive behavior. The addition of a shrinkage reducing agent was found to further improve the compressive behavior of the composite columns. An analytical model was developed to predict the behavior of the composite columns under axial loading.

Keywords: analytical techniques; confinement; fiber reinforced polymer (FRP); retrofit; steel columns; tubes

3.2. Introduction

In United States, composite columns were first utilized in selected buildings in Pittsburgh in 1898 primarily to increase the fire resistance of steel sections by encasing them in concrete (Moore 1987; Uy 2001). Currently, composite columns are widely used in high-rise buildings, offshore structures, bridges and warehouses, particularly in regions of high seismic risk due to the high strength-to-weight ratio and increased deformability (Kilpatrick and Rangan 1997; Tao and Han 2006). Various types of composite columns

are reported in the literature, however, the two most common composite columns are the concrete-filled steel tubular (CFST) columns (Fig. 3.1(a)) and concrete-encased steel columns (Fig. 3.1(b)).

In CFST columns longitudinal and lateral reinforcing bars are replaced by a single steel tube, which enhances the compressive strength and deformability of the concrete by providing continuous confinement in addition to acting as formwork. The concrete core in turn enhances the capacity of the column by providing stability against inward local buckling and overall buckling. Consequently, utilizing CFST columns in construction results in smaller column cross sections and significantly reduces construction time and labor costs, which makes CFST columns more economical than traditional reinforced concrete columns. Replacing steel columns in high-rise buildings with CFST columns can result in a 60% reduction in steel (Zhong 1988). The main disadvantages of CFST columns are their low fire and corrosion resistance as a result of using an exposed steel tube. To overcome corrosion related issues, some studies have suggested replacing the carbon steel tube with a cold-formed stainless steel or aluminum tube for higher corrosion resistance and aesthetic appearance (Young and Ellobody 2006; Zhou and Young 2008).

In concrete-encased steel (CES) columns, the encased steel section provides additional compressive and shear resistance and ductility to the column and the concrete further enhances local and overall buckling of the steel column (Uy 2001). Fire resistance of CES columns is considerably higher than CFST columns. The main disadvantages of CES columns are the need for formwork and placing lateral reinforcement cages to prevent spalling of the concrete cover under compressive loading which are labor intensive.

Wang et al. (2004) introduced a new composite column by inserting a steel section into a CFST column, which incorporates advantages of CES and CFST columns (Fig. 3.1(c)). In this study, the steel tube is replaced with a fiber reinforced polymer (FRP) tube as shown in Fig. 3.2(a). FRP is well recognized for its high strength-to-weight ratio and durability.

Replacement of the steel jacket with FRP provides a significantly lighter formwork for the concrete resulting in considerable weight reduction and labor costs. It also aids in protecting the column against corrosion. Similar rectangular composite column constructed using a concrete-filled wet lay-up FRP jacket was previously proposed by Karimi et al. (2010). Replacing the rectangular wet lay-up FRP jacket with a circular FRP tube in this study is expected to increase confinement efficiency by providing more uniform confinement. In addition, construction of the composite columns using FRP tubes involves less labor compared to the columns constructed using a wet lay-up FRP jacket.

Combining FRP composites with traditional construction materials including steel and concrete to form a hybrid column has been investigated by Teng et al. (2007) in an attempt to integrate advantages of all the constituent materials to achieve higher structural performance. The hybrid column cross section comprised of an inner steel tube and an outer FRP tube, with concrete placed between them. The possibility of inward local buckling of the inner steel tube can influence performance of such columns, however, this is not an issue in the composite columns proposed in this study.

The proposed composite system in this paper can also be applied as a retrofit technique for strengthening existing steel columns subjected to gravity loads that exceed original design loads including for example steel bridge piers under increased traffic loading. Due to interference of other structural elements in placing the FRP tube around an existing steel column, in retrofit applications the FRP jacket can be manufactured by bonding split FRP tubes together using epoxy as shown in Fig. 3.2(b). A similar technique was used by Liu et al. (2005) to recover axial capacity of corroded steel columns by locally applying the composite retrofit scheme around the corroded segment. In strengthening steel columns using the composite retrofit scheme proposed in this study, the columns are retrofitted along their entire length to increase the compressive strength, stiffness and energy dissipation capacity. Performance of the composite columns constructed using

solid or split GFRP tubes are postulated to be similar if adequacy of the bond between the epoxy and the GFRP tube is ensured. The composite columns tested in this study were constructed using a solid GFRP tube.

This study investigates the compressive behavior of the proposed composite columns at the cross sectional level. To avoid stability-related failure, all tested specimens are selected as short (stub) columns. The effect of concrete shrinkage on the confinement mechanism is also investigated by adding a shrinkage reducing agent to the concrete mix in one composite specimen. An analytical model is developed to predict the cross sectional behavior of the composite columns. A simplified approach is employed in development of the analytical model such that it can be used as a practical design tool.

3.3. Experimental Program

A total of seven columns were tested in the experimental program. Three steel column specimens were tested for comparison purposes in employing the composite system as a retrofit technique. The remaining four composite columns were tested to evaluate the proposed composite system. The FRP tubes comprised of unidirectional glass fiber reinforcement oriented in the circumferential direction and are referred to as GFRP tubes hereafter. In constructing the composite column specimens, the GFRP tube was placed around the steel column and subsequently filled with concrete. The steel column was held concentric with respect to the GFRP tube using a temporary spacer as shown in Fig. 3.3(a). The selected steel stub columns were 500 mm long W150×14 sections with the cross section classified as a compact section based on the Canadian steel code, CAN/CSA-S16-09 (CSA 2009). These dimensions ensured cross sectional yielding prior to the onset of local or overall buckling. Fig. 3.3(b) shows cross sectional dimensions of the composite specimens.

3.3.1. Material Properties

The dimensions and mechanical properties of the two GFRP tubes used in this study are presented in Table 3.1. Two different types of concrete mix were used, one with and one without a shrinkage reducing agent. The average compressive strength of concrete at the time of testing was 48.3 MPa. The average yield and ultimate tensile strength values of the steel were 411 MPa and 526 MPa, respectively.

3.3.2. Test Matrix

The test matrix is presented in Table 3.2. The letters "C" and "R" in the assigned designations indicate control (steel column specimens) and composite (retrofitted) specimens, respectively. The first digit indicates the specimen number in each category and the second digit specifies the type of GFRP tube. The letter "S" at the end of the specimen designation indicates the concrete mix contains a shrinkage reducing agent.

3.3.3. Test Setup and Instrumentation

A self reacting test frame was used to conduct the compression tests. The load was applied to the specimen using a 5,000 kN capacity actuator and measured using a load cell with similar capacity. An MTS controller was used to apply the displacement controlled loading at a rate of 0.1 mm/min. Fig. 3.4 shows a photograph and a schematic of the test setup.

Fig. 3.5 shows the instrumentation layout used in this experimental program. Four displacement transducers, mounted between the end plates, were used to measure the axial deformation of the columns over their full height. Four additional displacement transducers were used to measure the axial deformation of the columns over a gauge length of 160 mm at the mid-height region. Eight stain gauges were used to measure axial and lateral strain at mid-height. A photograph of a gauged specimen is shown in Fig. 3.6.

3.3.4. Test Results

The test results are presented in the following sections and discussed in terms of load-displacement characteristics, enhanced properties, enhancement factors, state of stress in the FRP tube, confinement effects, shrinkage effects, and failure modes.

3.3.4.1. Load-Displacement Characteristics

The axial load-displacement relationship of the stub columns under compressive loading can be influenced by the deformation measurement method. Three different measurement techniques employed to establish deformation behavior of stub columns are reported in the literature: (1) measuring axial deformation over the full height using displacement transducers (Schneider 1998; Johansson and Gylltoft 2002; Giakoumelis and Lam 2004; Sakina et al. 2004), (2) measuring axial deformation over a certain gauge length at the mid-height region (Wu and Xiao 2000), (3) axial strain recording at mid-height of the specimen (Han and Yao 2004; Han et al. 2005).

Yu et al. (2007) reported the axial deformation measurement method 2 introduced above as the most accurate deformation measurement technique in developing the axial load-displacement relationship of stub columns. It was also shown capable of estimating the post failure deformation of the columns.

In an effort to establish a suitable method of measuring axial deformation, the axial load-axial strain relationship of the tested specimens obtained based on the three axial deformation measurement methods described above are presented and compared in Fig. 3.7. From this figure, it can be seen that the axial load-axial strain diagrams obtained based on methods 2 and 3 are in close agreement. Axial deformation recordings using method 1 were generally larger than the values obtained from the two other methods as they included the end constraint effects of the capped areas at the top and bottom of the specimens with the exception of specimen *R3* where the displacement transducers in the mid-height region recorded the largest axial deformations due to the localized failure in

this region. Also, strain gauge recordings in specimen *R3*, were not valid over the entire displacement range due to debonding of the strain gauges from the mounted surface resulting from crack formation and GFRP tube rupture at larger deformations. Therefore, deformation measurement method 2 provides a reliable axial deformation recording and is subsequently used to establish the overall load-deformation behavior of the specimens in this study.

3.3.4.2. Enhanced Properties

To highlight the significant enhancement in the axial behavior due to confinement and composite action, separate contributions from the constituent materials were analytically evaluated and superimposed as denoted by $P_s+P_c+P_{g,I}$ and $P_s+P_c+P_{g,II}$ in Fig. 3.8, for the two types of GFRP tubes used, in comparison with load-deformation behavior of the tested composite specimens. In developing these diagrams, the GFRP tube and the steel were assumed to be elastic and elastic-plastic materials, respectively. The axial stress-strain diagram for the unconfined concrete was calculated using the concrete model proposed by Popovics (1973). The axial force corresponding to each level of strain is obtained using the following formula:

$$P = \sigma_{a,s}A_s + \sigma_{a,c}A_c + \sigma_{a,g}A_t \tag{3.1}$$

where, $\sigma_{a,s}$, $\sigma_{a,c}$ and $\sigma_{a,g}$ are the axial stress in the steel, concrete and GFRP tube, respectively, and A_s, A_c and A_t are the corresponding cross sectional areas.

Fig. 3.8 reveals significant improvement in the peak strength and the ultimate axial strain of the composite specimens compared to $P_s+P_c+P_{g,I}$ and $P_s+P_c+P_{g,II}$ diagrams due to the confinement and composite action between the constituent materials. From this figure, it can also be inferred that the confinement and the composite action have a minor influence on the elastic stiffness, which is attributed to negligible confinement occurring in the elastic range.

The compressive properties of the tested specimens are presented in Table 3.3. In this table, P_u is the compressive strength, ε_{au} the ultimate axial strain and ε_{lu} the ultimate lateral strain in the GFRP tube; $\sigma_{au,g}$ and $\sigma_{lu,g}$ are the axial and lateral stress in the GFRP tube at the failure, respectively; f'_{co} is the compressive strength of unconfined concrete and f'_{cc} is the compressive strength of the confined concrete core evaluated from test results assuming yielding of the steel at failure and accounting for the load carrying capacity of the GFRP tube.

Table 3.3, also shows the increase in P_u, elastic axial stiffness and ε_{au} of the composite specimens compared to the control specimens to evaluate the enhancement in the axial behavior of retrofitted steel column specimens. The compressive strength of the composite specimens was approximately 4.5-5.5 times greater than that of the control specimens primarily due to the increase in strength of the confined concrete which was approximately doubled in the specimens constructed using Type II GFRP tube. The composite specimens achieved an axial stiffness and ultimate axial strain of approximately 4 and 2 times those of the steel specimens, respectively. The significantly larger ultimate axial strains achieved in composite specimens compared to the steel specimens indicates the considerable enhancement in the energy dissipation capacity of retrofitted columns.

3.3.4.3. Enhancement Factors

To further highlight the enhanced axial behavior of steel columns retrofitted using the proposed composite scheme, enhancement factors are presented and evaluated. These factors include composite action index (*C.A.I*), confinement ratio (*C.R.*) and ductility index (*D.I.*) defined as:

$$C.A.I. = \frac{A_s f_y + A_c f'_{cc}}{A_s f_y + A_c f'_{co}} \tag{3.2}$$

$$C.R. = \frac{A_t \sigma_{lu,g}}{A_c f_{co}^{'}} \tag{3.3}$$

$$D.I. = \frac{\varepsilon_u}{\varepsilon_y} \tag{3.4}$$

where, f_y is the yield strength of the steel section; ε_u and ε_y are the ultimate and yield axial strain, respectively.

C.A.I. and *C.R.* factors were introduced by Yang et al. (2008) to evaluate the degree of confinement and composite action between the constituent materials in a study on the axial behavior of CFST columns. *D.I.*, as defined in Eq. (3.4), was applied by Woods et al. (2007) to evaluate failure ductility of concrete columns. The enhancement factors were later applied by Karimi et al. (2009) in evaluating the enhanced behavior of retrofitted steel columns and were found correlated to the enhancement in the compressive strength of the retrofitted columns.

Table 3.4 presents the evaluated enhancement factors for the columns tested in this study. An increase in the confinement ratio (*C.R.*) typically resulted in a more pronounced composite action existing between the constituent materials (higher *C.A.I*), which subsequently enhanced load carrying capacity of the retrofitted columns. The greater *D.I.* for the composite specimens compared to the steel specimens indicates a more ductile failure, which is attributed to confinement and composite action.

3.3.4.4. State of Stress in the FRP Tube

In the composite specimens, the GFRP tube is under a biaxial state of stress. Based on the mechanics of composite materials and using the ultimate axial and lateral strains measured on the GFRP tube, $\sigma_{au,g}$ and $\sigma_{lu,g}$ are evaluated as (Bank 2006):

$$\sigma_{au,g} = \frac{E_{a,g}}{1-\nu_{al}\nu_{la}}\varepsilon_{au} + \frac{\nu_{al}E_{a,g}}{1-\nu_{al}\nu_{la}}\varepsilon_{lu} \tag{3.5}$$

$$\sigma_{lu,g} = \frac{\nu_{la}E_{l,g}}{1-\nu_{al}\nu_{la}}\varepsilon_{au} + \frac{E_{l,g}}{1-\nu_{al}\nu_{la}}\varepsilon_{lu} \tag{3.6}$$

where, $E_{a,g}$ and $E_{l,g}$ are the axial compressive and lateral tensile modulus of the GFRP tube, respectively.

Comparing $\sigma_{au,g}$ and $\sigma_{lu,g}$ in Table 3.3 with the axial compressive and lateral tensile strength of the GFRP tubes presented in Table 3.1, indicates that the GFRP tubes, at collapse, reached neither the axial compressive strength nor the lateral tensile strength due to the biaxial stress state. The Tsai-Wu failure criterion was applied to the GFRP tubes at collapse and was found to slightly exceed unity for the tested specimens indicating rupture of the tube. The failure criterion for an orthotropic GFRP tube under biaxial state of stress along the principal axes is determined as (Daniel and Ishai 2006):

$$F_l\sigma_{lu,g} + F_a\sigma_{au,g} + F_{ll}\sigma^2_{lu,g} + F_{aa}\sigma^2_{au,g} + 2F_{la}\sigma_{lu,g}\sigma_{au,g} = 1 \tag{3.7}$$

where,

$$F_l = \frac{1}{S_{l,t}} - \frac{1}{S_{l,c}} \tag{3.8}$$

$$F_a = \frac{1}{S_{a,t}} - \frac{1}{S_{a,c}} \tag{3.9}$$

$$F_{ll} = \frac{1}{S_{l,t}S_{l,c}} \tag{3.10}$$

$$F_{aa} = \frac{1}{S_{a,t}S_{a,c}} \tag{3.11}$$

$$F_{la} = -\frac{1}{2}\sqrt{F_{ll}F_{aa}} \tag{3.12}$$

where, $S_{l,t}$ and $S_{l,c}$ are the tensile and compressive strength of the GFRP tube in the lateral direction, respectively, and $S_{a,t}$ and $S_{a,c}$ are the tensile and compressive strength values in the axial direction, respectively.

3.3.4.5. Confinement Effects

The maximum confining pressure is the dominant parameter that specifies the shape of the stress-strain relationship. Based on this parameter, three types of stress-strain diagrams have been observed in the literature from tests on FRP confined concrete cylinders (Lam and Teng 2003). Specimens with high confinement show a monotonically increasing bi-linear curve, whereas specimens with average or low confinement undergo a post-peak descending branch and reach their peak-strength prior to failure. For columns with average confinement the strength at rupture is higher than the unconfined strength of concrete and are considered as sufficiently confined columns. However, for specimens with low confinement the failure stress is lower than the unconfined concrete strength and are considered as insufficiently confined columns having low strength enhancement. Confinement efficiency also depends on the concrete strength and is less efficient for the columns poured with higher strength concrete (Li et al. 2005; Wu et al. 2009).

Based on the above definitions and considering the axial load-strain relationship of the retrofitted specimens in this study shown in Fig. 3.8, specimen *R1* can be classified as a moderately confined column undergoing a post-peak strain softening branch with failure stress in the concrete core higher than the unconfined concrete strength. Specimens *R2*, *R3* and *R4,* which show a monotonically ascending behavior in the nonlinear region, are categorized as highly confined specimens. It is postulated that the lower confinement in specimen *R1* is attributed to the lower lateral tensile strength of the Type I GFRP tube and the lack of shrinkage reducing agent in the concrete mix.

Fig. 3.9 shows the axial load versus the strain ratio relationships for the composite specimens. The strain ratio (v) is defined as the average lateral strain divided by the

absolute value of the average axial strain. An increase in the strain ratio indicates increased confinement. As shown in Fig. 3.9, the strain ratio increases slowly in the elastic range of the compressive behavior of the composite columns and it is approximately equal to the poison's ratio of the FRP tube material (ν_{la}=0.11). However, the strain ratio increases rapidly beyond the elastic range and continues to increase until failure. It was found to exceed unity in some of the composite columns indicating significant concrete confinement resulting in enhanced column compressive strength.

The confinement efficiency is highly dependent on the uniformity of confinement (Ozbakkaloglu and Oehlers 2008). Fig. 3.10 shows the distribution of lateral strains over the perimeter of the composite columns for selected axial strain levels. It can be observed that the distribution of lateral strains was relatively uniform. Confinement uniformity decreased at high levels of axial strain. It is postulated that this was a result of the cracking propagation in the concrete followed by local buckling of the steel column at high axial load levels.

3.3.4.6. Shrinkage Effects

The effect of concrete shrinkage can be evaluated by comparing the peak strength for the specimens *R1* and *R2* (3,197 kN and 3,821 kN, respectively), which were constructed using the same type of GFRP tube but with shrinkage reducing agent added to the concrete mix in specimen *R2*. Although the GFRP tube provides partial sealing to the concrete, shrinkage was found to reduce the compressive strength of the composite columns. Naguib and Mirmiran (2002) evaluated shrinkage strain of the concrete core in FRP tubes as 10%-20% of exposed concrete.

Shrinkage delays the confinement action as the concrete must attain higher volumetric dilation for the FRP tube to engage and apply lateral confinement. This can potentially deteriorate the enhancement in the load carrying capacity and ultimate displacement of the retrofitted columns. Harries and Carey (2003) investigated effect of delaying

confinement on the behavior of FRP confined concrete columns by introducing a gap between concrete and FRP tube and found it negligible on the overall efficiency of the FRP tube. However, this finding seems to be questionable by comparing the axial load-strain relationships of specimens *R1* and *R2*, which indicates the shrinkage reducing agent added to the concrete in specimen *R2* changed the confinement level from moderate to high. This resulted in approximately a 20% increase in compressive strength of the specimen and the confined concrete core (Table 3.3). Specimen *R2* was also found to have a 22% higher stiffness value compared to the other three specimens that were constructed using concrete without shrinkage reducing agent as a result of earlier initiation of confinement.

3.3.4.7. Failure Modes

Fig. 3.11 presents photographs of the failed test specimens. Failure of the steel specimens was typically initiated by steel yielding over the entire cross section followed by local buckling of the steel flanges and web as highlighted in Fig. 3.11(a), 3.11(b) and 3.11(c). Failure of the composite columns initiated by rupture of the GFRP tube followed by crushing and spalling of the concrete core. Failure ductility can be further improved by utilizing angular fiber jackets instead of unidirectional jackets; however, they are not as efficient as unidirectional jackets with circumferentially oriented fibers in terms of strength enhancement (Au and Buyukozturk 2005).

As previously evaluated from the recorded ultimate axial and lateral strains, the GFRP tube failed under lateral tension in specimens *R1* and *R2* and under axial compression in specimens *R3* and *R4*. Local buckling of the steel flanges and web was observed after removal of the GFRP tube in all the composite specimens.

3.4. Analytical Model

This section describes the development of an analytical model to predict the behavior of the proposed composite columns under axial load. The axial force, corresponding to a

level of axial strain, is estimated by superimposing the contribution of the steel, the confined concrete and the GFRP tube in carrying the load. σ_c in Eq. (3.1) is replaced by the axial stress acting over the confined concrete core (σ_{cc}). In this model, the steel is assumed to be elastic-plastic with strain hardening from the yield stress to the ultimate stress shown in Fig. 3.12(a). In this figure, ε_{sy} and ε_{su} are the yield and ultimate strain of the steel, respectively, and E_s is the elastic modulus. The GFRP tube is assumed to behave in a linear elastic manner both in the longitudinal and the circumferential directions. Fig. 3.12(b) shows the stress-strain relationship for the GFRP tube under uniaxial compression, where ε_t is the axial strain of the GFRP tube.

Steel-confined concrete models available in the literature overestimate the compressive capacity resulting in an unconservative design if applied to concrete confined by FRP, as they are unable to evaluate dilatancy of the confined concrete accurately (Mirmiran and Shahawy 1997). Consequently, a confinement model that is specifically developed for FRP confined concrete must be employed to accurately evaluate the load carrying capacity of the composite columns.

The confined concrete core was modelled using the constitutive relationship proposed by Lam and Teng (2003) for FRP-confined concrete shown in Fig. 3.12(c). The axial stress-strain relationship consists of a parabolic curve followed by a linear branch. The influence of confinement is assumed negligible in the parabolic segment. Nani and Bradford (1995) also noted negligible FRP confinement effect under stress conditions below f'_{co}. The proposed axial stress-strain model for the confined concrete is expressed as:

$$\sigma_{cc} = \begin{cases} E_c\varepsilon_{cc} - \dfrac{(E_c - E_2)^2}{4f'_{co}}\varepsilon_{cc}^2 & \left(0 \le \varepsilon_{cc} \le \varepsilon_{cc,t}\right) \\ f'_{co} + E_2\varepsilon_{cc} & \left(\varepsilon_{cc,t} \le \varepsilon_c \le \varepsilon_{au}\right) \end{cases} \tag{3.13}$$

where, ε_{cc} and E_c are the axial strain and the elastic modulus of the unconfined concrete, respectively, and E_2 is the slope of the linear branch. The transition axial strain at the intersection of the linear and parabolic branches, $\varepsilon_{cc,t}$, is given by:

$$\varepsilon_{cc,t} = \frac{2f'_{co}}{E_c - E_2} \tag{3.14}$$

E_2, can be calculated as:

$$E_2 = \frac{f'_{cc} - f'_{co}}{\varepsilon_{au}} \tag{3.15}$$

From Eq. (3.13), it can be seen that the two key parameters in establishing the stress-strain relationship of the confined concrete are the ultimate axial strain and the compressive strength (ε_{au} and f'_{cc}).

Lam and Teng (2003) demonstrated dependency of the ultimate axial strain of the confined concrete on the stiffness of the FRP and the lateral confining pressure and proposed the following expression to evaluate ε_{au}:

$$\frac{\varepsilon_{au}}{\varepsilon_{co}} = 1.75 + 12.0\left(\frac{f_l}{f'_{co}}\right)\left(\frac{\varepsilon_{lu}}{\varepsilon_{co}}\right)^{0.45} \tag{3.16}$$

where, ε_{co} is the axial strain corresponding to peak strength of the unconfined concrete, commonly taken as 0.002, and f_l is the lateral confining pressure. The above expression is calibrated against a large database of experimental tests on concrete cylinders confined by different types of FRP with various stiffness values (Lam and Teng 2003). In the composite columns tested in this study, ε_{au} can be estimated by substituting Eqs. (3.5) and (3.6) into (3.7) and using Eq. (3.16).

The lateral confining pressure can be evaluated considering the free body diagram of the GFRP tube shown in Fig. 3.13(a) at failure. Equilibrium of the GFRP tube requires that:

$$f_l = \frac{2\sigma_{lu,g}t}{d} \tag{3.17}$$

where, t and d are the wall thickness and the inner diameter of the tube, respectively. Utilizing the proposed composite system in retrofit applications by bonding split FRP tubes shown in Fig. 3.2(b), requires minimum shear strength of the bond between the epoxy glue and the GFRP tube to ensure f_l evaluated above can be achieved. The minimum required shear strength of the bond between the epoxy and the GRFP tube can be estimated considering the free body diagram of the split GFRP tube shown in Fig. 3.13(b) at failure by:

$$\tau_b = f_l = \frac{2\sigma_{lu,g}t}{d} \tag{3.18}$$

where, τ_b is the shear stress in the bond between the epoxy and the GFRP tube at failure. Therefore, the shear strength of the epoxy-GFRP bond should be greater than τ_b.

The compressive strength of the confined concrete is expressed as a function of the lateral confining pressure using the following relationship (Lam and Teng 2003):

$$f_{cc}^{'} = f_{co}^{'} + 3.3f_l \tag{3.19}$$

3.5. Comparison of Analytical and Experimental Results

Results from the analytical model are presented in Table 3.5 in terms of various parameters including the compressive strength, elastic axial stiffness and ultimate axial strain of the composite specimens. Ratios of the analytically evaluated parameters to their corresponding experimental values are also shown in Table 3.5. It can be observed that

the analytical model predictions are in good agreement with experimentally obtained values for the presented parameters. Analytical predictions are more accurate for specimens *R1*, *R3* and *R4* (error of less than approximately 10% for the evaluated parameters) compared to the specimen *R2*, as shrinkage effects are not considered in the current model.

The overall axial load-axial strain relationship for the four composite specimens generated based on the developed analytical model are shown in Fig. 3.14 with the experimental results for comparison. As can be observed, the analytical predictions are generally in good agreement with the experimental results, particularly in the linear range. Deviation of the analytical predictions from the experimental data over the inelastic range for specimens *R1* and *R2* can be attributed to the assumed stress-strain relationship with a strain-hardening behavior for concrete in the analytical model (specimen *R1* showed strain softening behavior) and the incapability of the model of accommodating shrinkage effects in specimen *R2*. Although some discrepancy exists between the experimental and predicted relationships for specimens *R3* and *R4* over the inelastic range in Fig. 3.14, the analytical model satisfactorily estimates the elastic and overall inelastic stiffness, ultimate axial strain and peak strength values.

3.6. Conclusions

A new type of composite column consisting of steel, concrete and FRP was introduced and tested under compressive loading. The proposed composite systems can be utilized in new construction or retrofit applications to increase the load carrying capacity, axial stiffness and energy dissipation capacity of existing steel columns. Seven stub columns were tested in the experimental program, three were steel column control specimens and the remaining four were composite specimens. To construct the composite specimens, the GFRP tube was placed around the steel section and the void between the steel section and the GFRP tube was filled with concrete. In the proposed composite columns, the GFRP

tube serves as the formwork, provides confinement and enhances the concrete and steel durability.

Two different types of GFRP tubes, having different mechanical properties, were used in construction of the composite specimen. In addition, concrete mixes with similar compressive strength were used with and without an additional shrinkage reducing agent. Experimental results showed a 40%-80% increase in the compressive strength of the concrete in the composite specimens. The composite specimens exhibited axial failure strains of approximately 2 times those of the steel columns. The significant increase in compressive strength and failure axial strain of the composite columns compared to the steel columns indicates the enhanced energy dissipation capacity of the retrofitted steel columns. It was also shown that confinement and composite action do not significantly affect the axial stiffness of the retrofitted columns in the elastic range. The increased axial stiffness of such columns is primarily due to the elastic stiffness of the added materials. Composite columns constructed using Type II GFRP tube (with higher lateral tensile strength and lower rupture lateral strain) attained approximately 25% and 20% higher compressive strength and ultimate axial strain, respectively, compared to the columns retrofitted with Type I GFRP tube. Adding the shrinkage reducing agent to the concrete mix resulted in 20% increase in the compressive strength, 22% increase in the elastic axial stiffness and 24% increase in the ultimate axial strain of the composite columns.

Evaluating strain ratios at mid-height of the composite specimens indicated minor confinement effect in the elastic range up to an axial strain level of approximately 0.002. The strain ratio increased rapidly afterwards indicating significant confinement in the inelastic stage.

Failure of the steel columns occurred due to yielding followed by local buckling of the flanges and web. Failure of the composite specimens occurred due to rupture of the GFRP

tube under lateral tension (Type I GFRP tube) or axial compression (Type II GFRP tube) followed by crushing and spalling of the concrete.

An analytical model was developed to predict the axial behavior of the composite columns. Analytical predictions were generally in good agreement with the experimental results. As the current model does not account for concrete shrinkage, it underestimated the axial stress of the specimens constructed with the concrete mix containing shrinkage reducing agent, over the inelastic branch.

Appendix 3.1. Notation

A_c = cross sectional area of the concrete;

A_s = cross sectional area of the steel;

A_t = cross sectional area of the GFRP tube;

C.A.I. = composite action index;

C.R. = confinement ratio;

D.I. = ductility index;

d = inside diameter of the GFRP tube;

ε_{au} = ultimate axial strain;

$\varepsilon_{a,85\%}$ = post failure axial strain at the point where the strength of the column degrades to 85% of the ultimate load;

ε_{co} = axial strain corresponding to peak strength of the unconfined concrete;

ε_{cc} = axial strain of the confined concrete;

$\varepsilon_{cc,t}$ = The transition axial strain at the intersection of the linear and parabolic branches in axial stress-strain relationship of the confined concrete;

ε_{lu} = ultimate lateral strain;

ε_{sy} = yield strain of the steel;

ε_{su} = ultimate strain of the steel;

ε_g = axial strain of the GFRP tube;

ε_y = yield strain of the steel;

$E_{a,g}$ = axial compressive modulus of the GFRP tube;

E_c = elastic modulus of the unconfined concrete;

E_2 = slope of the linear branch in the axial stress-strain relationship of the confined concrete;

$E_{l,g}$ = lateral tensile modulus of the GFRP tube;

f'_{co} = compressive strength of unconfined concrete;

f'_{cc} = compressive strength of confined concrete;

f_l = lateral confining pressure;

f_y = yield strength of the steel;

f_{su} = ultimate strength of the steel;

v_{la} = Poisson's ratio of the GFRP tube when the load is applied in the axial direction and contraction occurs in the lateral direction;

v_{al} = Poisson's ratio of the GFRP tube when the load is applied in the lateral direction and contraction occurs in the axial direction;

P_u = compressive strength;

$\sigma_{a,c}$ = axial stress in the unconfined concrete;

$\sigma_{a,g}$ = axial stress in the GFRP tube;

$\sigma_{au,g}$ = axial stress in the GFRP tube at failure;

$\sigma_{a,s}$ = axial stress in the steel;

σ_{cc} = compressive axial stress in the confined concrete core;

$\sigma_{lu,g}$ = lateral stress in the GFRP tube at failure;

$S_{a,c}$ = axial compressive strength of the GFRP tube;

$S_{a,t}$ = axial tensile strength of the GFRP tube;

$S_{l,c}$ = lateral compressive strength of the GFRP tube;

$S_{l,t}$ = lateral tensile strength of the GFRP tube;

t = thickness of the GFRP tube;

τ_b = shear stress in the bond between the epoxy and the GFRP tube at failure;

Appendix 3.2. References

Au C, and Buyukozturk O. Effect of fiber orientation and ply mix on fiber reinforced polymer-confined concrete. J. Compos. Constr. 2005, 9(5): 397-407.

Bank, L. C. (2006). "Composites for construction." John Wiley & Sons, Hoboken, New Jersey.

CSA. (2009). "Limit states design of steel structures. Standard CAN/ CSA S16-09." Canadian Standards Association, Mississauga, Ont.

Daniel, I. M., and Ishai, O. (2006). "Engineering mechanics of composite materials." 2nd ed. Oxford University Press: New York, NY.

Giakoumelis, G., and Lam, D. (2004). "Axial capacity of circular concrete-filled tube columns." *J. Constr. Steel Res.*, 60(7):1049–1068.

Han, L. H., and Yao, G. H. (2004). "Experimental behaviour of thin-walled hollow structural steel (HSS) columns filled with self-consolidating concrete (SCC)." *J. Thin Walled Struct.*, 42(9):1357–1377.

Han, L. H., Yao, G. H., and Zhao, X. L. (2005). "Tests and calculations for hollow structural steel (HSS) stub columns filled with self-consolidating concrete (SCC)." *J. of Constr. Steel Res.*, 61(9):1241–1169.

Harries KA, and Carey SA. Shape and gap effects on the behavior of variably confined concrete. J. Cement and Concr. Res. 2003, 33: 881–890.

Johansson, M., and Gylltoft, K. (2002). "Mechanical behavior of circular steel–concrete composite stub columns." *J. of Struct. Eng.*, 128(8):1073–1081.

Karimi. K, Tait, M. J., and El-Dakhakhni, W. W. (2009). "A Novel retrofit technique for strengthening steel columns using FRP." *Proceedings of CSCE 2009 Annual General Conference*, St. John's, Canada.

Karimi, K., El-Dakhakhni, W. W., and Tait, M. J. "Performance enhancement of steel columns using concrete-filled composite jackets." *J. Perform. Constr. Facil.*, doi:10.1061/(ASCE)CF.1943-5509.0000162.

Kilpatrick, A. E., and Rangan, B. V. (1997). "Tests on high-strength composite concrete columns. Research Report No. 1/97, School of Civil Engineering, Curtin University of Technology, Perth, Western Australia.

Lam, L., and Teng, J. G. (2003). "Design-oriented stress-strain models for FRP-confined concrete." *J. Constr. and Build. Mat.*, 17: 471-489.

Li, G., Torres, S., Alaywan, W., and Abadie, C. (2005). "Experimental study of FRP tube-encased concrete columns." *J. Compos. Mat.*, 39(13): 1131-1145.

Liu, X., Nanni, A., and Silva, P. F. (2005). "Rehabilitation of compression steel members using FRP pipes filled with non-expansive and expansive light-weight concrete." *J. Adv. in Struct. Eng.*, 8(2): 129-142.

Mirmiran A, and Shahawy M. Behavior of concrete columns confined by fiber composites. J. Struct. Eng. 1997, 123(5): 583–590.

Moore, W. P. (1987). "keynote address: An overview of composite construction in the United States; Composite construction in steel and concrete." *Proceedings of An Engineering Foundation Conference*, ASCE, Henniker, New Hampshire.

Naguib W, and Mirmiran A. Time-dependent behavior of FRP-confined concrete columns: experiments and modeling. ACI Struct. J. 2002, 99(2): 142–148.

Nanni A, and Bradford NM. FRP jacketed concrete under uniaxial compression." J. Constr. and Build. Mat. 1995, 9(2): 115-124.

Ozbakkaloglu, T., and Oehlers, D. J. (2008). "Manufacture and testing of a novel FRP tube confinement system." *J. Eng. Struct.*, 30: 2448–2459.

Popovics, S. (1973). "A numerical approach to the complete stress-strain curves for concrete." *J. Cement and Concr. Res.*, 3(5): 583-599.

Sakina, K., Nakahara, H., Morino, S., and Nishiyama, I. (2004). "Behavior of centrally loaded concrete-filled steel-tube short columns." *J. of Struct. Eng.*, 130(2):180–188.

Schneider, S. P. (1998). "Axially loaded concrete-filled steel tubes." *J. of Struct. Eng.*, 124(10): 1125-1138.

Tao, Z., and Han, L. H. (2006). "Behaviour of concrete-filled double skin rectangular steel tubular beam-columns." *J. Constr. Steel Res.*, 62: 631-646.

Teng, J. G., Yu, T., Wong, Y. L., and Dong, S. L. (2007). "Hybrid FRP-concrete-steel tubular columns: concept and behavior." *J. Constr. Build. Mater.*, 21: 846-854.

Uy, B. (2001). "Local and post-local buckling of fabricated steel and composite cross sections." *ASCE J. Struct. Eng.*, 127(6): 666-677.

Wang, Q., Zhao, D., and Guan, P. (2004). "Experimental study on the strength and ductility of steel tubular columns filled with steel-reinforced concrete." *J. Eng. Struct.*, 26, 907-915.

Woods, J. M., Kiousis, P. D., Ehsani, M. R., Saadatmanesh, H., and Fritz, W. (2007). "Bending ductility of rectangular high strength concrete columns." *J. Eng. Struct.*, 29, 1783-1790.

Wu, H., and Xiao, Y. (2000). "Compressive stress–strain behavior of concrete confined by carbon fiber jackets." *Proceedings of the 6th ASCCS conference*, Los Angeles, USA: 919–926.

Wu, H. L., Wang, Y. F., Yu, L., and Li, X. R. (2009). "Experimental and computational studies on high-strength concrete circular columns confined by aramid fiber-reinforced polymer sheets." *J. Compos. for Constr.*, 13(2): 125-134.

Yang, H., Lam, D., and Gardner, L. (2008). "Testing and analysis of concrete-filled elliptical hollow sections." *J. Eng. Struct.*, 30(12): 3771-3781.

Young, B., and Ellobody, E. (2006). "Experimental investigation of concrete-filled cold-formed high strength steel tube columns." *J. Constr. Steel Res.*, 62: 484-492.

Yu, Z. W., Ding, F. X., and Caib, C. S. (2007). "Experimental behavior of circular concrete-filled steel tube stub columns." *J. Constr. Steel Res.*, 63: 165-174.

Zhong, S. (1988). "The development of concrete filled tubular structures in China." *Proceedings of the Int. Conf. on Concrete Filled Steel Tubular Structures*, China.

Zhou, F., and Young, B. (2008). "Test of concrete-filled aluminum stub columns." *J. Thin Walled Struct.*, 46: 573-583.

Table 3.1. Dimensions and material properties of the GFRP tubes

			Type I	Type II
Inside Diameter		(mm)	211	211
Outside Diameter		(mm)	219	220
Structural Wall Thickness		(mm)	3.2	3.6
Lateral Tensile Strength		(MPa)	275	342
Lateral Tensile Modulus		(GPa)	15.9	29
Axial Compressive Strength		(MPa)	138	171
Axial Tensile Strength		(MPa)	138	161
Axial Compressive Modulus		(GPa)	10.3	18.5
Axial Tensile Modulus		(GPa)	10.3	18.5
Poisson's Ratio[(a)]	ν_{la}	---	0.11	0.11
	ν_{al}	---	0.19	0.19

[(a)] The first subscript denotes the contraction direction and the second subscript denotes direction of the applied force. "*a*" and "*l*" denotes axial and lateral direction, respectively.

Table 3.2. Test matrix

Test No.	Specimen ID	Type of the GFRP Tube	Shrinkage Reducing Agent
1	C1	N/A	N/A
2	C2	N/A	N/A
3	C3	N/A	N/A
4	R1-I	I	No
5	R2-I-S	I	Yes
6	R3-II	II	No
7	R4-II	II	No

Table 3.3. Experimental results

Specimen ID	P_u		Elastic Axial Stiffness		ε_{au}		$\sigma_{au,t}$	ε_{lu}	$\sigma_{lu,t}$	f'_{cc}	
	(kN)	Increase (Ratio)	(kN/ mm)	Increase (Ratio)	(micro strain)	Increase (Ratio)	(MPa)	(micro strain)	(MPa)	(MPa)	f'_{cc}/f'_{co}
C1	726	N/A	753	N/A	4,000	N/A	N/A	N/A	N/A	N/A	N/A
C2	719	N/A	725	N/A	5,700	N/A	N/A	N/A	N/A	N/A	N/A
C3	726	N/A	723	N/A	5,500	N/A	N/A	N/A	N/A	N/A	N/A
R1-I	3,197	4.42	2,647	3.61	9,400	1.85	74.7	12,000	178.6	70.6	1.46
R2-I-S	3,821	5.28	3,244	4.42	11,700	2.31	100.5	11,400	163.5	86.7	1.80
R3-II	3,995	5.51	2,668	3.64	11,100	2.19	182.2	7,600	188.6	85.1	1.76
R4-II	4,093	5.65	2,607	3.55	11,300	2.23	177.4	10,100	261.5	88.4	1.83

Table 3.4. Evaluated enhancement factors for the tested specimens

	C.A.I	C.R.	D.I.
Avg. (C1,C2,C3)	---	---	2.53
R1-I	1.32	0.30	4.70
R2-I-S	1.55	0.28	5.85
R3-II	1.53	0.36	5.55
R4-II	1.58	0.50	5.65

Table 3.5. Predicted values in comparison with the experimental results

Specimen ID	P_u		Elastic Axial Stiffness		ε_{au}		$\sigma_{au,Tube}$		ε_{lu}		$\sigma_{lu,Tube}$		f'_{cc}	
	(kN)	Analy. /Exp.	(kN/ mm)	Analy. /Exp.	(micro strain)	Analy. /Exp.	(MPa)	Analy. /Exp.	(micro strain)	Analy. /Exp.	(MPa)	Analy. /Exp.	(MPa)	Analy. /Exp.
R1-I	3,229	1.01	2,354	0.89	9,279	0.99	74.3	0.99	11,690	0.97	173.3	0.97	65.6	0.93
R2-I-S		0.84		0.75		0.79		0.74		1.03		1.06		0.76
R3-II	3,859	0.96	2,428	0.91	10,688	0.96	171	0.94	8,600	1.13	219.9	1.16	73.1	0.86
R4-II		0.94		0.93		0.95		0.96		0.85		0.84		0.83

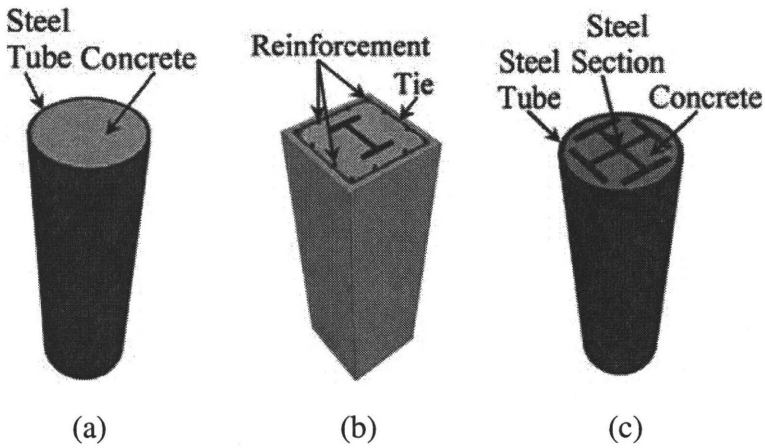

Figure 3.1. (a) CFST column (b) concrete-encased steel column (c) steel tubular column filled with steel reinforced concrete

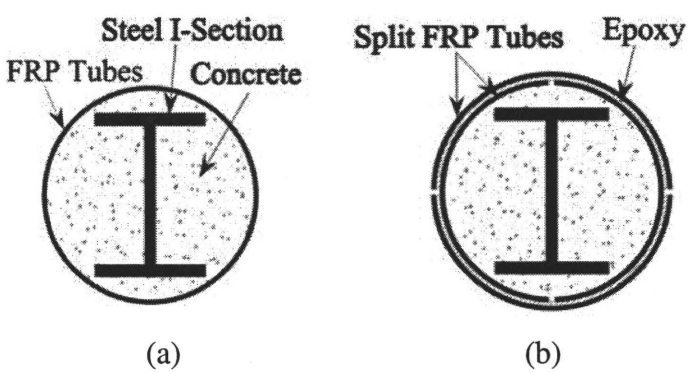

Figure 3.2. Proposed composite system (a) new construction (b) retrofit of existing steel columns

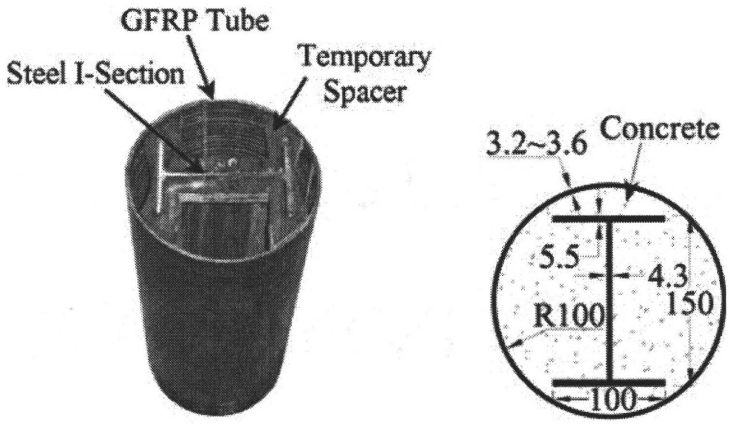

Figure 3.3. (a) Photograph of the composite specimen before pouring concrete (b) dimensions of the composite cross section

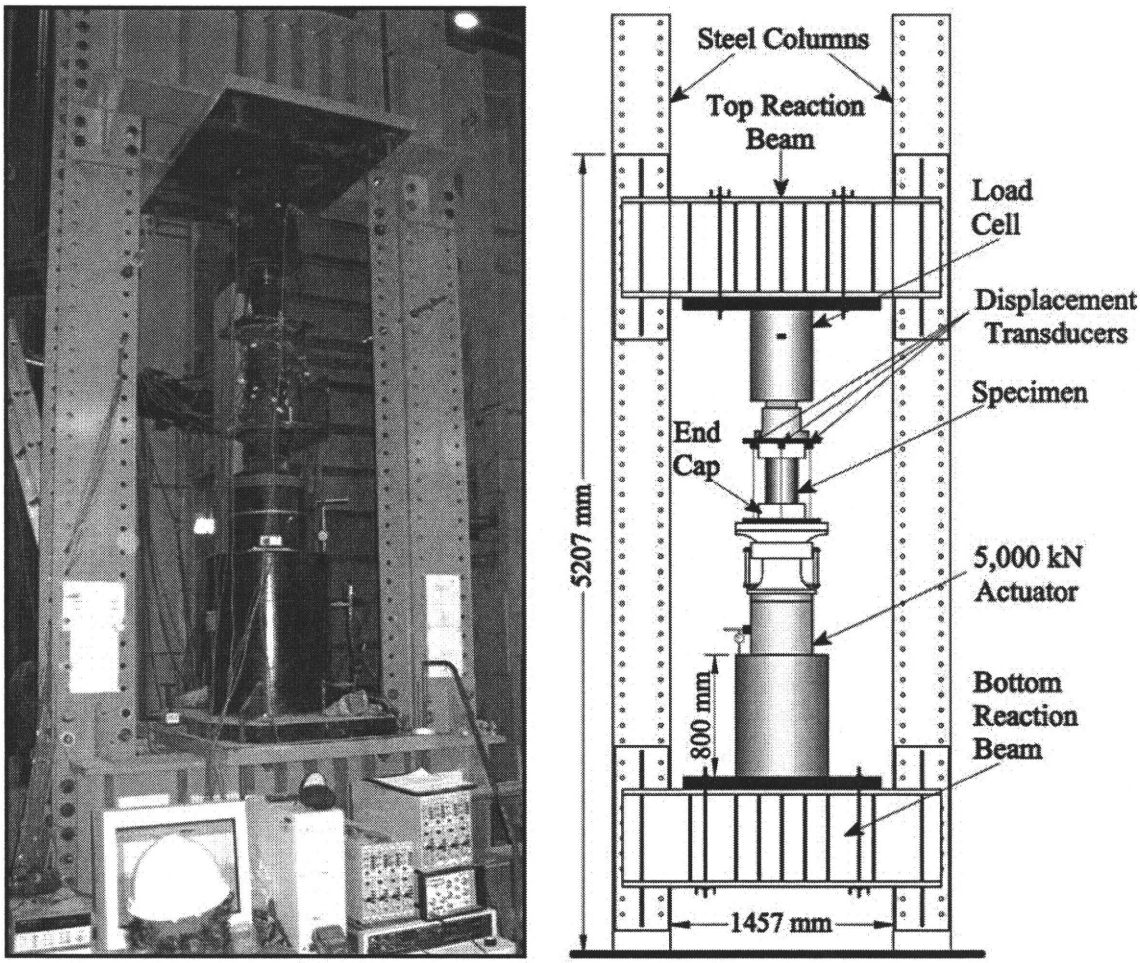

(a) (b)

Figure 3.4. Test setup (a) photograph (b) schematic view

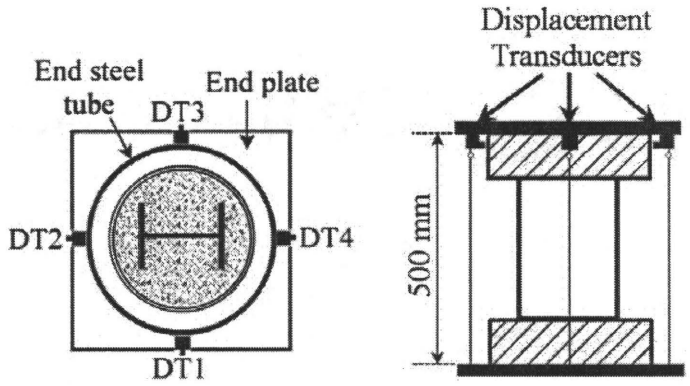

(i) Plan view (ii) Elevation view

(a) Displacement transducers (DT) over the full height

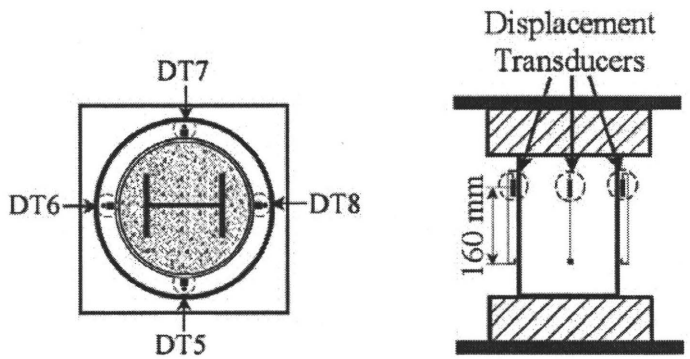

(i) Plan view (ii) Elevation view

(b) Displacement transducers (DT) in the mid-height region

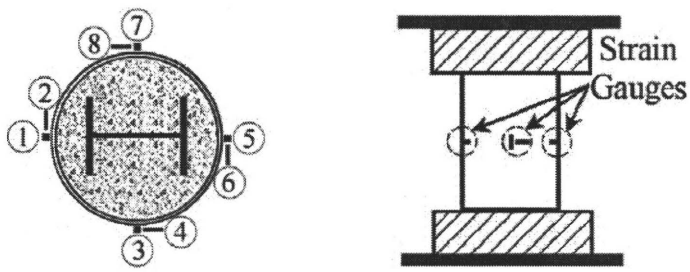

(i) Plan view (ii) Elevation view

(c) Strain gauges (SG) at mid-height

Figure 3.5. Instrumentation layout

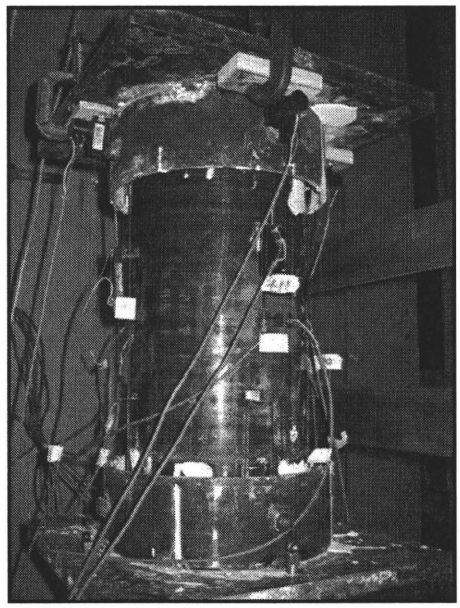

Figure 3.6. Photograph of a gauged specimen

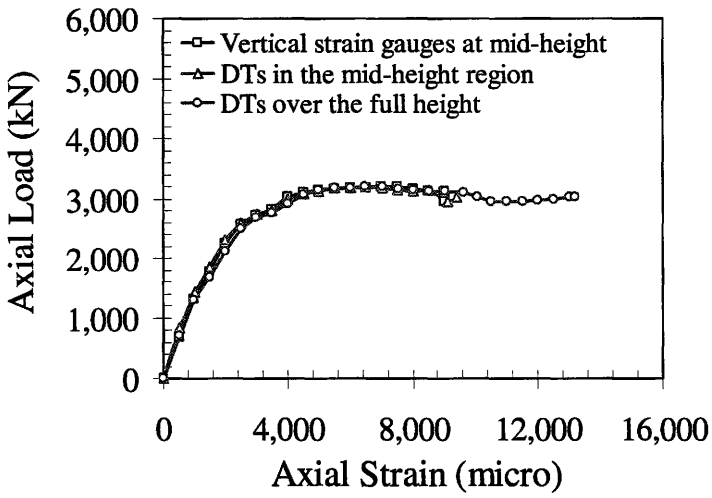

(a) R1-I

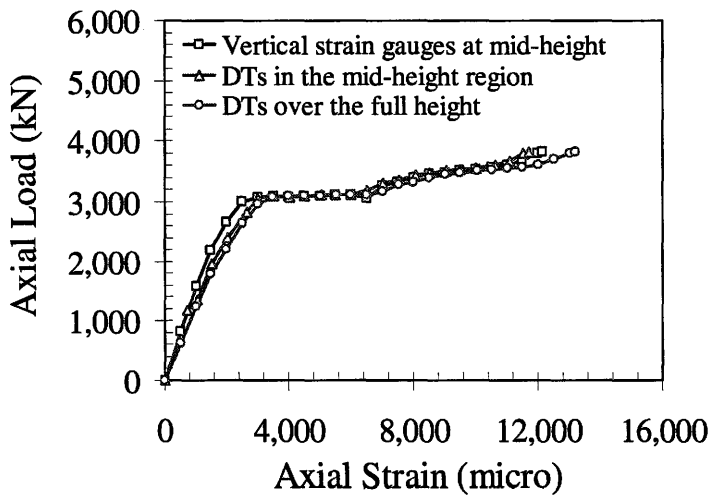

(a) R2-I-S

Figure 3.7. Comparison of axial load versus axial strain relationships obtained from the strain gauge readings at mid-height, displacement transducer readings in the mid-height region and displacement transducer readings over the full height of the specimens

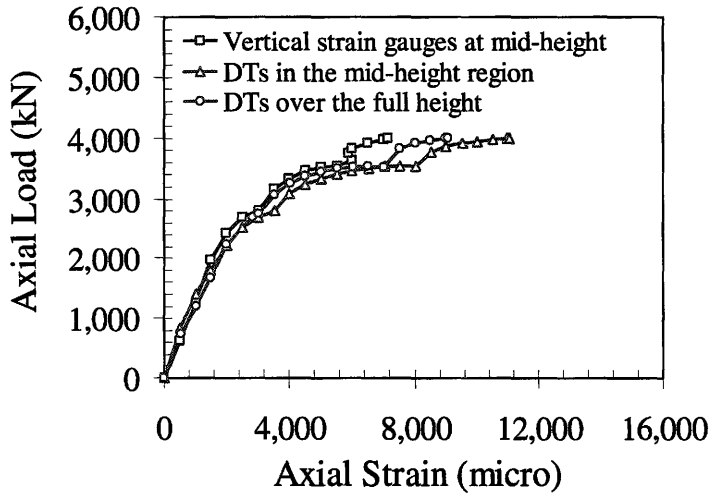

(b) R3-II

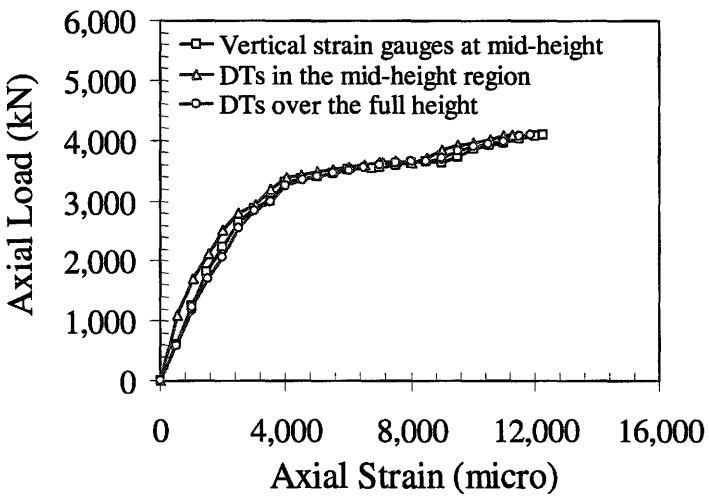

(b) R4-II

Figure 3.7. Continued

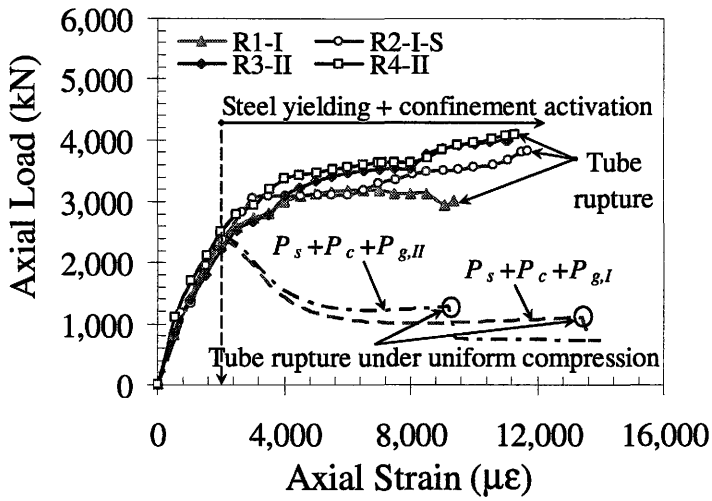

Figure 3.8. Axial load versus axial strain diagrams based on displacement transducer readings in the mid-height region over 160mm gauge length

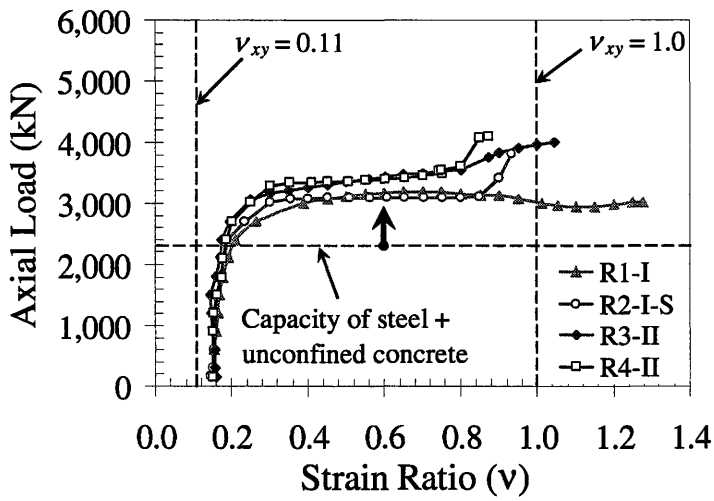

Figure 3.9. Comparison of axial load versus strain ratio diagrams

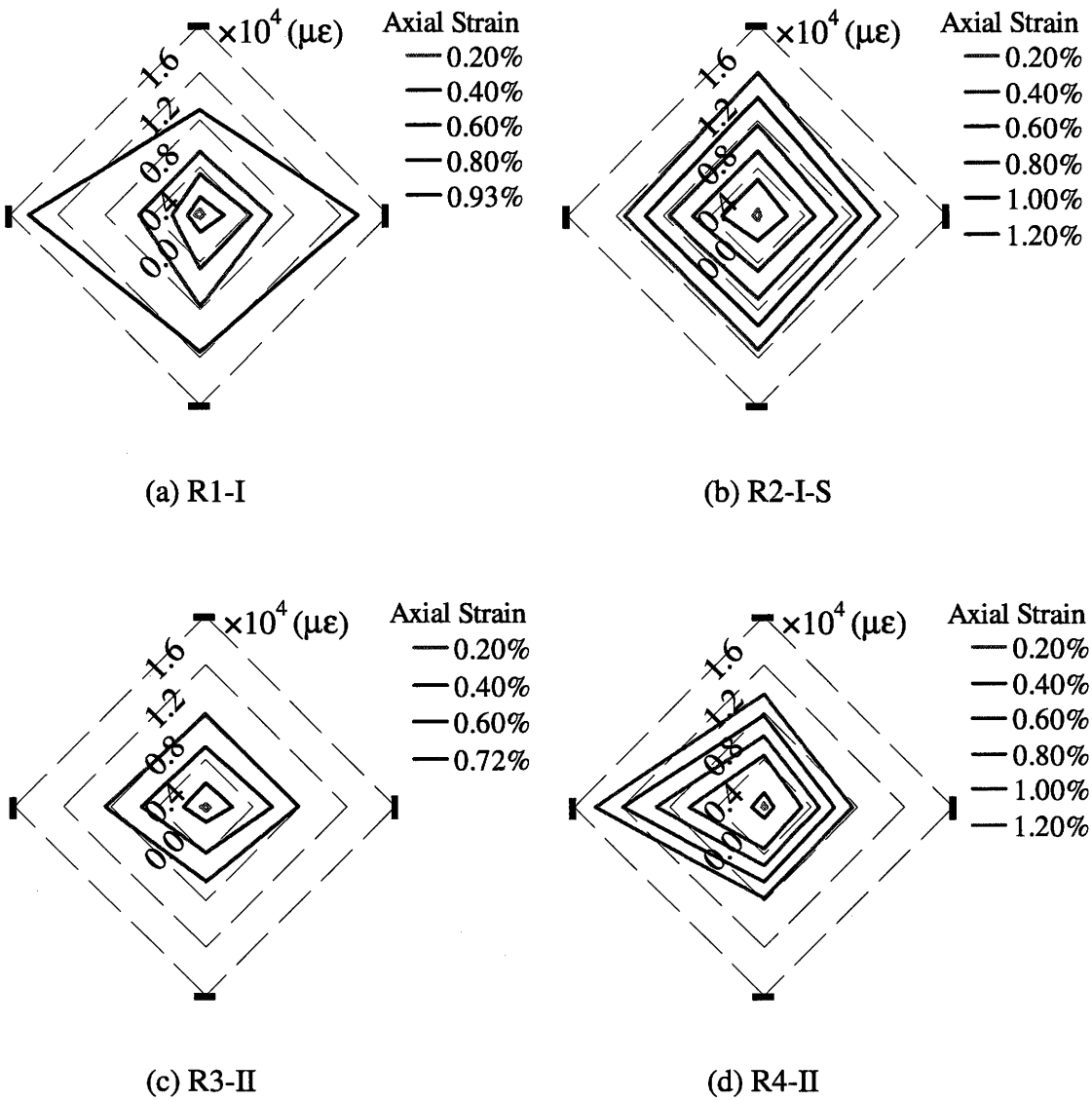

(a) R1-I (b) R2-I-S

(c) R3-II (d) R4-II

Figure 3.10. Distribution of lateral strains for selected axial strain levels

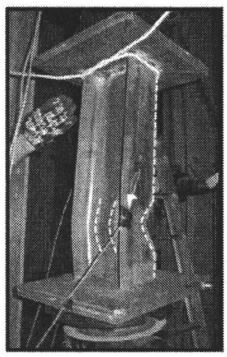

(a) C1

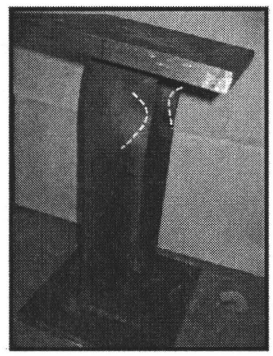

(b) C2

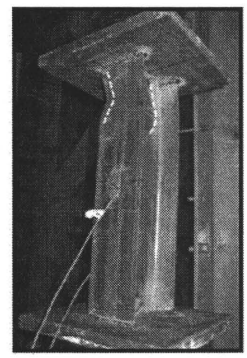

(c) C3

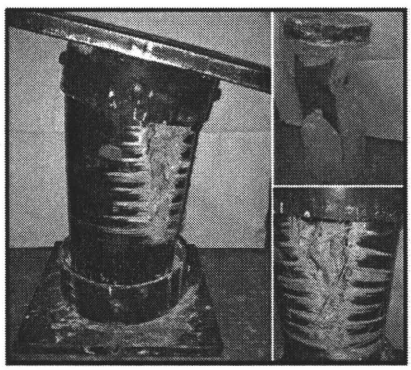

(d) R1-I

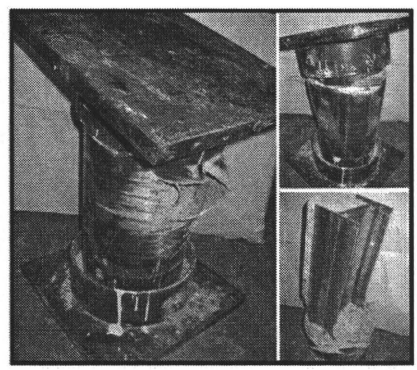

(e) R2-I-S

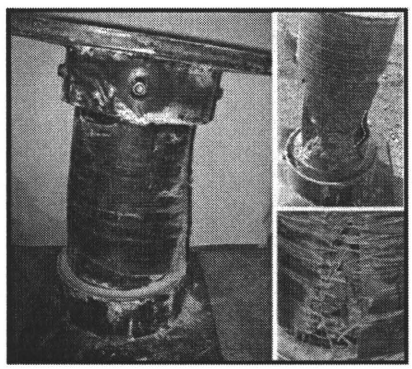

(f) R3-II

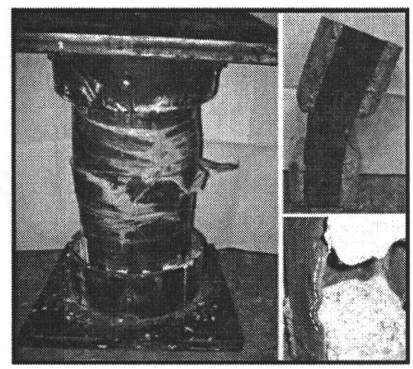

(e) R4-II

Figure 3.11. Photographs of the tested specimens after failure

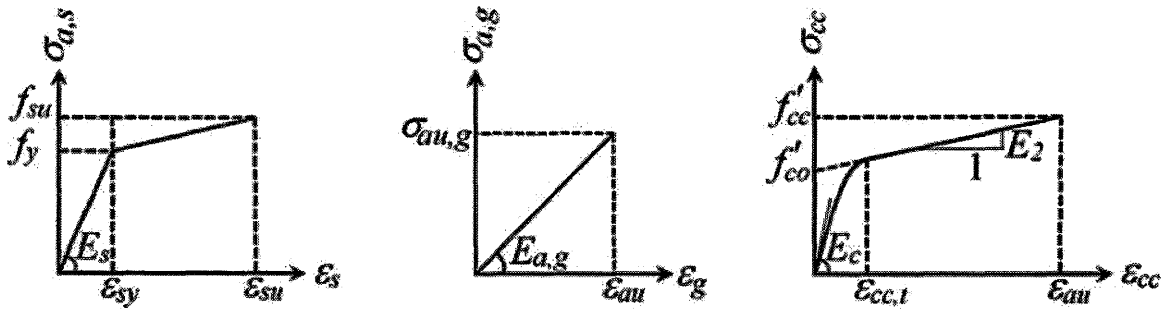

Figure 3.12. The stress-strain relationship for (a) steel (b) GFRP tube (c) confined concrete under axial compression

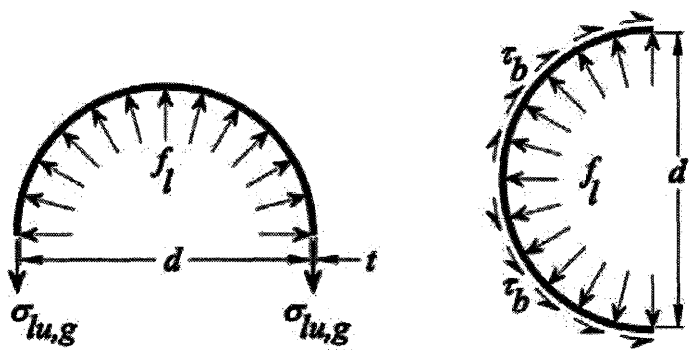

Figure 3.13. Free body diagram of the GFRP tube (a) continuous and split tubes (b) split tubes in retrofit applications

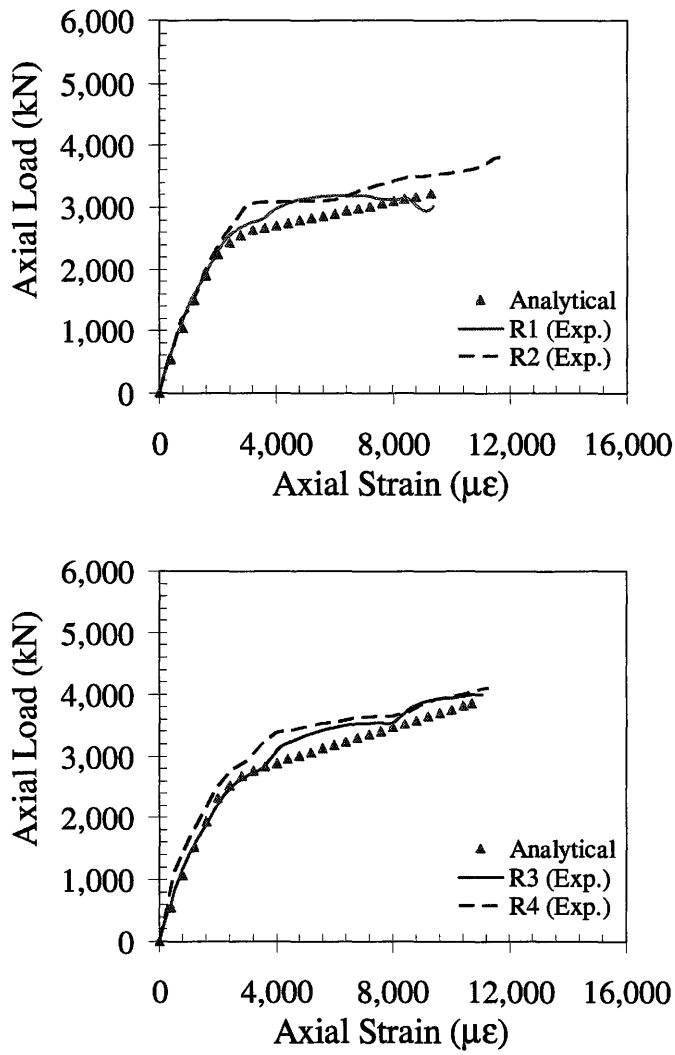

Figure 3.14. Comparison of the analytical model and experimental axial load-strain results

Chapter 4: Slenderness Effects on the Behavior of Steel-Concrete Composite Columns Wrapped with FRP Jackets

4.1. Summary

This paper studies the influence of slenderness ratio on the behavior of steel-concrete composite columns encased in Fiber Reinforced Polymer (FRP) jackets. The composite columns are composed of steel I-sections that are partially-encased by concrete and fully-wrapped with epoxy-saturated glass and carbon FRP (GFRP and CFRP) sheets. A total of nine specimens where tested with different slenderness ratios and heights ranging between 500 mm and 3,000 mm. The confining pressure provided by the FRP jacket and the composite action between the constituent materials resulted in enhanced compressive behavior of the composite columns. The compressive strength, elastic axial stiffness and energy dissipation capacity of the composite columns increased by a ratio of up to 5.2, 2.5 and 14.0, respectively, compared to that of the bare steel columns of equivalent length. A buckling strength relationship was developed for the composite columns based on the experimental results, which can be used to predict the load carrying capacity in design of such columns.

Keywords: buckling, confinement, composite columns, fiber reinforced polymer (FRP), retrofitting, slenderness ratio, steel columns, sheets

4.2. Introduction

Composite steel columns are compression members in which steel interacts with other construction materials such as concrete in carrying the applied load (Oehlers and Bradford 1995). The combination of steel and concrete provides an ideal composite section as the concrete is the most economical material in providing compression and steel provides significant tension capacity and results in lightweight and rapid construction (Mursi and Uy 2004). The high load carrying capacity of composite columns, with their light weight and enhanced deformability, has resulted in their adoption in bridges, offshore structures and high-rise buildings, particularly in regions of high seismic risk (Kilpatrick and Rangan 1997; Tao and Han 2006).

With the introduction of Fiber Reinforced Polymers (FRP) in civil engineering, new types of composite columns have been introduced and investigated. FRP materials have been effectively applied in retrofitting concrete columns due to their high strength-to-weight ratio, durability and ease of application (Mirmiran and Shahawy 1997; Saafi and Toutanji 1999; ISIS 2001; Pessiki et al. 2001). FRP wrapping enhances the strength and ductility of reinforced concrete (RC) columns by providing passive confinement. Despite the higher cost of FRP compared to other conventional constructional materials, its superior properties have made it an economical alternative for several structural applications. Furthermore, the reduction in manufacturing cost of the FRP during the past few decades has led to the significant growth in use of these materials in transportation infrastructure (Bakis et al. 2002).

Currently, a significant portion of the steel bridge stock in the United States and Canada are structurally deficient due to corrosion, aging and increasing traffic volume (AASHTO 2001). Recently, FRP has been extensively utilized in strengthening metallic bridges such as Tickford Bridge and Hythe Brdige in United Kingdom (CIRIA 2004). FRP composites have also been combined with conventional construction materials in hybrid structural members to achieve superior structural performance (Teng et al. 2007). In composite

columns, FRP is mainly utilized in providing confinement to the concrete. Confinement efficiency depends on the shape of the cross section. More efficient confinement is developed in circular columns compared to columns with square or rectangular cross sections. In rectangular sections, confinement is not uniform and may develop through arching action within four parabolic areas while the column central core remains unconfined (Mirmiran et al. 1998; Lam and Teng 2003a). Although confinement efficiency is lower in rectangular columns compared to circular columns, experimental studies have shown that failure of most FRP confined short rectangular columns occurred due to FRP rupture, indicating effective confinement (Rochette and Labossiere 2000).

In confined composite columns, confinement efficiency is severely reduced with increased slenderness as the failure mode changes from strength (cross sectional) to stability loss. Although a substantial amount of research on confinement effects in short RC columns has been reported in the literature, few studies have investigated the effects of slenderness ratio on the behavior of confined composite columns. Mirmiran et al. (2001) investigated the behavior of concrete-filled FRP tubes with various slenderness ratios and found that the strength and ductility of the columns decreased with increased slenderness, however, a greater reduction in ductility was found to occur. Pan et al. (2007) also studied the effect of slenderness on the behavior of FRP-wrapped reinforced concrete columns and found that strengthening effects were considerably reduced by an increase in the slenderness ratio.

The current study aims at investigating the behavior of a rectangular steel-concrete composite column wrapped with FRP sheets (shown in Fig. 4.1) through a set of experimental tests on columns with various slenderness ratios. In the proposed composite column, the steel provides ductility and shear resistance whereas the concrete enhances local and overall buckling capacity of the steel column and provides additional compressive strength. In addition, the FRP jacket replaces the transverse steel reinforcement required in conventional concrete-encased steel columns and provides

confinement to the concrete in addition to protecting the steel and concrete from environmental deterioration. The FRP jacket also participates in developing the composite action between the steel and concrete by holding the two materials together and resisting outward local buckling of steel flanges.

The use of the proposed composite columns in the construction of high-rise buildings could result in smaller columns cross sections compared to traditional RC columns due to their enhanced compressive strength. The composite system proposed in this study may also be applied as a retrofit technique in strengthening existing steel columns, piles and bridge piers.

4.3. Experimental Program

A total of nine column specimens were tested in the experimental program. Six specimens were composite columns and three specimens were bare steel columns, which were tested for comparison purposes and to quantify the effects of utilizing the composite system as a retrofit technique. A W150×14 (CISC 2008) compact section was chosen for the steel columns to ensure yielding of the entire cross section prior to the onset of local buckling (CSA 2009).

The following steps summarize the construction procedure of the composite column specimens: 1) The steel surface was cleaned using a wire brush and acetone; 2) formwork was placed around the longer sides of the columns and the voids were filled with concrete; 3) formwork was removed after the concrete set and the specimens were cured for a minimum of 28 days prior to FRP jacketing; 4) FRP sheets were cut to appropriate sizes; 5) a two component epoxy was uniformly blended by a ratio of 100:42 using a low speed mixer at 400-600 RPM 6) FRP sheets were fully saturated in the epoxy matrix; 7) the specimens were wrapped with one layer of saturated GFRP sheet followed by two additional CFRP wraps; 8) an overlap of 200 mm was provided in the FRP jacket to prevent any premature failure due to debonding of the FRP warps; 9) the specimens were

cured for an additional minimum 48 hours prior to testing. Figure 4.2 shows photographs of the composite specimens during construction.

4.3.1. Material Properties

The GFRP and CFRP sheets utilized in construction of the composite columns were uni-directional fabrics made of glass and carbon fibers, respectively. Material properties of the FRP composite laminate and the epoxy are presented in Table 4.1. The average compressive strength of concrete at the time of testing was 48.3 MPa and the average yield strength of steel was 411 MPa.

4.3.2. Test Matrix

The test matrix is presented in Table 4.2 where each specimen is assigned a designation consisting of a letter and a number. The letters "C" and "R" denotes control (bare steel column specimens) and composite specimens, respectively, followed by the height, H, of the specimens in meters.

4.3.3. Test Setup

The specimens were tested under axial loading using a compression test setup shown in Fig. 4.3. The setup was a self-reacting steel frame consisting of two steel columns and four girders which were bolted to the column at the top and bottom of the setup. The load was applied to the specimens using a 5,000 kN actuator under displacement control at a rate of 0.1 mm/min. A load cell with similar capacity attached to the top girders was used to measure the applied load. The specimen was placed between the actuator and the load cell. The top girders were unbolted and moved accordingly for each test to accommodate the appropriate height of the specimen. The boundary conditions were simulated as pin-pin by using swivels at the top and bottom of specimens (See Fig. 4.3(a)).

4.3.4. Instrumentation

Axial deformation of the specimens over their full height was measured by four displacement transducers (DT) mounted between the specimen ends. Lateral deformation of the columns was measured using additional horizontal DTs at equally-spaced locations along the column height for both weak and strong axis bending. Axial deformation was also measured closer to the columns mid-height over a gauge length of equal to half of the column height. Strain gauges were mounted on the FRP jacket at mid-height and quarter-height from the top of the specimen in longitudinal and transverse directions to measure axial and lateral strains, respectively. Figure 4.4 shows the instrumentation layout.

4.3.5. Load Transfer Mechanism

Axial loading was applied to the specimen through thick steel plates and the specimens were capped to ensure uniform loading over the entire cross section. Figure 4.5 shows method of capping the specimen ends. The steel I-section was in direct contact with the end plates and the small gap between the concrete and the plate were filled with hydrostone. Special care was taken in placing the specimens concentrically with respect to the loading axis by aligning a dowel attached to the specimen end with a hole at the steel plate center.

4.3.6. Experimental Results

Experimental results are discussed in terms of the axial load-deformation characteristics, energy dissipation capacity, confinement evaluation, lateral deflections, buckling strength relationship and failure modes.

4.3.6.1. Axial Load-Deformation Characteristics

Figure 4.6 shows the axial load versus axial displacement relations of the tested specimens. Axial displacement is represented by the average axial strain recorded over the full height of the specimens. To quantify the confinement and composite action influence in enhancing compressive behavior of the composite column, separate

contributions of the steel and unconfined concrete in carrying the axial load are superimposed and denoted by P_s+P_c in Fig. 4.6. In developing this diagram, the steel was assumed as an elastic-perfectly plastic material and the compressive behavior of unconfined concrete was evaluated based on the axial stress-strain relationship proposed by Popovics (1973).

Comparing P_s+P_c with the axial load versus axial strain relationship of the composite specimens *R-0.5* and *R-1.0* in Fig. 4.6 reveals the enhanced load carrying capacity and ultimate axial displacement of the composite columns due to the confinement and composite action between the constituent materials. Failure of composite columns longer than 1,000 mm (*R-1.5* thought *R-3.0*) occurred due to the loss of stability prior to any effective confinement activation. Confinement becomes activated once a minimum volumetric strain develops inside the concrete. Confinement is commonly assumed negligible in elastic range below 0.002 axial strain (Lam and Teng 2003b; Nani and Bradford 1995). Consequently, elastic axial stiffness was not affected by confinement.

Figure 4.6 also shows the enhanced behavior of the composite columns compared to the corresponding steel columns. The enhancement is indicated in terms of the increased compressive strength, elastic axial stiffness and ultimate axial strain in Table 4.3. The compressive strength of the composite columns was 2-5 times greater than that of the corresponding bare steel columns. The elastic stiffness of the composite columns increased by a ratio of up to 2.5 compared to the corresponding bare steel columns. The enhancement in the compressive strength and failure displacement generally increased with the height of the specimens when the columns failed due to loss of stability (overall buckling). However, stiffness enhancement was approximately similar for all the composite columns.

The compressive strength of the bare steel columns of 1.0, 2.0 and 2.5 m height was estimated using the column strength equation provided in the Canadian Standards

Association CAN/CSA S16-09 (CSA 2009) and the corresponding axial strain was taken as the failure strain. The elastic stiffness was estimated as $E_{St}A/L$.

The increased compressive strength and failure displacement of the composite column specimens indicates significant enhancement in the energy dissipation capacity of the columns. Compressive strength and failure strain were severely influenced by increasing the composite column height and decreased by approximately 60% and 80%, respectively, in specimen *R-3.0* compared to the shortest composite column specimen (*R-0.5*).

4.3.6.2. Energy Dissipation Capacity

The ability of columns to dissipate energy in the structures under dynamic loading such as earthquake or impact is estimated by calculating the area under the load-displacement relationship until failure. The load-deformation curve is idealized by an elastic perfectly plastic relationship in Fig. 4.7 and the energy dissipation capacity (E_d) is evaluated as:

$$E_d = \frac{1}{2} P_u \delta_y + P_u (\delta_u - \delta_y) \tag{4.1}$$

where, P_u and δ_u are the compressive strength and ultimate axial deformation, respectively. δ_y is the yield axial deformation which is taken as $\delta_{75\%}/0.75$ where, $\delta_{75\%}$ is the axial deformation prior to failure corresponding to 75% of the ultimate load (Tao et al. 2007).

The energy dissipation capacity is evaluated for the tested column specimens and summarized in Table 4.4. The energy dissipation capacity of composite columns was 2-14 times greater than that of the corresponding bare steel columns, which indicates the proposed composite columns can act as energy dissipative elements to control structural response under extreme dynamic loading. The energy dissipation capacity of the steel columns, which were not tested, was evaluated analytically by estimating the compressive

strength based on CAN/CSA S16-09 (CSA 2009) and using the stress-strain relationship of steel. The enhancement in energy dissipation capacity of the composite columns generally increased with increased column height except in the slender column *R-3.0*.

4.3.6.3. Confinement Evaluation

The level of confinement can be assessed by evaluating the ultimate lateral stains developed in the FRP jacket as a measure of the confining pressure. The average ultimate lateral strains recorded on the FRP jacket are presented in Table 4.5. Similar ultimate lateral strains were recorded in specimens *R-0.5* to *R-2.5* and were considerably reduced in specimen *R-3.0* indicating low confinement. The recorded lateral strains in the FRP jacket at the column failure were significantly smaller than the ultimate tensile strain of the FRP jacket (12,000 με) indicating that the FRP remained intact upon the specimen failure.

The ultimate compressive stress of the confined concrete ($\sigma_{u,cc}$) in the composite columns is evaluated from the experimental results and presented in Table 4.5. Confinement provided by the FRP jacket resulted in 8%-17% increase in the compressive strength of the unconfined concrete (f'_{co}) in the composite columns except specimen *R-3.0* which failed at an axial strain below 0.002 prior to confinement activation.

Confinement efficiency depends on the uniformity of confinement (Lam and Teng 2003a; Ozbakkaloglu and Oehlers 2008). Figure 4.8 shows distribution of lateral strains over the perimeter of the FRP jacket indicating confinement non-uniformity which is expected in rectangular or square cross sections. Confinement uniformity can be improving by modifying the shape of the composite cross section to an elliptical or circular section (Pan et al. 2007).

Yu et al. (2007) proposed evaluating the strain ratio as another method of assessing confinement efficiency. Strain ratio is defined as the absolute value of the lateral strain

divided by the axial strain. Figure 4.9 shows axial load versus strain ratio relationship for the tested composite columns. In general, the strain ratio increased gradually in the elastic range, which indicates low confinement in this region (up to 0.002 axial strain). The strain ratio increased more rapidly in the inelastic region in specimens *R-0.5* and *R-1.0* which failed at an ultimate axial strain above the elastic limit indicating considerable confinement.

4.3.6.4. Lateral Deflections

Figure 4.10 shows that lateral deflections increased gradually under increased loading due to the initial eccentricity of the columns and increased rapidly near the column failure. The higher initial slope of the axial load versus lateral deflection relationships of the composite columns compared to the corresponding bare steel columns in Fig. 4.10 indicates the enhanced stability of the columns against lateral deflections.

As a sample of the results, lateral deflections are also plotted for specimen *R-3.0* along the column height at different axial load levels in Fig. 4.11 in which n is the ratio of the applied load to the ultimate load. Although lateral deflections increased continuously about both column axes due to the initial eccentricity, they increased significantly about the column weak axes near ultimate load due to overall buckling of the specimen.

As previously mentioned, lateral deflections and the columns compressive strength are significantly influenced by the initial eccentricity in loading due to out-of-straightness of the specimens or misalignments in the test setup (Shaat and Fam 2006). Behavior of the tested columns can be evaluated more accurately knowing the amount of eccentricity. The maximum initial eccentricity is estimated using the moment-curvature relationship of the columns at the mid-height given by:

$$\frac{\varepsilon_{max} - \varepsilon_{min}}{d} = \frac{P\delta'}{EI} \tag{4.2}$$

where, ε_{max} and ε_{min} are the maximum and minimum recorded axial strains at the column mid-height; d is the shorter dimension of the column; P is the applied load; δ is the maximum initial eccentricity at the column mid-height and EI is the flexural stiffness of the composite column evaluated as the summation of EI from each of the column components given by:

$$EI = (EI)_{St.} + (EI)_{Conc.} \tag{4.3}$$

where, E and I denotes the elastic modulus and moment of inertia, respectively.

The estimated initial eccentricities corresponding to bending about the columns week axis are shown in Table 4.2. In general, eccentricity increased with the column height due to the greater out-of-straightness of the long columns compared to the short columns.
The ultimate curvature corresponding to the weak axis bending was evaluated for the tested composite specimens using the ultimate axial strain recordings on the opposite sides of the FRP jacket as shown in Fig. 4.12. Specimen *R-1.5* attained the largest ultimate curvature due to the relatively large initial eccentricity.

4.3.6.5. Buckling Strength Relationship

Column compressive strength normalized by the cross sectional strength (P_y) is plotted as a function of the slenderness parameter in Fig. 4.13. P_y can be estimate using the analytical model proposed by Karimi et al. (2010) for predicting *cross-sectional* capacity of partially-encased steel-concrete columns confined by FRP composites. The slenderness parameter proposed by Kato (1996) is used in developing the buckling strength relationship given by:

$$\lambda = \sqrt{\frac{P_y}{P_{cr}}} \tag{4.4}$$

where, P_{cr} is the elastic Euler buckling strength. λ is evaluated for the tested columns as presented in Table 4.2.

Figure 4.13 shows that all the composite columns failed at load levels below the cross section capacity and consequently are classified as long columns. However, the composite columns showed smaller slenderness parameter values compared to the corresponding bare steel columns indicating effectiveness of the proposed composite system in enhancing stability of column against overall buckling (see Fig. 4.13). Stability enhancement was found to be more significant in the longer specimens.

4.3.6.6. Failure Modes

Figure 4.14 shows photographs of the tested specimens. Failure of the short steel column specimen *C-0.5* was associated with yielding of the entire cross section followed by local buckling of the steel flanges and web. Failure of the remainder steel columns and all the composite columns occurred due to overall buckling accompanied by significant bending of the specimens.

The onset of overall buckling can be determined from Fig. 4.15 when the maximum and minimum axial strain recording diverged significantly from the average value. Figure 4.15 shows that the composite column specimens *R-0.5*, *R-1.*0, *R-1.5* and *R-2.0* failed at an axial strain value exceeded or near the elastic axial strain limit (taken as 2,000 με) indicating inelastic overall buckling. However, specimens *R-2.5* and *R-3.0* failed due to elastic overall buckling at an axial strain considerably smaller than the elastic axial strain limit. In all the tested composite columns no sign of local buckling of the steel section was observed after removal of the FRP jacket (see Fig. 4.14). In addition, FRP jacket remained undamaged in specimens *R-2.5* and *R-3.0.*

Failure of the long steel specimens *C-1.5* and *C-3.0* was associated with inelastic and elastic overall buckling, respectively, according to the maximum compressive strain

recording at failure shown in Fig. 4.15. Specimen *C*-3.0 returned to its undeflected shape after unloading (see Fig. 4.14).

4.4. Conclusions

In this study the slenderness influence on the behavior of a FRP-wrapped partially-encased steel-concrete composite column was investigated. The composite column was constructed by filling the voids between the flanges and web of an I-shape steel section with concrete and subsequently wrapping the column with FRP sheets. The proposed composite scheme may also be applied as a retrofit technique to increase the load carrying capacity, axial stiffness and energy dissipation capacity of existing steel columns.

A total of nine specimens were tested, six were composite columns and the remaining three were bare steel columns tested for comparison. The steel columns ranged between 500 mm and 3,000 mm with a slenderness parameter of 0.3 and 1.5, respectively. The slenderness parameter of the corresponding composite columns was between 0.2 and 1.3.

The FFP jacket provided considerable confinement to the concrete which resulted in up to 17% increase in the compressive strength of concrete. No confinement was achieved in the composite column with a slenderness parameter of greater than 1.0 due to overall buckling of the column at small axial strains prior to confinement activation.

The ratio of the compressive strength, elastic axial stiffness and ultimate axial strain of the composite columns were respectively 2.0-5.2, 2.1-2.5 and 1.0-2.6 compared to the corresponding steel columns. The energy dissipation capacity of the composite columns was 2-14 times larger than that of the corresponding steel columns. The enhancement in the compressive strength and ultimate axial strain generally increased with the specimen height. Furthermore, the enhancement in the elastic axial stiffness was not influenced by the height of the specimens.

Failure of the short steel column specimen having a slenderness parameter of 0.3 occurred due to yield of the entire cross-section followed by local buckling of the flanges and web. The remainder steel columns and all the composite columns failed by overall buckling due to loss of stability.

The slenderness parameter of the long composite columns specimen were considerably smaller than the corresponding steel columns indicating effectiveness of the proposed composite system in providing lateral stability against overall buckling and consequently enhancing buckling capacity of long steel columns.

Appendix 4.1. Notation

The following symbols are used in this paper:

A = cross sectional area;

d = the shorter dimension of the column;

$D.I.$ = ductility index;

δ = lateral deflection at the column mid-height;

δ' = maximum initial eccentricity recorded at mid-height of the columns;

E = elastic modulus;

$E_{St.}$ = elastic modulus of the steel;

δ_y = yield axial deformation;

δ_u = ultimate axial deformation;

$\varepsilon_{75\%}$ = axial deformation prior to failure corresponding to 75% of the ultimate load;

ε_{max} = maximum recorded axial strain at the mid-height of the column specimens;

ε_{min} = minimum recorded axial strain at the mi-height of the column specimens;

ϕ = curvature;

f'_{co} = compressive strength of unconfined concrete;

H = height of the column specimen;

I = moment of inertia;

L = unbraced length for column buckling about the week axis;

λ = slenderness parameter;

P = applied axial load;

P_y = cross sectional compressive strength;

P_{cr} = elastic Euler buckling strength;

P_u = ultimate axial load;

$\sigma_{u,cc}$ = the ultimate compressive strength of the confined concrete in the composite column;

Appendix 4.2. References

American Association of State Highway and Transportation Officials (AASHTO). (2001). "Weekly transportation report." *AASHTO Journal*, 101(1), 1-8.

Bakis, C. E., Bank, L. C., Brown, V. L., Cosenza, E., Davalos, J. F., Lesko, J. J., Machida, A., Rizkalla, S. H. and Triantafillou, T. C. (2002) "Fiber-reinforced polymer composites for construction-State-of-the-art review" *J. Compos. for Constr.*, 6(2): 73-87.

Canadian Institute of Steel Construction (CISC) (2008) "Handbook of Steel Construction." Ninth Edition, Toronto, Ontario.

CIRIA (2004) "Strengthening metallic structures using externally-bonded fibre-reinforced-polymers-C595." London, CIRIA.

CSA. (2009) "Limit states design of steel structures. Standard CAN/ CSA S16-09." *Canadian Standards Association*, Mississauga, Ont.

Karimi, K., El-Dakhakhni, W. W., and Tait, M. J. (2010) "Performance enhancement of steel columns using concrete-filled composite jackets." *J. of Perform. Constr. Facil.*, DOI: 10.1061/(ASCE)CF.1943-5509.0000162.

Kilpatrick, A. E., and Rangan, B. V. (1997) "Tests on high-strength composite concrete columns." *Research Report No. 1/97*, School of Civil Engineering, Curtin University of Technology, Perth, Western Australia.

Intelligent Sensing for Innovative Structures (ISIS) (2001) "Design manual no. 4: Strengthening reinforced concrete structures with externally bonded fiber reinforced polymers" *ISIS Canada*, Winnipeg, Canada.

Kato, B. (1996) "Column curves of steel-concrete composite members" *J. Constr. Steel Res.*, 39(2): 121-135.

Lam, L. and Teng, J. G. (2003a) "Design-oriented stress-strain model for FRP-confined concrete in rectangular columns." *J. Reinf. Plast. Compos.*, 22(13), 1149-1186.

Lam, L., and Teng, J. G. (2003b) "Design-oriented stress-strain models for FRP-confined concrete." *J. Constr. and Build. Mat.*, 17, 471-489.

Mirmiran, A., and Shahawy, M. (1997) "Behavior of concrete columns confined by fiber composites." *J. Struct. Eng. ASCE*, 23(5):583–90.

Mirmiran, A., Shahawy, M., Samaan, M., and El Echary, H. (1998) "Effect of column parameters on FRP-confined concrete." *J. Compos. for Constr. ASCE*, 2(4):175–185.

Mirmiran, A., Shahawy, M. and Beitleman, T. (2001) "Slenderness limit for hybrid FRP-concrete columns." *J. Compos. for Constr.*, 5(1): 26-34.

Mursi, M., and Uy, B. (2004) "Strength of slender concrete filled high strength steel box columns." *J. Constr. Steel Res.*, 60: 1825-1848.

Nanni, A., and Bradford, N. M. (1995) "FRP jacketed concrete under uniaxial compression." *J. Constr. Build. Mater.*, 9(2): 115-124.

Oehlers D. J., Bradford M. A. (1995) "Composite steel and concrete structural members: fundamental behaviour."

Ozbakkaloglu, T., and Oehlers, D. J. (2008) "Manufacture and testing of a novel FRP tube confinement system." *J. Eng. Struct.*, 30: 2448–2459.

Pan, J. L., Xu, T., and Hu Z. J. (2007) "Experimental investigation of load carrying capacity of the slender reinforced concrete columns wrapped with FRP." *J. Constr. Build. Mater.*, 21: 1991-1996.

Pessiki, S., Harries, K., Kestner J. T., Sause, R, and Ricles J. (2001) "Axial behavior of reinforced concrete columns confined with FRP jackets." *J. Compos Constr.*, 5(4):237–245.

Popovics, S. (1973) "A numerical approach to the complete stress-strain curves for concrete." *J. Cement and Concr. Res.*, 3(5): 583-599.

Rochette, P., and Labossiere, P. (2000) "Axial testing of rectangular column models confined with composites." *J. Compos. for Constr. ASCE*, 4(3): 129–136.

Saafi, M., Toutanji, H. A., and Li, Z. (1999) "Behavior of concrete columns confined with fiber reinforced polymer tubes." *ACI Mater. J.*, 96(4):500–509.

Shaat, A., and Fam., A. (2006) "Axial loading tests on short and long hollow structural steel columns retrofitted using carbon fibre reinforced polymers." *Can. J. Civ. Eng.*, 33: 458-470.

Tao, Z., Han, L. H., and Zhuang, J. P. (2007) "Axial loading behavior of CFRP strengthened concrete-filled steel tubular stub columns." *J. Adv. Struct. Eng.*, 10(1): 37-46.

Teng, J. G., Yu, T., Wong, Y. L., and Dong, S. L. (2007) "Hybrid FRP-concrete-steel tubular columns: concept and behavior." *J. Constr. Build. Mater.*, 21: 846-854.

Yu, Z. W., Ding, F. X. and Cai, C. S. (2007) "Experimental behavior of circular concrete-filled steel tube stub columns." *J. Constr. Steel Res.*, 63: 165-174.

Table 4.1. Material properties of the CFRP and GFRP composite laminates and the epoxy

	Tensile Strength (MPa)	Tensile Modulus (GPa)	Ultimate Elongation (%)	Thickness (mm)
CFRP compsite laminate	876	72.4	1.2	1.0
GFRP compsite laminate	575	26.1	2.2	1.3
Saturant Epoxy	72.4	3.18	5.0	---

Table 4.2. . Test matrix, estimated slenderness parameter and the initial eccentricity of the tested specimens

Test I.D.	Height (H) (mm)	Slenderness Parameter (λ)	Maximum Initial Eccentricity (δ) (mm)
C-0.5	500	0.25	N/A
C-1.5	1500	0.76	0.6
C-3.0	3000	1.51	0.7
R-0.5	500	0.22	N/A
R-1.0	1000	0.44	0.5
R-1.5	1500	0.66	1.7
R-2.0	2000	0.89	0.5
R-2.5	2500	1.11	0.9
R-3.0	3000	1.33	1.9

Table 4.3. Axial capacity, stiffness and ultimate strain of the tested columns

Specimen I.D.	Compressive Strength		Elastic Axial Stiffness		Ultimate Axial Strain	
	(kN)	Increase (Ratio)	(kN/mm)	Increase (Ratio)	(με)	Increase (Ratio)
C-0.5	726	N/A	753	NA	4,034	N/A
C-1.5	497	N/A	271	NA	1,509	N/A
C-3.0	268	N/A	123	NA	748	N/A
R-0.5	1,440	1.98	1,702	2.26	3,899	0.97
R-1.0	1,447	2.40	805	2.32	2,834	1.40
R-1.5	1,354	2.72	573	2.11	2,026	1.34
R-2.0	1,361	4.12	412	2.38	2,147	2.19
R-2.5	1,236	5.17	342	2.47	1,716	2.57
R-3.0	590	2.20	265	2.15	819	1.09

Table 4.4. Energy dissipation capacity of the tested columns

Specimen I.D.	E_d	
	(kJ)	Increase (Ratio)
C-0.5	1.05	N/A
C-1.5	0.61	N/A
C-3.0	0.31	N/A
R-0.5	1.94	1.85
R-1.0	2.47	3.67
R-1.5	2.31	3.76
R-2.0	3.21	9.55
R-2.5	2.82	13.96
R-3.0	0.78	2.55

Table 4.5. Ultimate lateral strain of the FRP jacket and compressive strength of the confined concrete in the composite columns

Specimen I.D.	Ultimate Lateral Strain	$\sigma_{u,cc}$	
	(με)	(MPa)	$\frac{\sigma_{u,cc}}{f'_{co}}$
R-0.5	300	53.8	1.11
R-1.0	330	54.3	1.12
R-1.5	380	47.3	0.98
R-2.0	450	47.8	0.99
R-2.5	290	46.2	0.95
R-3.0	100	22.1	0.46

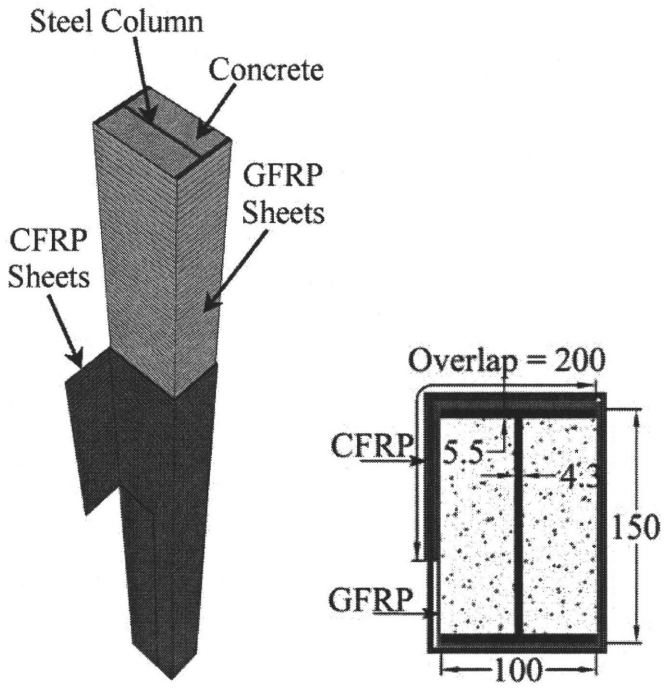

Figure 4.1. Schematic of the composite columns (all dimensions in *mm*)

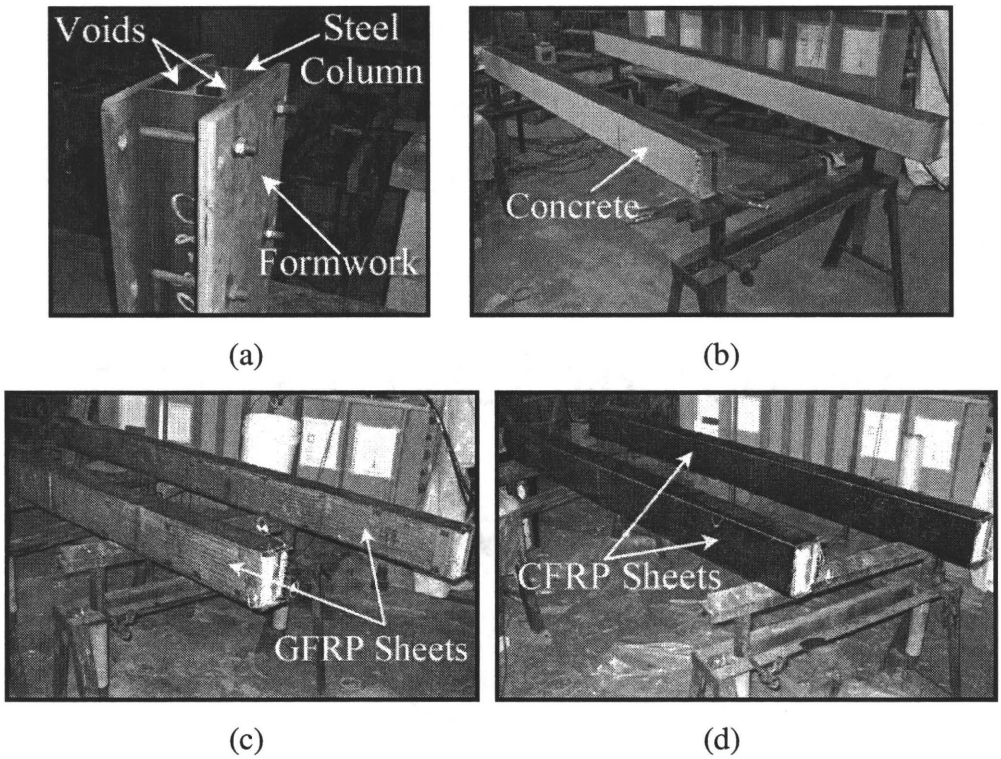

Figure 4.2. Photographs of the construction of the composite specimens (a) before pouring concrete (b) after pouring concrete (c) applying GFRP wraps (d) applying CFRP wraps

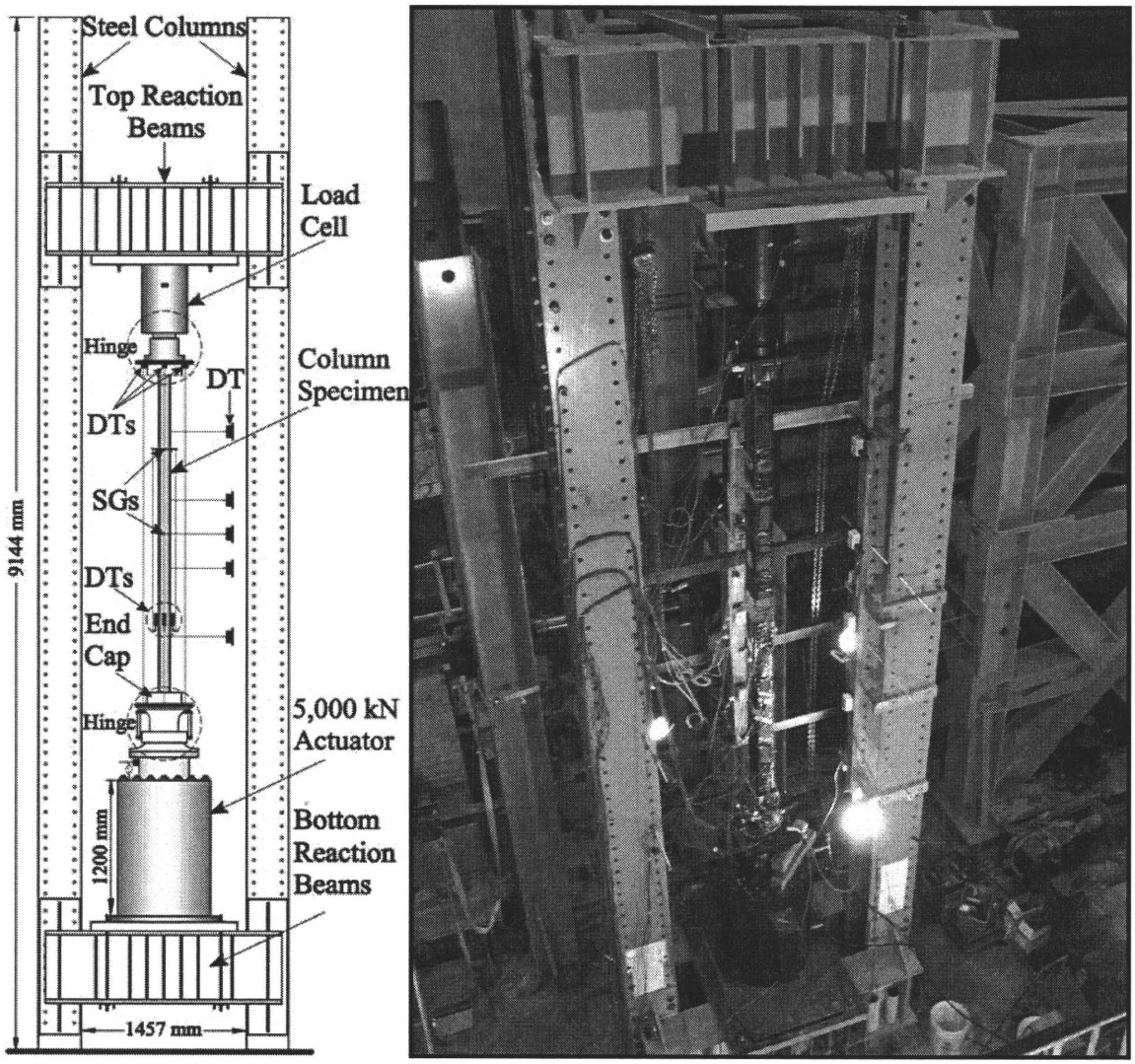

(a) (b)

Figure 4.3. Test setup (a) schematic view (b) photograph

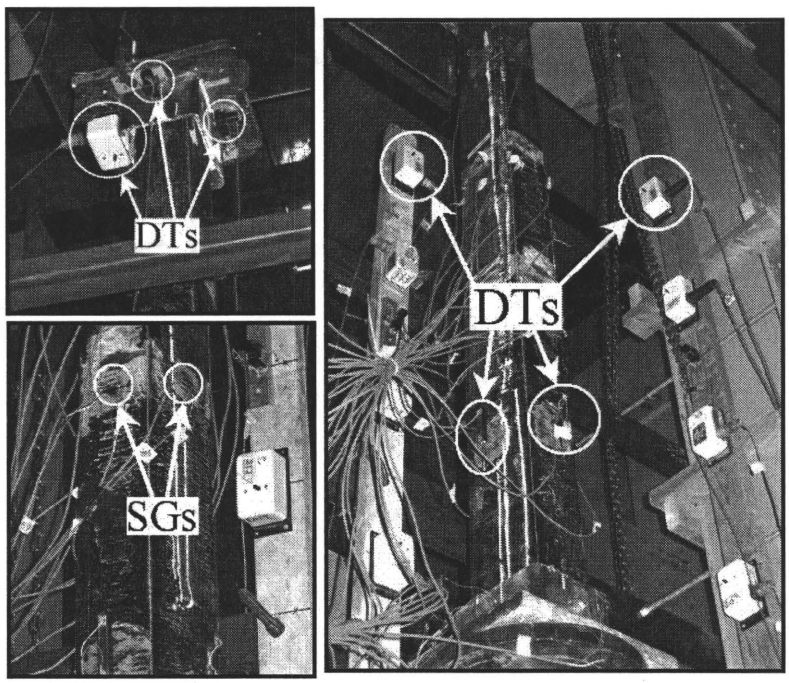

Figure 4.4. Instrumentations

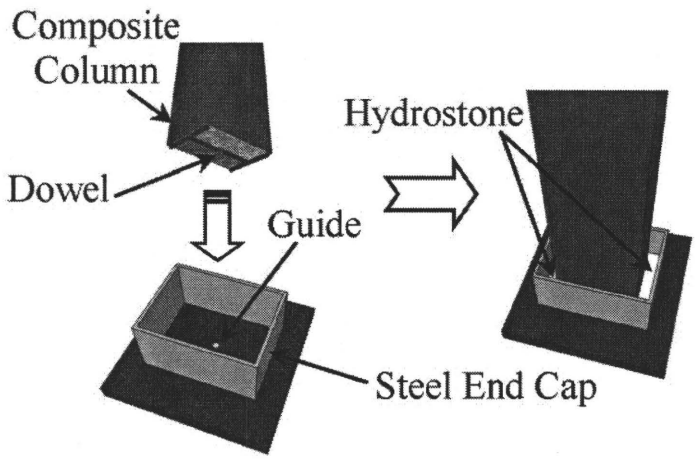

Figure 4.5. Method of capping the specimen ends to ensure uniform axial loading over the entire cross section

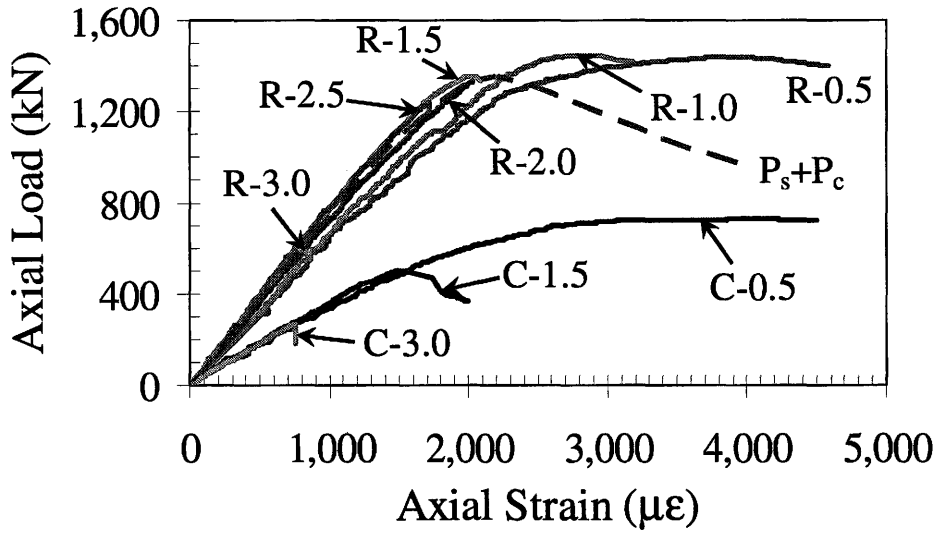

Figure 4.6. Load versus average axial strain curves for the tested specimens

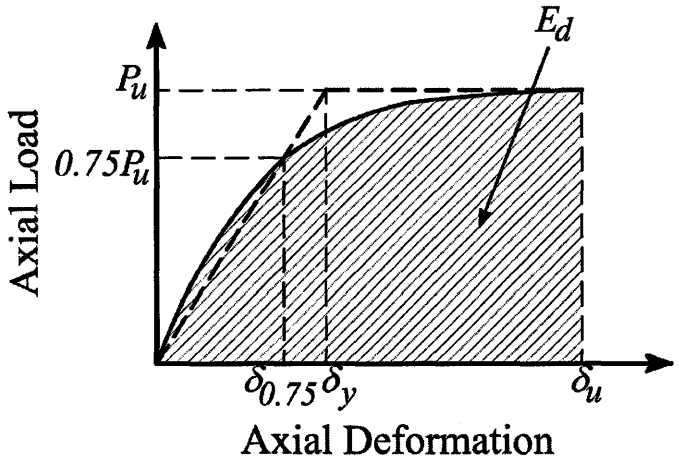

Figure 4.7. Definition of ductility index and energy dissipation capacity

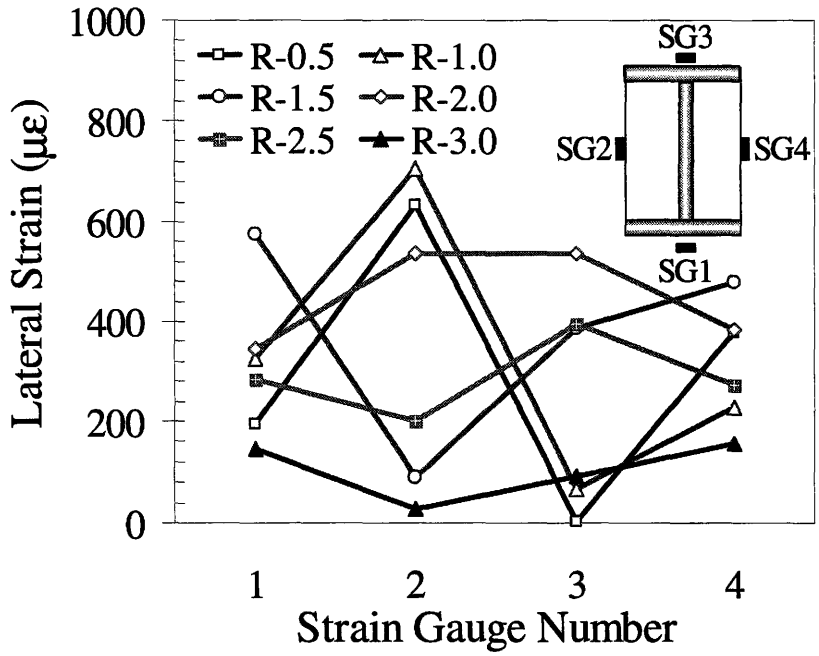

Figure 4.8. Axial load versus strain ratio (ν) diagrams for the tested composite specimens

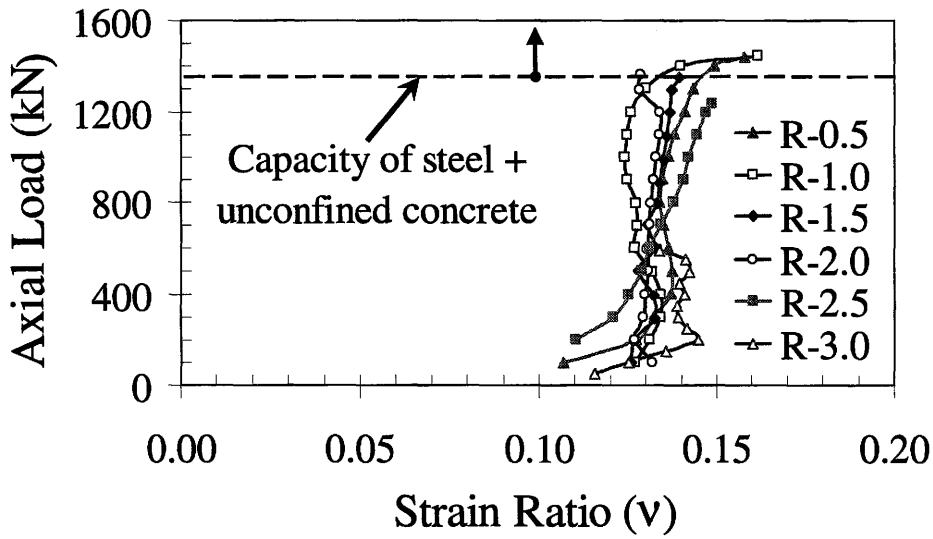

Figure 4.9. Axial load versus strain ratio (ν) diagrams for the tested composite specimens

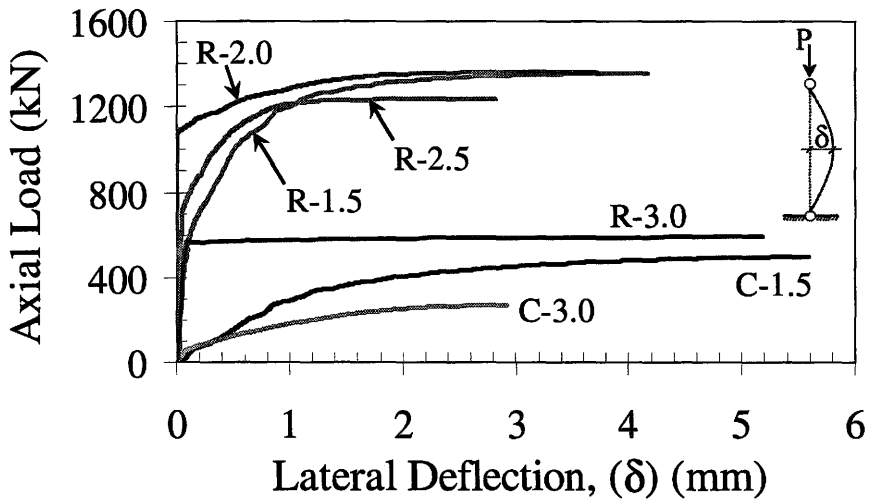

Figure 4.10. Axial load versus lateral deflection about the weak axis at the column mid-height

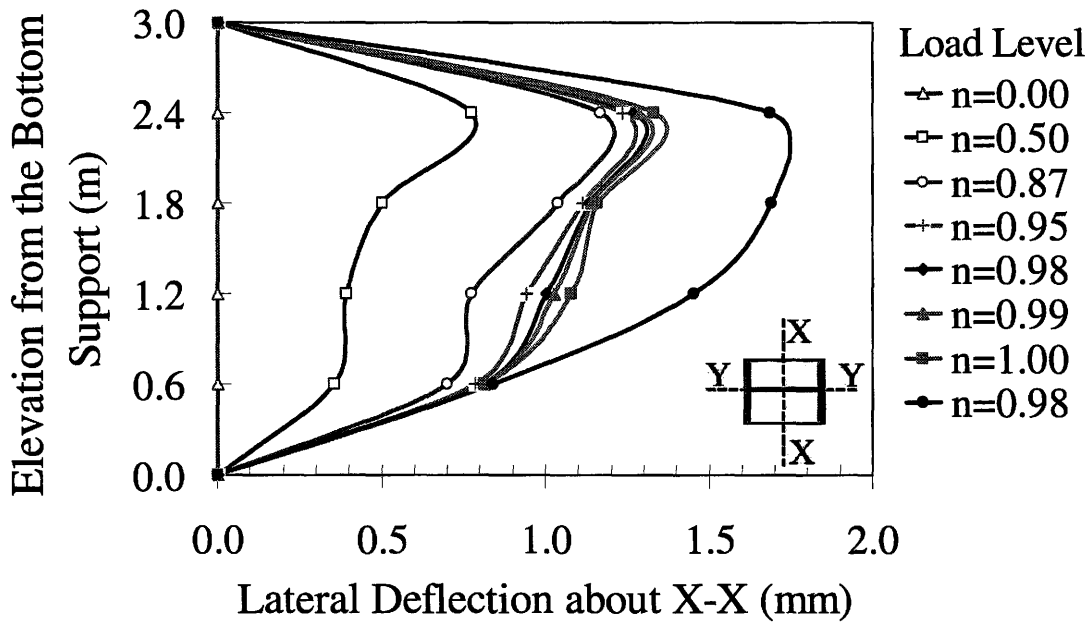

(a)

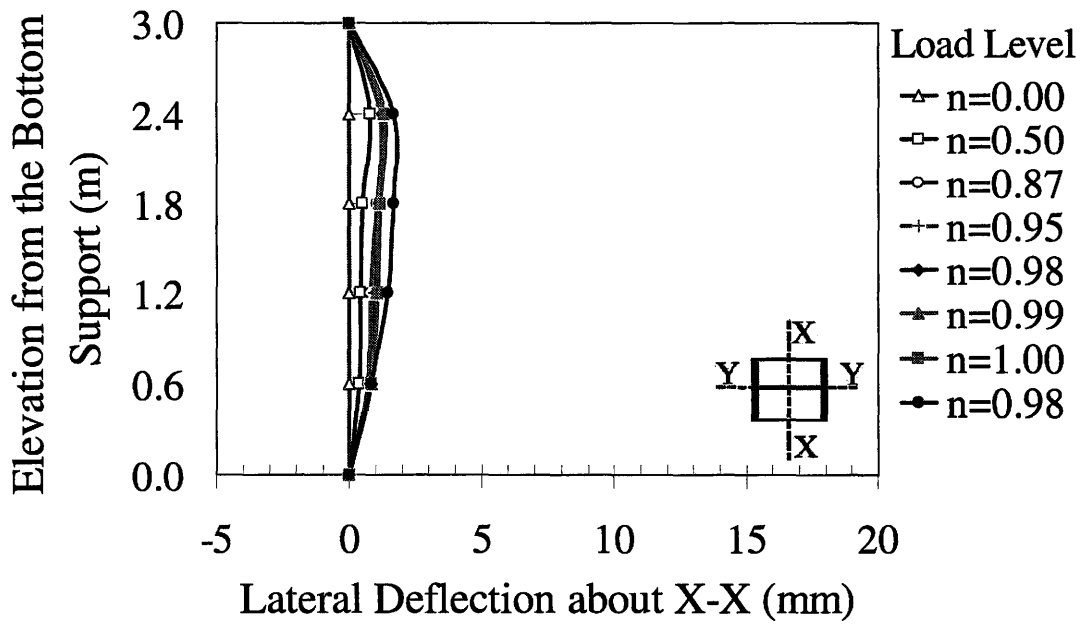

(b)

Figure 4.11. Lateral deflection along the height at the different axial load levels in specimens *R-3.0* (a) about the weak axis (b) about the strong axis

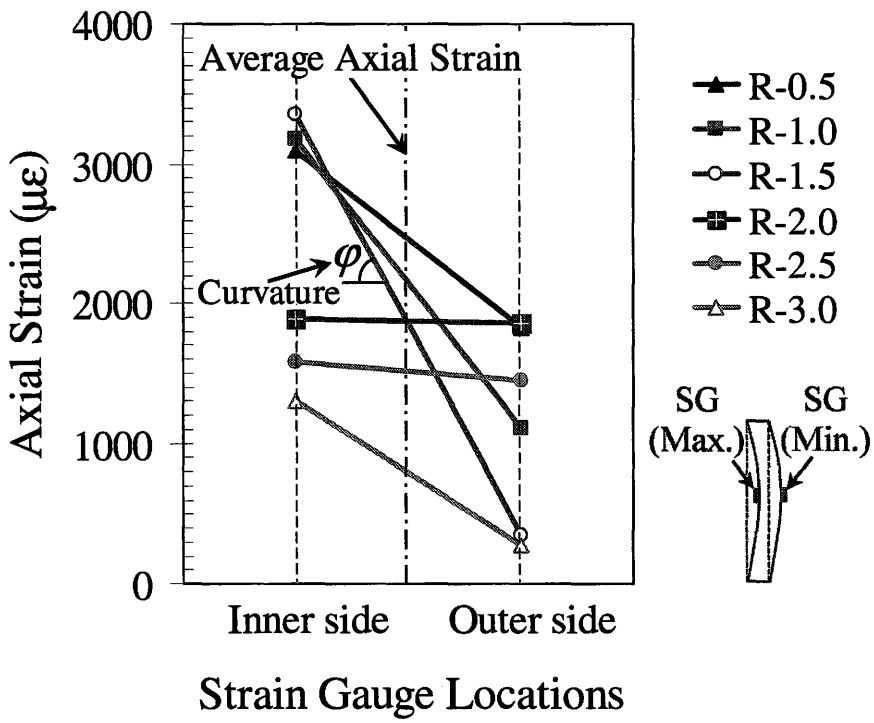

Figure 4.12. Ultimate axial strain recordings on the FRP jacket

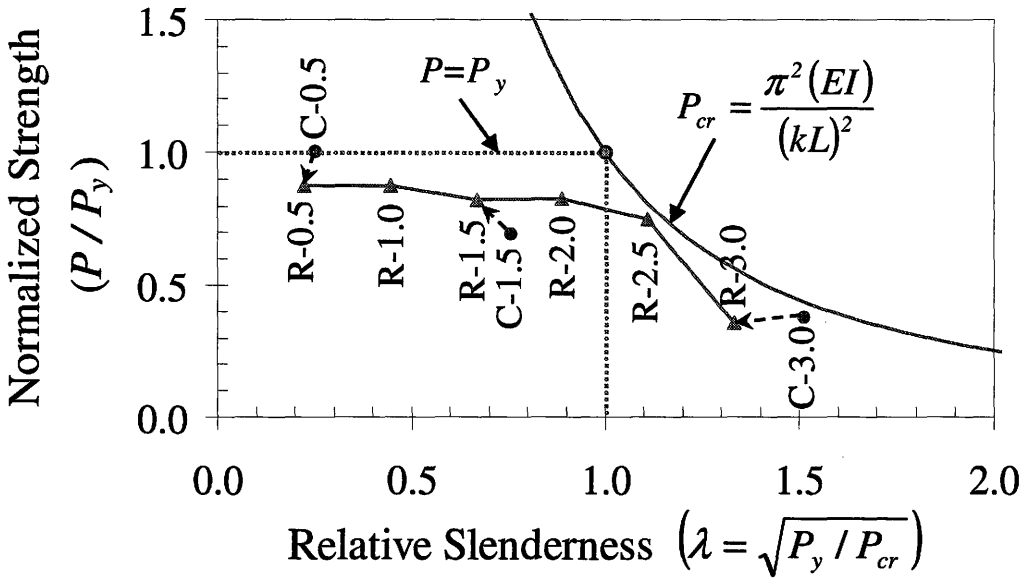

Figure 4.13. Normalized buckling strength curve for the columns specimens

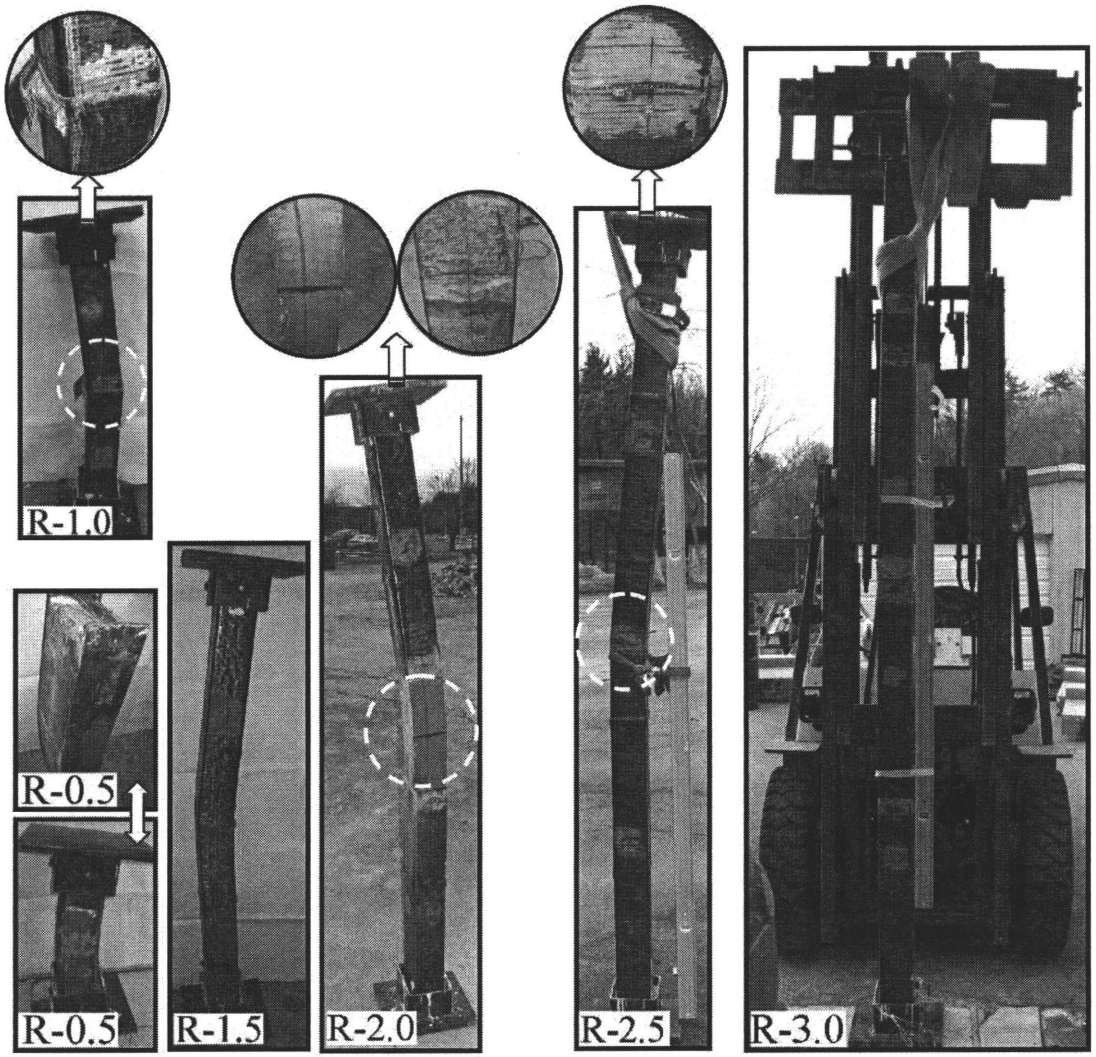

Figure 4.14. Photographs of the tested specimens after unloading

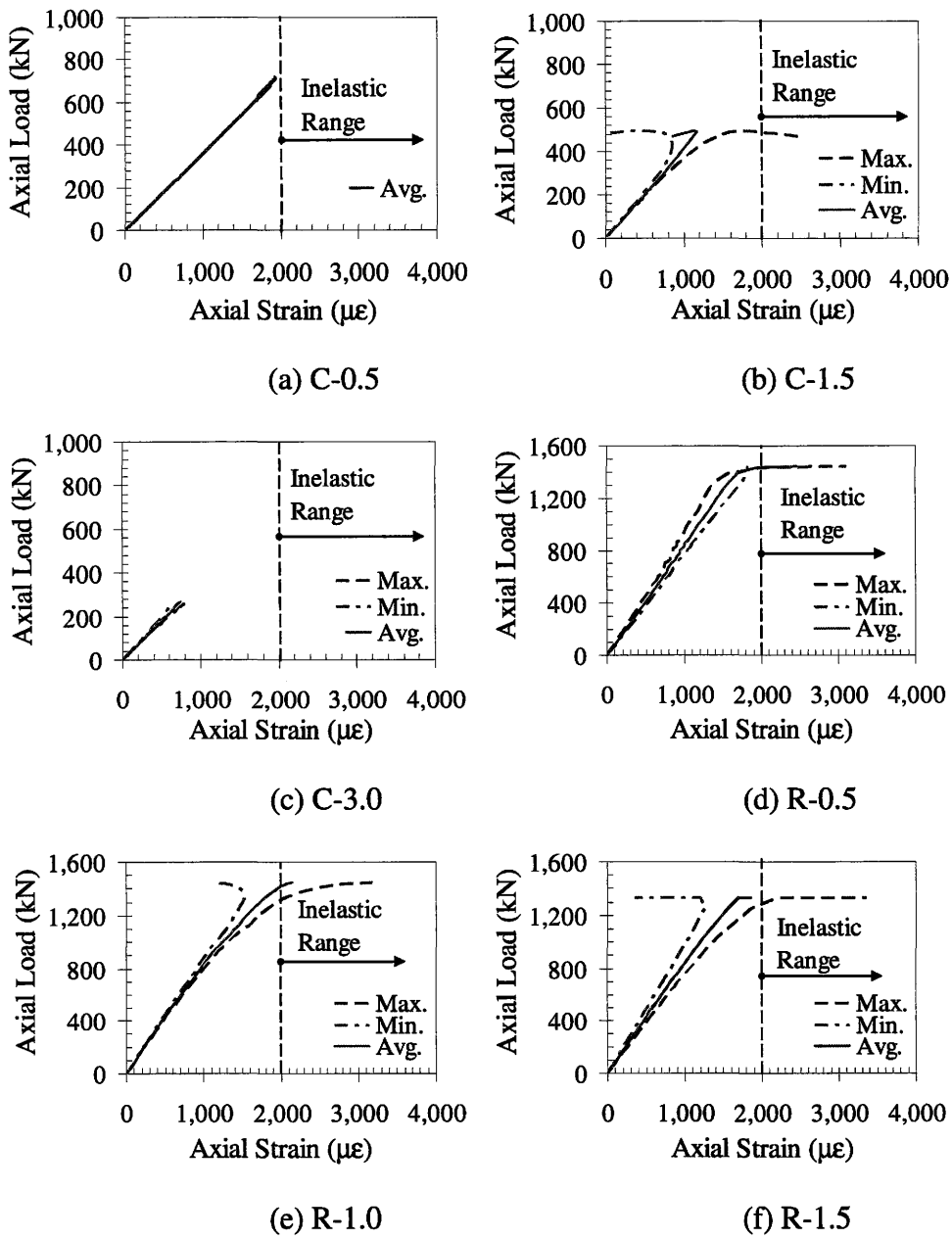

Figure 4.15. Axial load versus vertical strain gauges readings at the mid-height

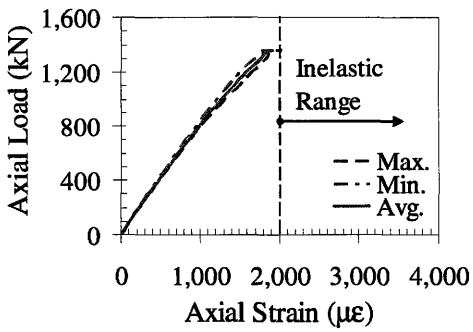

(g) R-2.0

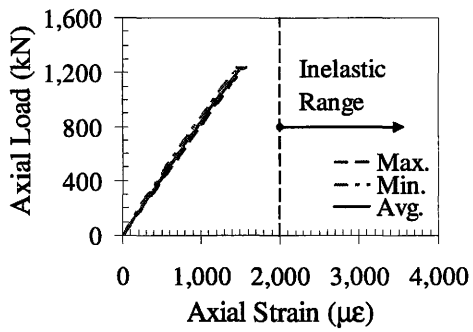

(h) R-2.5

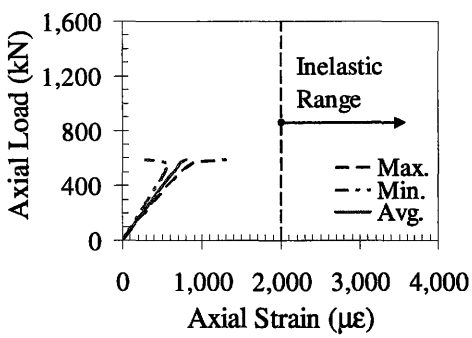

(i) R-3.0

Figure 4.15. Continued

Chapter 5: Influence of Slenderness on the Behavior of a FRP-encased Steel-Concrete Composite Column

5.1. Summary

The compressive behavior of a steel-concrete composite column encased in a fiber reinforced polymer (FRP) tube is evaluated experimentally for columns with various slenderness ratios. The composite column is comprised of a FRP tube surrounding a steel I-section, which is subsequently filled with concrete. A total of nine column specimens were tested ranging between 500 mm and 3,000 mm in height. Confinement and composite action resulted in enhanced compressive behavior of the composite columns. Maximum confinement occurred in the short column (slenderness parameter of smaller than 0.2). Confinement action reduced with increased height of the column specimens. The column load carrying capacity, ultimate axial strain and compressive strength of the confined concrete core in the longest specimen (slenderness parameter of 0.9) were reduced to approximately 59%, 14% and 51% of the short column values, respectively. A buckling strength curve of the composite columns was developed based on the experimental results, which can be used in predicting load carrying capacity of the columns with different slenderness ratios.

Keywords: buckling, confinement, composite columns, fiber reinforced polymer (FRP), retrofitting, slenderness ratio, steel columns, tubes

5.2. Introduction

Infrastructure safety, durability and serviceability have been significantly enhanced as a result of improved construction materials over the past two decades.

Despite the higher cost of FRP compared to conventional construction materials, its superior properties including excellent corrosion, fatigue and creep resistance, high stiffness, weather proofing properties and durability to freezing and thawing in cold climate regions makes FRP an attractive alternative material for infrastructure applications (Triantafillou 1998; Neale 2000). On a relative weight basis, FRP is 4-20 times as expensive as steel. However, it has a significantly higher strength-to-weight ratio compared to steel. A single kilogram of FRP is equivalent to approximately 28 kg steel on a strength basis. In addition, the FRP material cost in rehabilitation rarely exceeds 20% of the overall project cost. Accounting for the savings in the installation and traffic management costs, use of FRP can result in a increased approximately saving of 17.5% over steel cost (Hollaway and Cadei, 2002).

Increased demand placed on the composite material industry in the late 1980s and early 1990s facilitated reduction of their manufacturing costs, which consequently led to a growth in construction and infrastructure projects using composite materials (Bakis et al. 2002).

As of the year 2000, approximately 170,000 bridges in the United States were indentified as structurally deficient or functionally obsolete (AASHTO 2001). Deicing salt used for winter maintenance activities is considered the main cause of bridge corrosion. Therefore, use of corrosion resistant materials such as FRP in bridge construction extends the serviceability life of the structure and reduces maintenance costs. Application of FRP composites usually results in lighter and more durable structural elements and substantial saving in labor cost and construction time. FRP may also be utilized in construction of

hybrid structures where high performance FRP is combined with the low cost concrete resulting in a cost-effective system (Cheng and Karbhari, 2006).

Despite the substantial research effort that focuses on application of FRP in developing innovative composite structural schemes and corresponding design guidelines, particularly in the United States, most of these applications have focused on the use of FRP in concrete structures. Only a limited number of recently conducted studies have investigated the application of FRP in metallic structures. Furthermore, these studies have typically concentrated on strengthening steel girders (El Damatty et al. 2005; Phares et al. 2003; Shaat and Fam 2006b) and fatigue damaged connections (Fam et al. 2006; Shaat et al. 2004). Application of FRP in strengthening steel columns has been limited to hollow structural steel sections (HSS) wrapped with FRP sheets to increase stability against local and overall buckling (Shaat and Fam, 2006a and Teng and Hu. 2007).

The current study aims at evaluating the behavior of a new type of composite column that was recently introduced by Karimi et al. (2010) through a set of experimental tests on columns with various slenderness ratios. The composite column comprises of a fiber reinforced polymer (FRP) tube surrounding a steel column with the void between the FRP tube and the steel column filled with concrete. The FRP tube enhances the compressive performance of the composite columns by providing confinement to the concrete core. The steel column replaces the longitudinal reinforcements in traditional reinforced concrete (RC) columns and provides additional shear and compressive capacity in addition to enhancing column ductility. Moreover, the FRP tube acts as a stay-in-place form and protects the concrete as well as the steel section from deterioration and weathering. Enhancement in compressive strength of the proposed composite columns may result in smaller cross sections than equivalent RC columns. The proposed composite system may also be applied as a retrofit technique in strengthening existing steel columns. A schematic of the composite column is presented in Fig. 5.1.

Through confinement, FRP is known to increase the compressive strength of short RC columns by a ratio of between 1.5 and 3.0 (Lam and Teng 2003a). However, confinement efficiency is severely reduced by an increase in the slenderness ratio of the columns. Substantial research on behavior of short RC columns confined with FRP has been reported in the literature. However, very few studies have investigated behavior of slender composite columns. Therefore, composite and steel columns ranging between 500 mm and 3,000 mm in height were tested in this study with the primary objective of investigating the influence of the slenderness ratio on the enhancement in compressive behavior of the proposed composite columns.

5.3. Experimental Program

A total of nine columns were tested in the experimental program. Six specimens were composite columns constructed based on the described composite scheme. The remaining three specimens were bare steel columns tested for comparison purposes in employing the composite system as a retrofit technique. Fig. 5.2 shows photographs of the composite specimens. The selected steel section was W150×14 (CISC 2008) which is classified as a compact section according to CAN/CSA S16-09 (CSA 2009) to ensure yielding of cross-section prior to the onset of local buckling.

5.3.1. Material Properties

The FRP tube utilized in construction of the composite column specimens was made of unidirectional glass fibers oriented in the circumferential direction. The mechanical properties and dimensions of the FRP tube are presented in Table 5.1. Poisson's ratio values are given for the force applied in the axial or the lateral directions. In the assigned designation for Poisson's ratio values, the first subscript denotes the contraction direction and the second subscript denotes direction of the applied force where "*a*" and "*l*" denote the axial and the lateral directions, respectively.

The average compressive strength of concrete at the time of testing was 48.3 MPa and the average yield strength of steel was 411 MPa.

5.3.2. Test Setup, Instrumentation and Load Transfer Mechanism

The compression test setup shown in Fig. 5.3(a) and 5.3(b) was used to conduct tests of specimens under axial loading. The test frame consisted of two steel columns and four steel girders. A 5,000 kN actuator was used to apply the load under displacement control at a rate of 0.1 mm/min. A load cell fastened to the top girders measured the applied load. Two swivels located at the top and bottom of the specimens simulated pin-pin boundary conditions (see Fig. 5.3(c)).

Four displacement transducers (DT), mounted between the ends of the specimen, were used to measure the axial deformation of the columns over the full height. Additional DTs were oriented horizontally to measure the lateral displacement of the specimen at equally-spaced locations along the column height for weak and strong-axis bending. Four DTs were also installed near the column mid-height over a gauge length equal to half of the column height as an alternative method for measuring the axial deformation. Eight strain gauges (SG) were located at the column mid-height in both the longitudinal and the circumferential directions to measure the axial and the lateral strains, respectively. In specimens longer than 1,000 mm, the SGs were also mounted at quarter points along the column height. The instrumentation layout and photographs of an instrumented column are shown in Fig. 5.3(d).

Fig. 5.4 shows the method used to cap the column ends to ensure uniform application of the load over the entire cross section. Axial loading was applied over the column cross section through thick steel plates and the small voids between the plate and the column were filled with hydrostone. Special care was taken in placing the specimens concentric with respect to the axis of loading by aligning a dowel, attached to the center of the column, with a hole drilled at the center of the steel plate.

5.3.3. Test Matrix and Results

Table 5.2 shows the test matrix. Each specimen is assigned a designation consisting of a letter and a number. The letters "C" and "R" denotes control (bare steel column specimens) and composite specimens, respectively, followed by the height, H, of the specimen in meters.

The test results summarized in Table 5.2 are discussed in the following section in terms of the load-displacement characteristics, state of stress in the FRP tube, confinement effects and energy dissipation capacity. In addition, initial eccentricity, load versus lateral deflections, buckling strength relationship and failure modes are presented.

5.3.3.1. Load Displacement Characteristics

Axial load-displacement relationship of the tested specimens is shown in Fig. 5.5 in which the displacement is calculated as the average axial strain measured from the displacement transducer readings over the full column height. To quantify the confinement effect and the composite action between the constituent materials, separate contributions from the steel column, the unconfined concrete and the FRP tube in carrying the applied load were analytically calculated and superimposed. This superimposed relationship is denoted by $P_s+P_c+P_t$ in Fig. 5.5. In developing this relationship, the FRP tube and the steel were assumed as elastic and elastic-perfectly plastic materials, respectively, and the axial stress-strain relationship proposed by Popovics (1973) was used to evaluate the unconfined concrete contribution in carrying the load.

Comparing the axial load versus axial strain relationships of the composite column specimens and the $P_s+P_c+P_t$ curve shows the significant effect of confinement and composite action in enhancing the compressive strength and ultimate axial strain of composite specimens ranging between 500 mm and 2,000 mm in height. Composite columns longer than 2,000 mm (*R-2.5* and *R-3.0*) failed due to loss of stability at small

axial strain values prior to efficient confinement activation. This is attributed to the fact that a minimum level of volumetric strain must develop in the concrete before the FRP tube is engaged in providing efficient confinement.

The slope of the linear elastic segment in the axial load-strain diagrams shown in Fig. 5.5, was similar for all the tested composite columns indicating elastic axial stiffness is not affected by confinement. Lam and Teng (2003a) and Nani and Bradford (1995) also noted negligible confinement in the elastic range (axial strain values smaller than 0.002) in FRP confined concrete.

Figure 5.5 shows significant enhancement in the compressive behavior of the composite columns compared to the bare steel columns. In Table 5.2, the enhancement is expressed in terms of increased compressive strength, elastic axial stiffness and ultimate axial strain of the composite columns compared to the bare steel column counterparts. In this table, the compressive strength of the composite column specimens was 5-10 times greater than the corresponding steel columns. Enhancement in the compressive strength of the composite columns compared to the corresponding steel columns generally increased with the height of the specimens when the columns failed as a result of overall buckling. However, the compressive strength decreased with the height of columns and reached approximately 60% of the cross sectional capacity in specimen *R-3.0*. The compressive strength of 1,000 mm, 2,000 mm and 2,500 mm high steel columns (not tested) was estimated using the column strength equation of the Canadian Standards Association CAN/CSA S16-09 (CSA 2009).

The composite column specimens also attained significantly higher stiffness and failure displacement compared to the corresponding bare steel columns. In general, the elastic axial stiffness of the composite columns was 4-6 times greater compared to the bare steel columns. The elastic axial stiffness of 1,000 mm, 2,000 mm and 2,500 mm high steel columns (not tested) was taken as $E_{St}A/L$. The ultimate axial strain of the composite

column specimens was 2-3 times greater than the corresponding steel columns. However, the ultimate axial strain reduced with increased specimen height. The significant increase in the compressive strength and ultimate axial strain of the composite column specimens indicates considerable enhancement in the energy dissipation capacity of the composite columns.

5.3.3.2. State of Stress in the FRP Tube

The FRP tube in the composite column specimens is under a biaxial state of stress. Failure of the composite column specimens may occur due to rupture of the FRP tube under axial compression or lateral confining pressure. Failure of the FRP tube can be assessed by evaluating the ultimate state of stress in the tube through the following relationships (Bank 2006):

$$\sigma_{au,t} = \frac{E_{a,t}}{1-\nu_{al}\nu_{la}}\varepsilon_{au,t} + \frac{\nu_{al}E_{a,t}}{1-\nu_{al}\nu_{la}}\varepsilon_{lu,t} \tag{5.1}$$

$$\sigma_{lu,t} = \frac{\nu_{la}E_{l,t}}{1-\nu_{al}\nu_{la}}\varepsilon_{au,t} + \frac{E_{l,t}}{1-\nu_{al}\nu_{la}}\varepsilon_{lu,t} \tag{5.2}$$

where, $E_{a,t}$ and $E_{l,t}$ are the axial and lateral modulus of the FRP tube, $\sigma_{au,t}$ and $\sigma_{lu,t}$ are the ultimate axial and lateral stress, and $\varepsilon_{au,t}$ and $\varepsilon_{lu,t}$ are the ultimate axial and lateral strain in the FRP tube, respectively.

$\sigma_{au,t}$ and $\sigma_{lu,t}$ are evaluated based on strain gauge recordings at four locations on the FRP tube at the column mid-height as shown in Figs. 5.6(a) and 5.6(b), respectively. In Fig. 5.6, $\sigma_{au,t}$ and $\sigma_{lu,t}$ are normalized with respect to the axial compressive and lateral tensile strength of the FRP tube ($\sigma_{a,t}$, $\sigma_{l,t}$), respectively.

Figure 5.6(b) shows that the ultimate lateral stress in the FRP tube did not exceed 70% of $\sigma_{l,t}$ in any of the tested composite columns. Uniform distribution of the lateral stresses in the FRP tube in specimen *R-0.5* indicates efficient confinement in this specimen.

From Fig. 5.6, it is also observed that the FRP tube of specimen *R-1.0* failed at location 2, whereas the axial and lateral stresses evaluated at other locations at the column mid-height were below the axial and lateral strength of the FRP tube. Failure of the FRP at location 2 occurred due to bending of the column prior to failure as a result of initial eccentricity which will be discussed in further details later.

In the remainder of the column specimens the axial and lateral stresses, estimated at all locations at the column mid-height at failure, were below the axial and lateral strength of the FRP tube indicating inefficient use of the FRP tube in providing confinement (see Fig. 5.6). In fact, the FRP tube in specimens *R-2.0*, *R-2.5* and *R-3.*0, remained completely intact after column failure.

Figure 5.6(b) also shows that the lateral tensile stress in the FRP tube at failure generally decreased with increased specimen height indicating lower confinement in the longer columns.

5.3.3.3. Confinement Evaluation

As previously mentioned, the enhanced behavior of the composite column specimens shown in Fig. 5.5 was mainly due to the confinement and composite action between the constituent materials. The estimated compressive strength of the confined concrete (f'_{cc}) in the composite column specimens is shown in Table 5.2. The compressive strength of unconfined concrete (f'_{co}) was approximately doubled in the shortest composite column, specimen *R-0.5*, due to the confinement. However, f'_{cc} significantly decreased with the increased specimen height and reached 93% of f'_{co} in specimen *R-3.0* indicating no confinement.

The shape of the axial load-displacement relationship of the composite columns is governed by the maximum confining pressure. Highly confined composite columns show a strain hardening behavior in the inelastic range prior to failure (Lam and Teng 2003a) as

can be seen for specimen *R-0.5* in Fig. 5.5. The strain hardening inelastic segment of the axial load-displacement relationship became a plateau in specimen *R-1.0* and a strain softening branch in the longer composite column specimens indicating a reduction in confinement with increasing specimen height.

Confinement can be evaluated based on the lateral strain recordings on the FRP tube. Figure 5.7 shows the axial load versus lateral strain relationship of the composite column specimens recorded at mid-height. In general, lateral strain values were small in the elastic range indicating insignificant confinement and increased rapidly beyond the elastic limit. The average ultimate lateral strains in the FRP tube at failure are presented in Table 5.2. The largest ultimate lateral strain in the FRP tube (presented in Table 5.2) was recorded in specimen *R-0.5* and was approximately equal to 70% of the lateral tensile strain of the FRP tube at rupture under lateral tension (evaluated from Table 5.1, $\varepsilon_{l,t}$ = 0.017). Figure 5.7 also shows that the ultimate lateral strains decreased with an increase in height of the composite columns and were relatively small in specimens *R-2.5* and *R-3.0* indicating negligible confinement in these two specimens, which agrees with the corresponding f'_{cc} values in Table 5.2.

Confinement effectiveness is highly dependent on the uniformity of the confining pressure (Lam and Teng 2003b; Ozbakkaloglu and Oehlers 2008). Confinement uniformity can be assessed based on the distribution of the lateral strain over the perimeter of the FRP tube. Ultimate lateral strain recordings at different elevations normalized by the rupture lateral tensile strain of the tube ($\varepsilon_{l,t}$) are shown in Fig. 5.8. Uniform distribution of ultimate lateral strains in the short specimen *R-0.5* was distorted by the shift in the failure mode from the cross sectional failure to overall buckling in the long column specimens, which indicates low confinement in the long composite columns. The maximum and minimum ultimate lateral strains were respectively recorded on the compression and tension side of the long column specimens. Figure 5.8 shows that the maximum ultimate lateral strain does not necessarily exist at the mid-height cross section

of the long column specimens. Figure 5.8 also indicates similar ultimate lateral strain recordings by SG1 and SG3 (refer to Fig. 5.6) due to minor overall buckling of the long column specimens about their strong axis.

Another useful parameter to evaluate confinement effectiveness is the strain ratio proposed by Yu el al. (2007), which is defined as the absolute value of the lateral strain divided by the axial strain. Strain ratios evaluated for the tested composite column specimens at different axial strain values are shown in Fig. 5.9. Strain ratio increased gradually in the elastic range approximately equal to Poison's ratio of the FRP tube (ν_{la}=*0.11*) indicating low confinement in this region. The strain ratio increased rapidly beyond the elastic limit and reached near 1.0 at failure in specimens *R-0.5* and *R-1.0*.

5.3.3.4. Energy Dissipation Capacity

The energy dissipation capacity of the columns (E_d) is associated with the area under the load-deformation relationship. To simplify estimation of E_d, the load-deformation relationship is idealized by an elastic perfectly plastic curve shown in Fig. 5.10. E_d is given by:

$$E_d = \frac{1}{2} P_u \delta_y + P_u (\delta_u - \delta_y) \tag{5.3}$$

where, δ_u and δ_y are the axial ultimate and yielding deformation, respectively. δ_y is taken as $\delta_{75\%}$/0.75 where, $\delta_{75\%}$ is the axial deformation corresponding to 75% of the ultimate axial load (Tao et al. 2007).

E_d is evaluated for the tested column specimens and is presented in Table 5.2. The energy dissipation capacity of the composite columns was 15-25 times greater than that of the corresponding bare steel columns indicating effectiveness of the composite system to be utilized in enhancing energy dissipation capacity. It was found that E_d generally decreased with increased column height.

5.3.3.5. Initial Eccentricity

The strength enhancement of the long column specimens is highly dependent on the initial eccentricity in loading that can occur due to the geometric imperfection, out-of-straightness of the specimens or misalignments in the test setup (Shaat and Fam 2006a). As previously mentioned, rupture of the FRP tube in the compression side of specimen *R-1.0* occurred due to initial eccentricity that caused significant bending of the column prior to failure. Behavior of columns can be evaluated more accurately knowing the amount of the initial eccentricity inherent in test of the specimens. Initial eccentricity can be estimated based on the minimum and maximum axial strain recordings at the column mid-height as shown in Fig. 5.11. The moment at the mid-height cross section is then given by:

$$M = P\delta' \tag{5.4}$$

where, P is the applied load and δ' is the maximum initial eccentricity recorded at the column mid-height. The moment-curvature relationship in the elastic range requires that:

$$\varphi = \frac{M}{EI} \tag{5.5}$$

where, φ is the curvature and EI is the equivalent flexural stiffness of the composite column specimen calculated as:

$$EI = (EI)_{St.} + (EI)_{Conc.} + (EI)_{Tube} \tag{5.6}$$

where, $(EI)_{St.}$, $(EI)_{Conc.}$ and $(EI)_{Tube}$ are the flexural stiffness of the steel column, concrete and GFRP tube, respectively. E and I denoted the elastic modulus and moment of inertia, respectively. Elastic modulus of the concrete ($E_{Conc.}$) is evaluated using the equation provided in the Canadian Standards Association CSA A23.3-04 (CSA 2004) as:

$$E_{Conc.} = 4{,}500\sqrt{f'_{co}} \tag{5.7}$$

where, f'_{co} is the compressive strength of unconfined concrete in MPa. Curvature at mid-height of the specimens is estimated by:

$$\varphi = \frac{\varepsilon_{\max} - \varepsilon_{\min}}{d} \tag{5.8}$$

where, ε_{max} and ε_{min} are the maximum and minimum recorded axial strains at the mid-height of the column specimens and d is the outer diameter of the FRP tube. Ultimate curvature is evaluated in Fig. 5.12 based on the ε_{max} and ε_{min} values recorded on the inner (compression) and outer (tension) sides of the composite column specimens, respectively. Axial strains are normalized with respect to the strain of the FRP tube at rupture due to axial compression ($\varepsilon_{a,f}$=0.013). The largest ultimate curvature was recorded in specimen *R-1.0* which occurred due to the large initial eccentricity of this composite column specimen previously mentioned. The rest of the composite column specimens showed similar curvature at failure.

Substituting Eqs. (5.4) and (5.8) into Eq. (5.5) results in:

$$\frac{\varepsilon_{\max} - \varepsilon_{\min}}{d} = \frac{P\delta'}{EI} \tag{5.9}$$

The maximum initial eccentricity about the week axis of the column specimens was evaluated using a linear regression based on Eq. (5.9) as shown in Table 5.2. Specimens *R-1.0*, *R-2.5* and *R-3.0* exhibited relatively large initial eccentricities compared to the rest of the column specimens. Large initial eccentricities were expected in test of the long column specimens (*R-2.5* and *R-3.0*) due to the higher out-of-straightness of the

specimens compared to the short columns. However, eccentricity in test of the specimen *R-1.0* is attributed to the misalignments in the test setup.

5.3.3.6. Load versus Lateral Deflections

Lateral deflections increased continuously during the loading process (due to the initial eccentricity of the column specimens) and grew rapidly near failure (when the column specimens reached approximately 80% of their strength). As sample results, Fig. 5.13 shows the load versus the lateral deflection relationships for specimens *R-1.5* and *R-3.0* compared to corresponding bare steel specimens. Lateral deflection along the height of the column is also shown for specimen *R-3.0* at different axial load levels in Fig. 5.14. The axial load level is normalized and represented by n which is the ratio of the applied load to the ultimate load.

The higher initial slope of the load versus lateral deflection relationships of the composite column specimens compared to the corresponding bare steel specimens (see Fig. 5.13) indicates effectiveness of the proposed composite system in providing stability against lateral deflections by increasing flexural stiffness of the columns. Following initial bending of the column specimens due to the inherent eccentricity, the lateral deflections increased continuously about both the weak and the strong axes of the column specimens. However, the increase was significantly larger for bending about the week axis at axial load levels near the ultimate load.

5.3.3.7. Buckling Strength Relationship

The buckling strength relationship shows the column strength as a function of its slenderness ratio. These diagrams can be used as effective design aids. To develop the buckling strength relationship for the composite columns in this study, a slenderness parameter proposed by Kato (1996) was used, which is given by:

$$\lambda = \sqrt{\frac{P_y}{P_{cr}}} \tag{5.10}$$

where, P_y is the cross sectional compressive strength and P_{cr} is the elastic Euler buckling strength. P_y is taken as the compressive strength of the short columns which failed due to compressive failure of the cross section. P_{cr} is calculated as:

$$P_{cr} = \frac{\pi^2 (EI)}{(kL)^2} \tag{5.11}$$

where, EI is the flexural stiffness and k is taken as 1.0 for pin-pin boundary conditions. An equivalent flexural stiffness, defined in Eq. (5.6), was used for the composite columns.

Figure 5.15 shows the buckling strength relationship for the tested column specimens. In this figure, the compressive strength is normalized by the cross sectional strength (P_y) of the columns. The Euler buckling relationship is also plotted in Fig. 5.15. Buckling strength relationship can also be used to determine the slenderness ratio limit in classifying the specimens as short or long composite columns. Mirmiran et al. (2001) suggested that a column can be classified as a short column if its compressive strength is greater than 95% of the cross sectional compressive strength in compliance with the standard of practice for the reinforced concrete columns (MacGregor et al. 1970). Based on the strength criteria suggested by Mirmiran et al. (2001) a slenderness parameter limit of $\lambda = 0.2$ was obtained from Fig. 5.15 below which the composite column specimens are classified as short columns. Compressive strength of the composite column specimens with $\lambda \geq 0.2$ was influenced by stability and ,consequently, they are classified as long columns. Comparison of the buckling strength and Euler buckling relationships for the long composite column specimens shows that all of columns failed below the elastic Euler buckling strength and are subsequently classified as intermediate long columns.

Figure 5.15 also shows significantly smaller slenderness parameter values and larger normalized compressive strength for the composite column specimens compared to the corresponding bare steel specimens demonstrating the effectiveness of the proposed composite system in enhancing stability of the columns as previously observed in evaluating lateral deflections from Fig. 5.13.

The buckling strength relationship of the steel column specimens in Fig. 5.15 indicates that the control specimens tested in this study covered various groups of steel columns (in terms of the slenderness) that exist in practice, i.e., short, intermediate long and slender columns.

5.3.3.8. Failure Modes

Photographs of the tested specimens are shown in Fig. 5.16. The specimens generally failed due to cross-section failure or loss of stability (overall buckling) in short and long column specimens, respectively. Failure of the short composite specimen *R-0.5* was associated with rupture of the FRP tube in the circumferential direction followed by crushing and spalling of the concrete core. Failure of the remainder of the composite column specimens occurred due to overall buckling associated with considerable bending of the specimens.

At the onset of overall buckling, the maximum and minimum axial strain recordings on the FRP tube, presented in Fig. 5.11, diverged from the average value and the minimum axial strain increased in the tension direction. Fig. 5.11 shows that in all the composite column specimens the maximum compressive strain at failure exceeded the elastic axial strain limit (taken as 0.002) indicating inelastic overall buckling of the long composite columns, which agrees with the corresponding buckling strength relationship in Fig. 5.15.

In addition to the FRP tube rupture, crushing of concrete and local buckling of the steel section on the compression side of the column was observed in the specimens *R-1.0* and

R-1.5 after removal of the FRP tube whereas, no significant sign of damage of the FRP tube or the concrete core was observed in specimens *R-2.0*, *R-2.5* and *R-3.0*.

Failure of the short steel column specimen *C-0.5* occurred due to yielding of the entire cross section followed by local buckling of the steel flanges and web. The long steel specimens *C-1.5* and *C-3.0* failed due to inelastic and elastic overall buckling, respectively, based on the maximum compressive strain value at failure presented in Fig. 5.11. Specimen *C-3.0* returned to its undeflected shape after unloading as shown in Fig. 5.16.

5.4. Summary and Conclusions

The effect of slenderness ratio on the behavior of a FRP-encased steel-concrete composite column was investigated. The composite column specimens were constructed by placing a FRP tube around a steel column and the void between the steel section and the FRP tube was subsequently filled with concrete. The proposed composite system may also be applied in retrofit of existing steel columns to increase the load carrying capacity, axial stiffness and energy dissipation capacity.

Nine column specimens were tested in the experimental program, six were composite column specimens and the remaining three were bare steel column control specimens tested for comparative purposes. The steel column specimens comprised of short, intermediate long and slender columns varying between 500 mm and 3,000 mm in height with a slenderness parameter of 0.3 and 1.6, respectively. Slenderness parameter of the corresponding composite column specimens was between 0.1 and 0.9.

The FRP tube provided significant confinement to the concrete in the short composite column specimens, which resulted in 80% increase in the compressive strength of the concrete. Composite column specimens having a slenderness parameter of greater than

0.6 failed due to loss of stability at small axial strains prior to efficient confinement activation.

The ratio of the compressive strength, elastic axial stiffness and energy dissipation capacity of the composite column specimens to those of the steel column specimens were 5-10, 4-6 and 15-25, respectively. The enhancement in the compressive strength of the composite column specimens increased with the height of the specimens. Moreover, elastic axial stiffness was not influenced by confinement.

Failure of the short steel column specimen having a slenderness parameter of 0.3 occurred due to yielding of the entire cross section followed by local buckling of the steel flanges and web. Failure of the short composite column specimen having a slenderness parameter of 0.1 occurred due to the rupture of the FRP tube under lateral tension followed by crushing and spalling of the concrete. The steel and composite column specimens having a slenderness parameter of greater than 0.3 and 0.1, respectively, failed by overall buckling due to the loss of stability.

Using the buckling strength relationship, a slenderness parameter limit of 0.2 was established for the composite columns below which the columns are classified as short columns that are expected to fail due to loss of cross sectional capacity. The proposed composite system significantly reduced the slenderness parameter of long steel column specimens by providing stability against overall buckling resulting in enhanced compressive strength in the composite column specimens.

Appendix 5.1. Notation

The following symbols are used in this paper:

d = outer diameter of the FRP tube;

$D.I.$ = ductility index;

δ = maximum initial eccentricity recorded at mid-height of the columns;

δ_u = ultimate axial deformation;

δ_y = yielding axial deformation;

$E_{a,t}$ = axial modulus of the FRP tube;

$E_{l,t}$ = lateral modulus of the FRP tube;

$E_{Conc.}$ = elastic modulus of the concrete;

$\varepsilon_{a,t}$ = axial strain of the FP tube at rupture under axial compression;

$\varepsilon_{au,t}$ = ultimate axial strain in the FRP tube;

$\varepsilon_{l,t}$ = lateral tensile strain of the FRP tube at rupture under unidirectional lateral tension;

$\varepsilon_{lu,t}$ = ultimate lateral strain in the FRP tube;

ε_{max} = maximum recorded axial strain at the mid-height of the column specimens;

ε_{min} = minimum recorded axial strain at the mi-height of the column specimens;

ϕ = curvature;

f'_{cc} = compressive strength of the confined concrete;

f'_{co} = compressive strength of unconfined concrete;

H = height of the column specimen;

I = moment of inertia;

k = effective length factor;

L = unbraced length for column buckling about the week axis;

λ = slenderness parameter;

M = applied moment at the mid-height cross section;

P = applied axial load;

P_y = cross sectional compressive strength;

P_{cr} = elastic Euler buckling strength;

ν = Poisson's ratio;

$\sigma_{a,t}$ = axial compressive strength of the FRP tube;

$\sigma_{au,t}$ = ultimate axial stress in the FRP tube;

$\sigma_{l,t}$ = lateral tensile strength of the FRP tube;

$\sigma_{lu,t}$ = ultimate lateral stress in the FRP tube;

Appendix 5.2. References

American Association of State Highway and Transportation Officials (AASHTO). (2001). "Weekly transportation report." *AASHTO Journal*, 101(1), 1-8.

Bakis, C. E., Bank, L. C., Brown, V. L., Cosenza, E., Davalos, J. F., Lesko, J. J., Machida, A., Rizkalla, S. H., and Triantafillou, T. C. (2002). "Fiber-reinforced polymer composites for construction-State-of-the-art review" *J. Compos. for Constr.*, 6(2): 73-87.

Bank, L. C. (2006). "Composites for construction." *John Wiley & Sons*, Hoboken, New Jersey.

Cement Association of Canada (2006). "Concrete Design Handbook", Third Edition, Ottawa, Ontario.

Cheng, L., and Karbhari, M. (2006). "New bridge systems using FRP composites and concrete: A state-of-the-art review." *J. Prog. Struct. Engng. Mater.*, 8: 143-154.

Canadian Institute of Steel Construction (2008). "Handbook of Steel Construction." Ninth Edition, Toronto, Ontario.

CSA. (2009). "Limit states design of steel structures. Standard CAN/ CSA S16-09." Canadian Standards Association, Mississauga, Ont.

CSA. (2004). "Design of concrete structures. CSA standard A23.3-04." Canadian Standards Association, Mississauga, Ont.

El Damatty, A. A., Abushagur, M., and Youssef, M. A. (2005). "Rehabilitation of composite steel bridges using GFRP plates." *J. Appl. Compos. Mater.*, 12(5): 309-325. .

Fam, A., Witt, S., and Rizkalla, S. (2006). "Repair of damages aluminum truss joints of highway overhead sign structures using FRP." *J. Constr. Build. Mater.*, 20: 948-956.

Karimi, K., Tait, M. J., and El-Dakhakhni, W. W. (2010). "Testing and modeling of a novel FRP-encased steel-concrete composite column." *J. Compos. Struct.*, submitted manuscript COST-S-10-00699.

Kato, B. (1996). "Column curves of steel-concrete composite members" *J. Constr. Steel Res.*, 39(2): 121-135.

Lam, L., and Teng, J. G. (2003a). "Design-oriented stress-strain models for FRP-confined concrete." *J. Constr. and Build. Mat.*, 17, 471-489.

Lam, L., and Teng, J. G. (2003b). "Design-oriented stress-strain model for FRP-confined concrete in rectangular columns." *J. Reinf. Plast. Compos.*, 22(13), 1149-1186.

MacGregor, J. G., Breen, J. E., and Pfrang, E. O. (1970). "Design of slender columns." *ACI J.*, 67(1): 6-28.

Mirmiran, A., Shahawy, M., and Beitleman, T. (2001). "Slenderness limit for hybrid FRP-concrete columns." *J. Compos. for Constr.*, 5(1): 26-34.

Nanni, A., and Bradford, N. M. (1995). "FRP jacketed concrete under uniaxial compression." *J. Constr. Build. Mater.*, 9(2): 115-124.

Neale, K. W. (2000). "FRPs for structural rehabilitation: a survey of recent progress." *J. Prog. Struct. Engng. Mater.*, 2(133): 133-138.

Ozbakkaloglu, T., and Oehlers, D. J. (2008). "Manufacture and testing of a novel FRP tube confinement system." *J. Eng. Struct.*, 30: 2448–2459.

Phares, B. M., Wipf, T. J., Klaiber, F. W., Abu-Hawash, A., and Lee, Y. S. (2003). "Strengthening of steel girder bridges using FRP." *Proc., the Mid-Continent Transportation Research Symposium*, Ames, Iowa.

Popovics, S. (1973). "A numerical approach to the complete stress-strain curves for concrete." *J. Cement and Concr. Res.*, 3(5): 583-599.

Shaat, A., Schnerch, D., Fam, A., and Rizkalla, S. (2004). "retrofit of steel structures using fiber-reinforced polymers (FRP): State-of-the-art." *Transportation research board (TRB) annual meeting*, Washington, D.C., CD-ROM (04-4063).

Shaat, A., and Fam., A. (2006a). "Axial loading tests on short and long hollow structural steel columns retrofitted using carbon fibre reinforced polymers." *Can. J. Civ. Eng.*, 33: 458-470.

Shaat, A., and Fam, A. (2006b). "Rehabilitation of damaged steel-concrete composite beams using high modulus CFRP sheets." *Proc., the 7th International Conference on Short and Medium Span Bridges*, Montreal, Canada.

Tao, Z., Han, L. H., and Zhao, X. L. (1998). "Behavior of square concrete filled steel tubes subjected to axial compression." *Proc., the Fifth International Conference on Structural Engineering for Yong Experts*, Shenyang, PR China: 61-67.

Teng., J. G., and Hu., T. M. (2007). "Behavior of FRP-jacketed circular steel tubes and cylindrical shells under axial compression." *J. Constr. Build. Mater.*, 21: 827-838.

Triantafillou, T. C. (1998). "Strengthening of structures with advanced FRPs." *J. Prog. Struct. Mater. Eng.*, 1(2): 126-134.

Yu, Z. W., Ding, F. X., and Cai, C. S. (2007). "Experimental behavior of circular concrete-filled steel tube stub columns." *J. Constr. Steel Res.*, 63: 165-174.

Table 5.1. Mechanical properties and dimensions of FRP tube

Nominal Pipe Size		(mm)	200
Inside Diameter		(mm)	211
Outside Diameter		(mm)	219
Structural Wall Thickness		(mm)	3.2
Lateral Tensile Strength		(MPa)	275
Lateral Tensile Modulus		(GPa)	15.9
Axial Compressive Strength		(MPa)	138
Axial Compressive Modulus		(GPa)	10.3
Axial Tensile Strength		(MPa)	138
Axial Tensile Modulus		(GPa)	10.3
Poisson's Ratio	$\frac{\nu_{la}}{\nu_{al}}$		0.11 0.19

Table 5.2. Experimental results

Test I.D.	H	δ	Compressive Strength		Elastic Axial Stiffness		Ultimate Strain			f'_{cc}		E_d	
							Axial		Lateral				
	(mm)	(mm)	(kN)	Increase (Ratio)	(kN/ mm)	Increase (Ratio)	(με)	Increase (Ratio)	(με)	(MPa)	$\frac{f'_{cc}}{f'_{co}}$	(kJ)	Increase (Ratio)
C-0.5	500	N/A	726	N/A	753	NA	4,034	N/A	N/A	N/A	N/A	1.1	N/A
C-1.5	1500	0.6	497	N/A	271	NA	1,509	N/A	N/A	N/A	N/A	0.6	N/A
C-3.0	3000	0.7	268	N/A	123	NA	748	N/A	N/A	N/A	N/A	0.3	N/A
R-0.5	500	0.2	3,821	5.26	3,244	4.31	11,700	2.90	11,400	86.7	1.80	21.6	19.6
R-1.0	1000	4.9	3,040	5.05	1,324	3.83	9,388	N/A	8,986	64.5	1.33	24.2	N/A
R-1.5	1500	0.8	2,935	5.91	1,097	4.05	3,277	2.17	1,092	63.7	1.31	9.3	15.5
R-2.0	2000	0.5	2,545	7.71	991	5.73	2,840	N/A	937	53.6	1.11	8.6	N/A
R-2.5	2500	3.7	2,295	9.60	791	5.73	2,369	N/A	536	46.3	0.96	8.6	N/A
R-3.0	3000	3.0	2,251	8.40	570	4.63	1,903	2.54	420	44.9	0.93	7.4	24.7

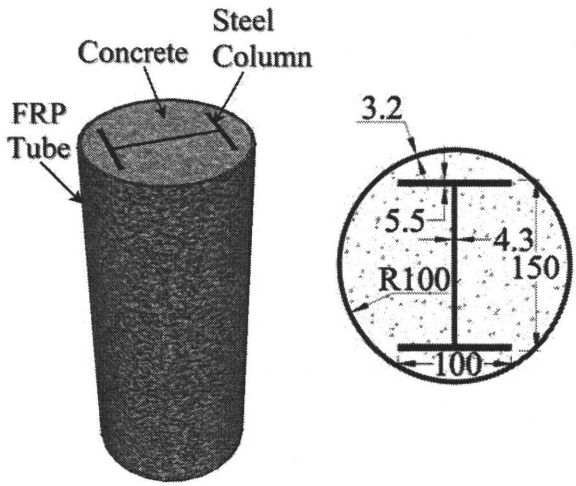

Figure 5.1. Schematic of the proposed composite columns (all dimensions in *mm*)

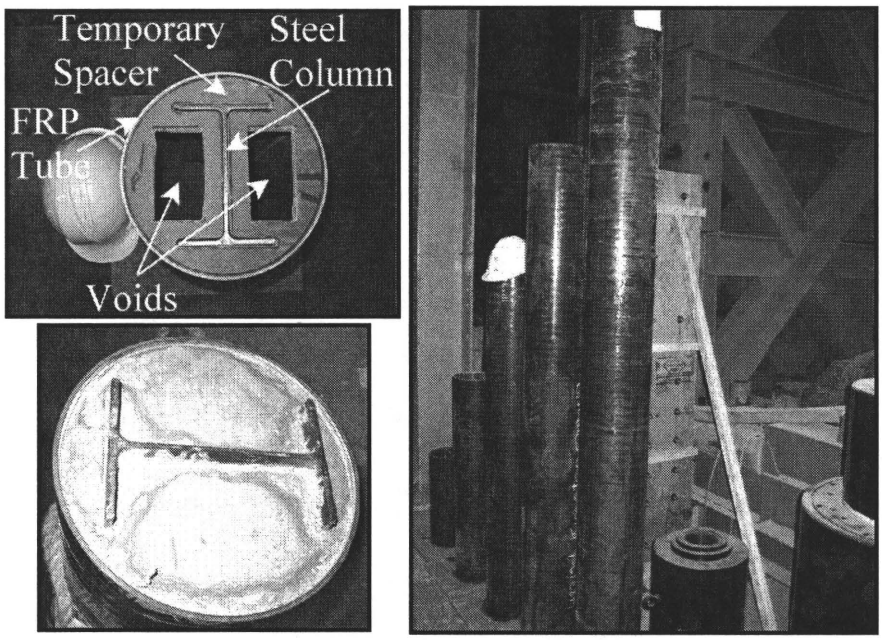

Figure 5.2. Photographs of the composite specimens before and after pouring the concrete

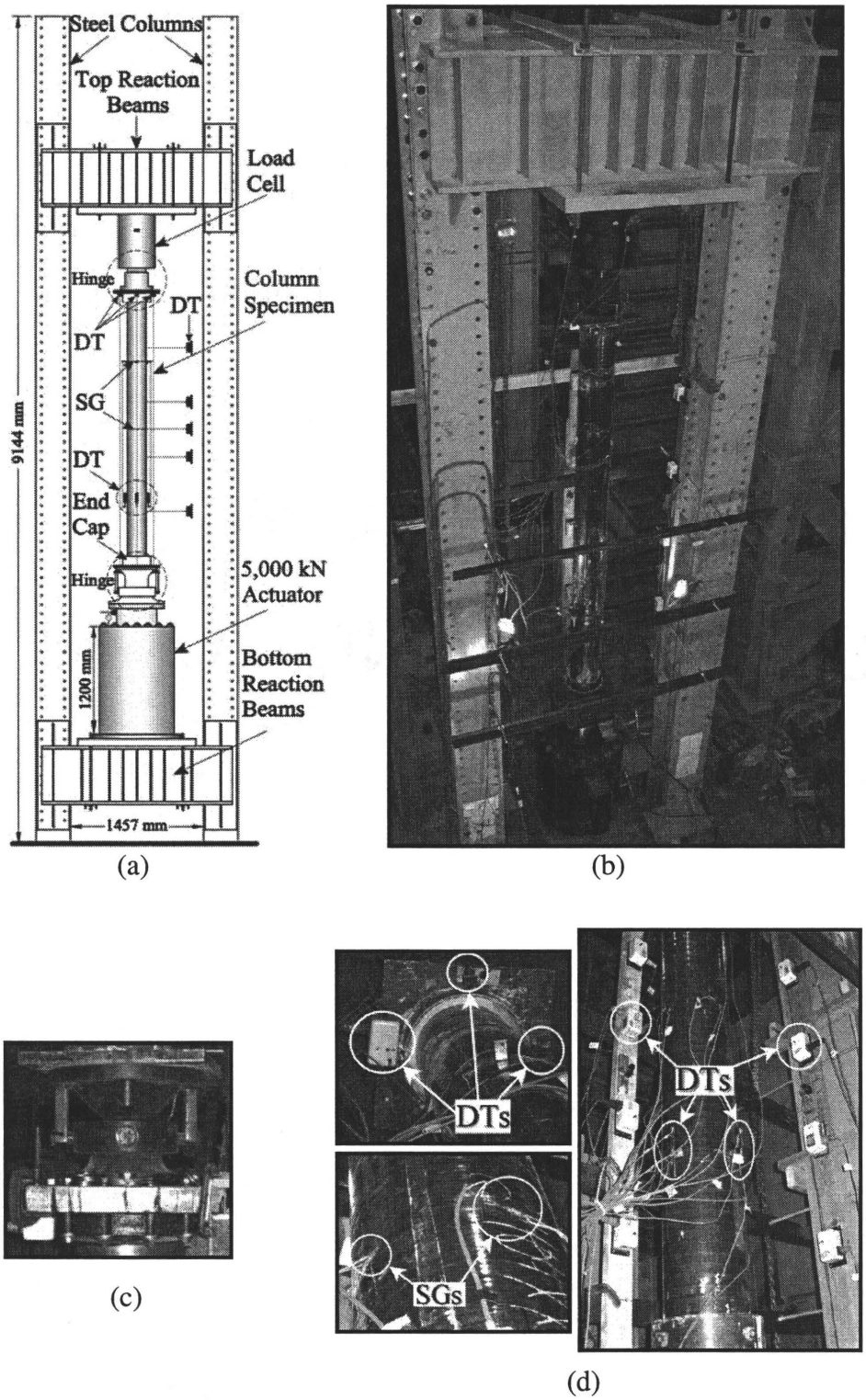

Figure 5.3. (a) Schematic of the test setup (b) photograph of the test setup (c) Bottom swivel representing pin support (d) instrumentation

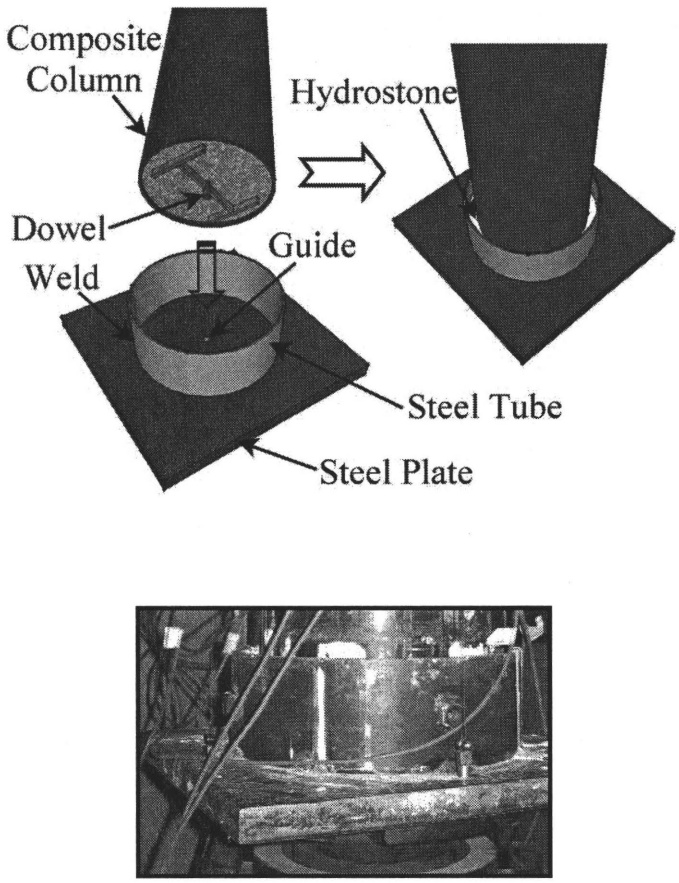

Figure 5.4. Method used to cap ends of the specimen to ensure uniform axial load over the entire cross section

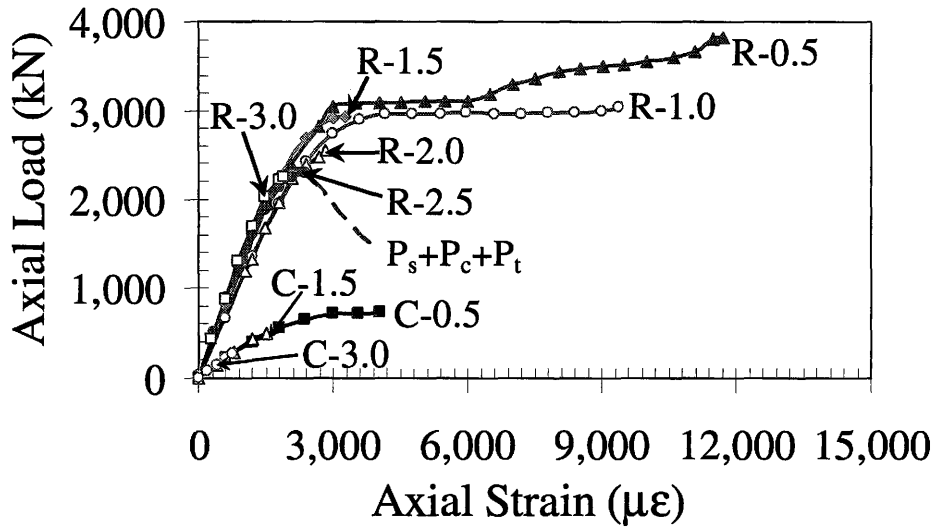

Figure 5.5. Load versus average axial strain curves for the tested specimens

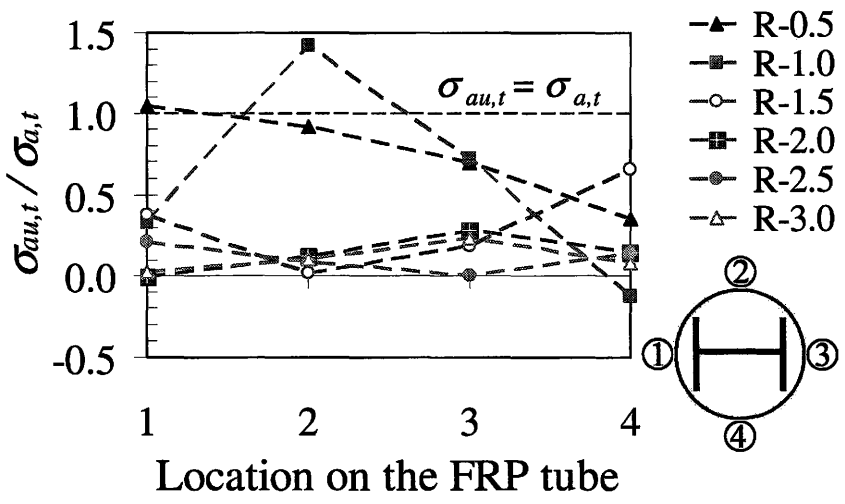

(a)

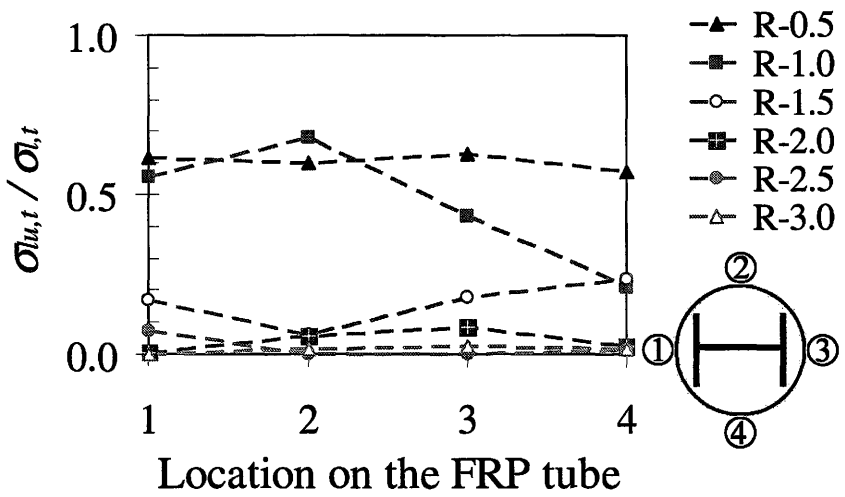

(b)

Figure 5.6. State of stress in the FRP tube at the columns mid-height at failure of the specimens (a) normalized compressive axial stress (b) normalized tensile lateral stress

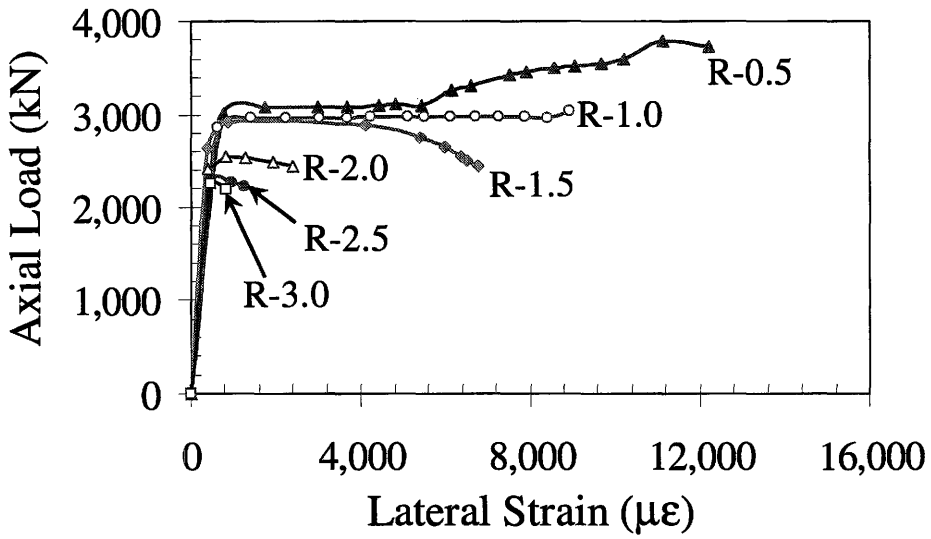

Figure 5.7. Load versus average lateral strain at the mid-height

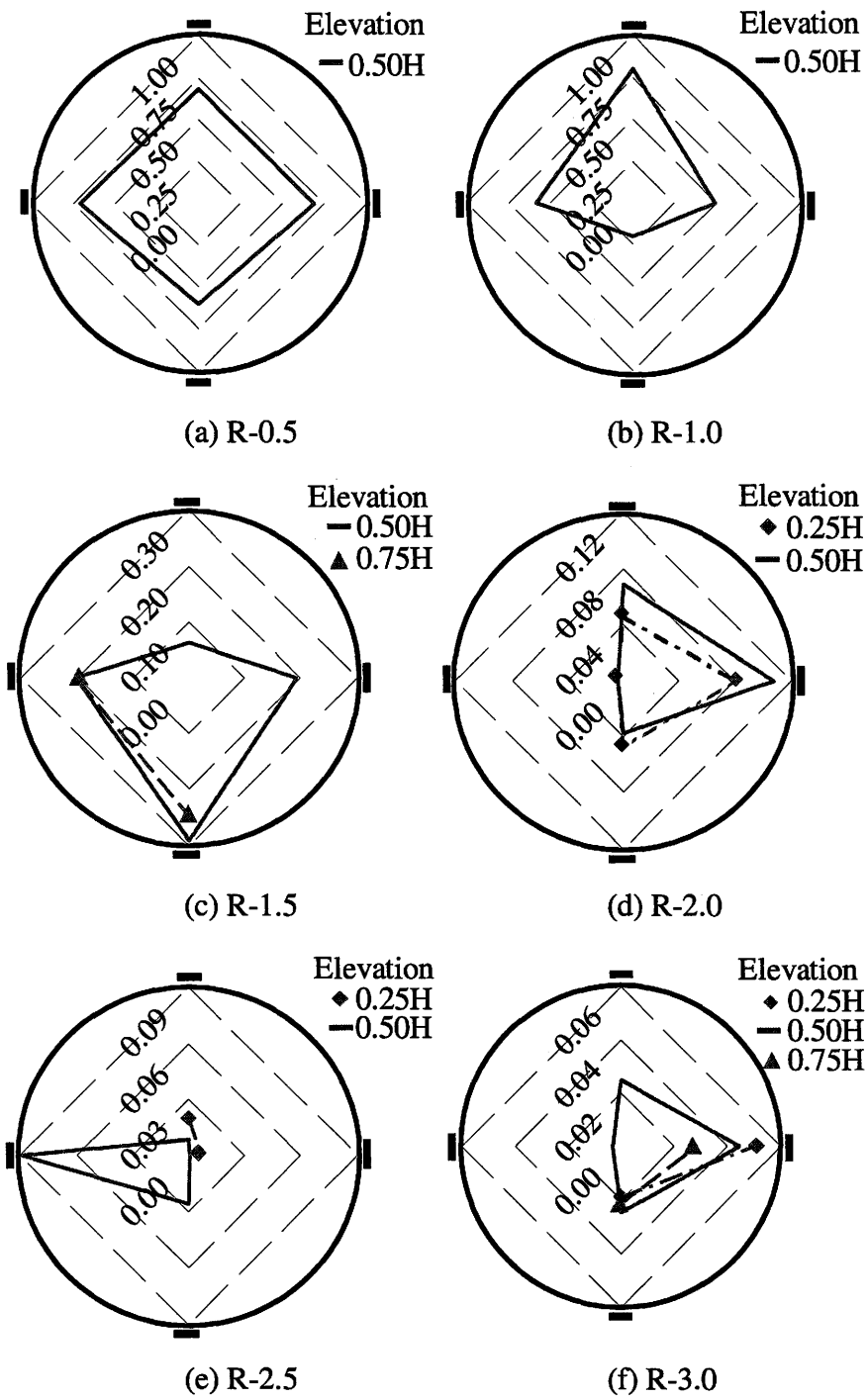

Figure 5.8. Normalized ultimate lateral strains ($\varepsilon_{lu}/\varepsilon_{l,t}$) recorded on the FRP tube at difference elevations

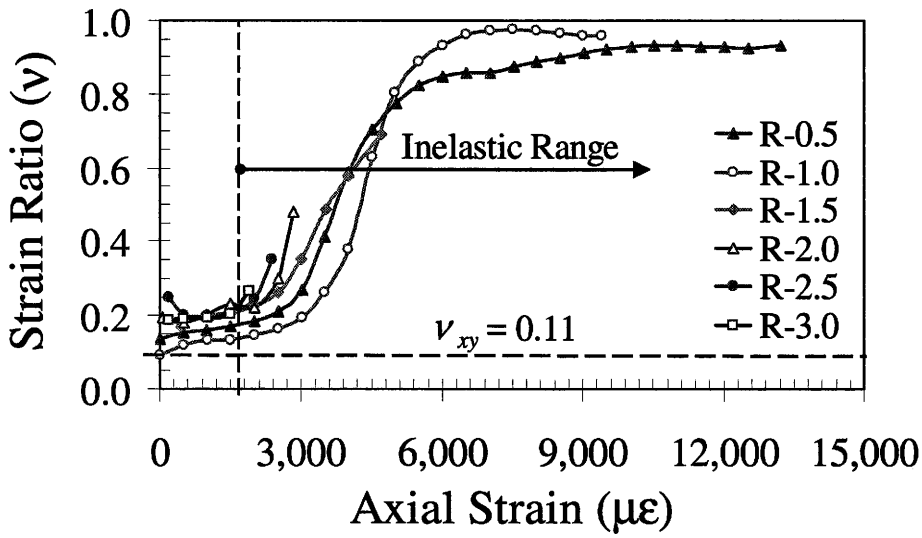

Figure 5.9. Comparison of the strain ratio (ν) versus axial strain diagrams obtained for the tested specimens

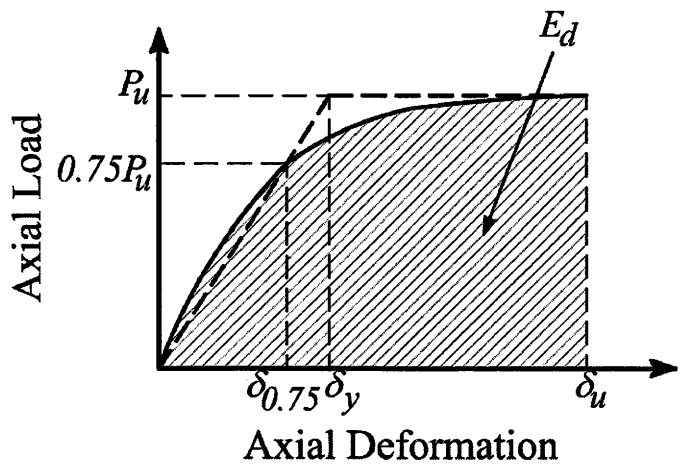

Figure 5.10. Definition of energy dissipation capacity

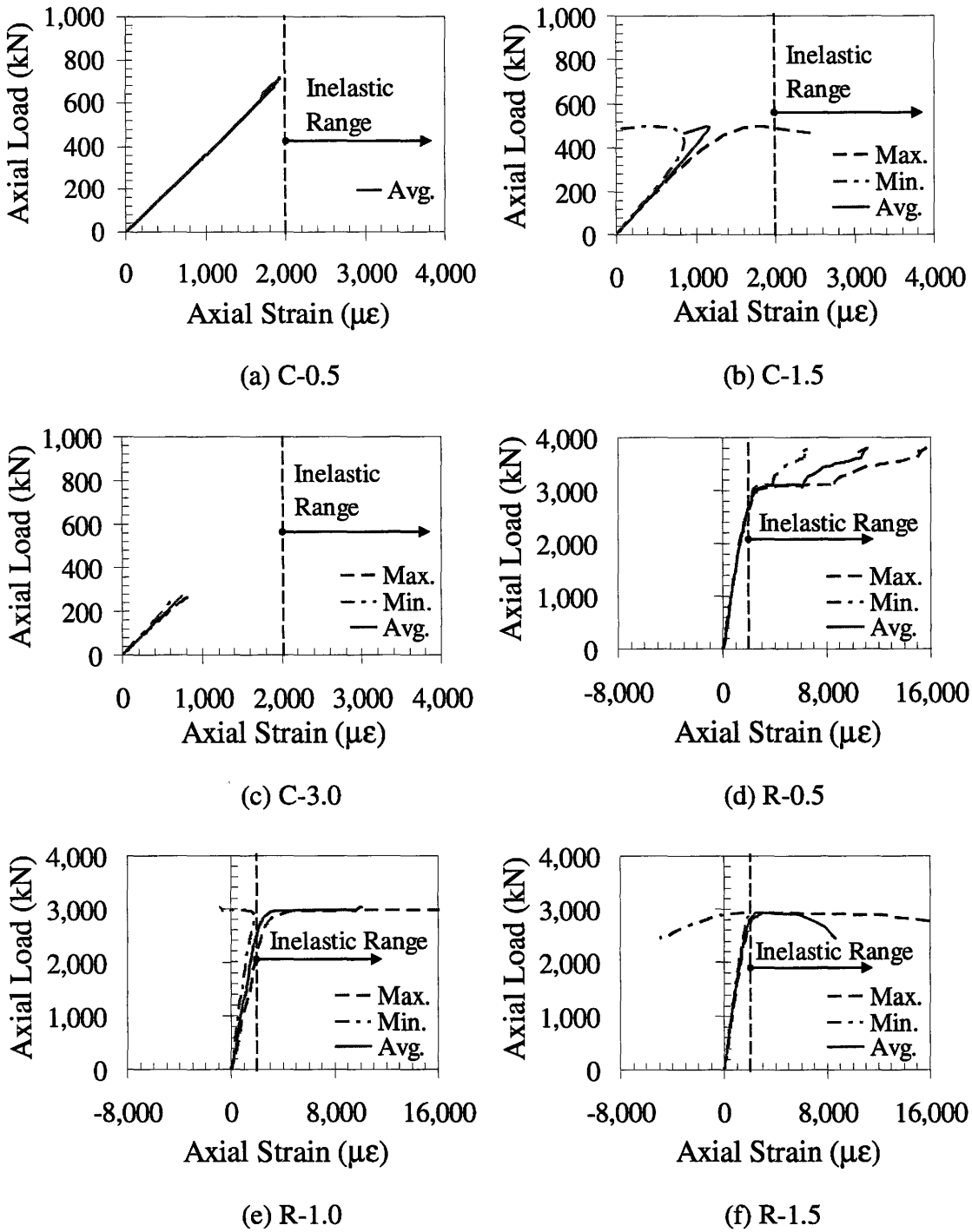

Figure 5.11. Axial load versus vertical strain gauges readings at the mid-height

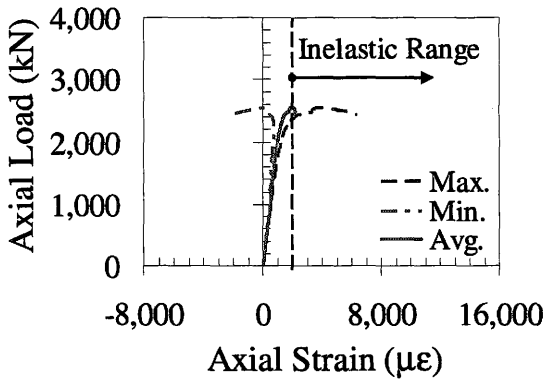

(g) R-2.0

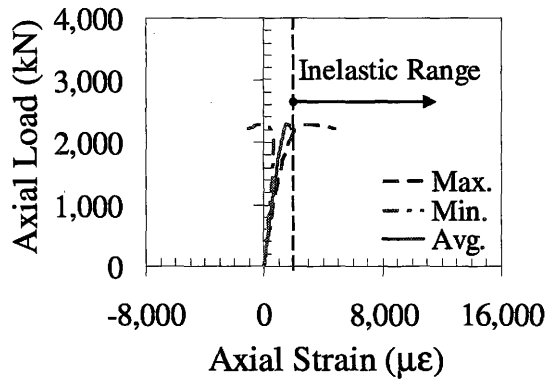

(h) R-2.5

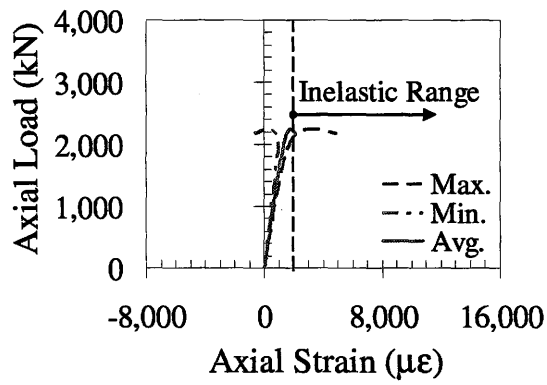

(i) R-3.0

Figure 5.11. Continued

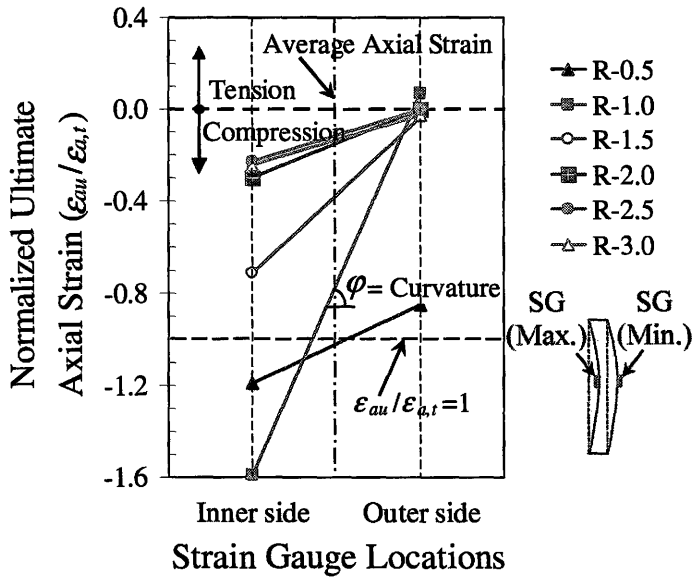

Figure 5.12. Axial strains at failure recorded on the compression and tension side of the specimens

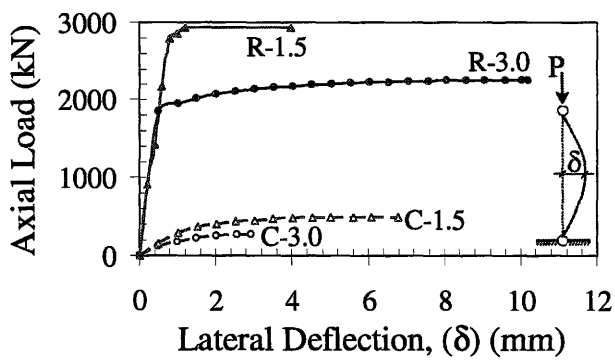

Figure 5.13. Axial load versus lateral deflection about the weak axis at the mid-height

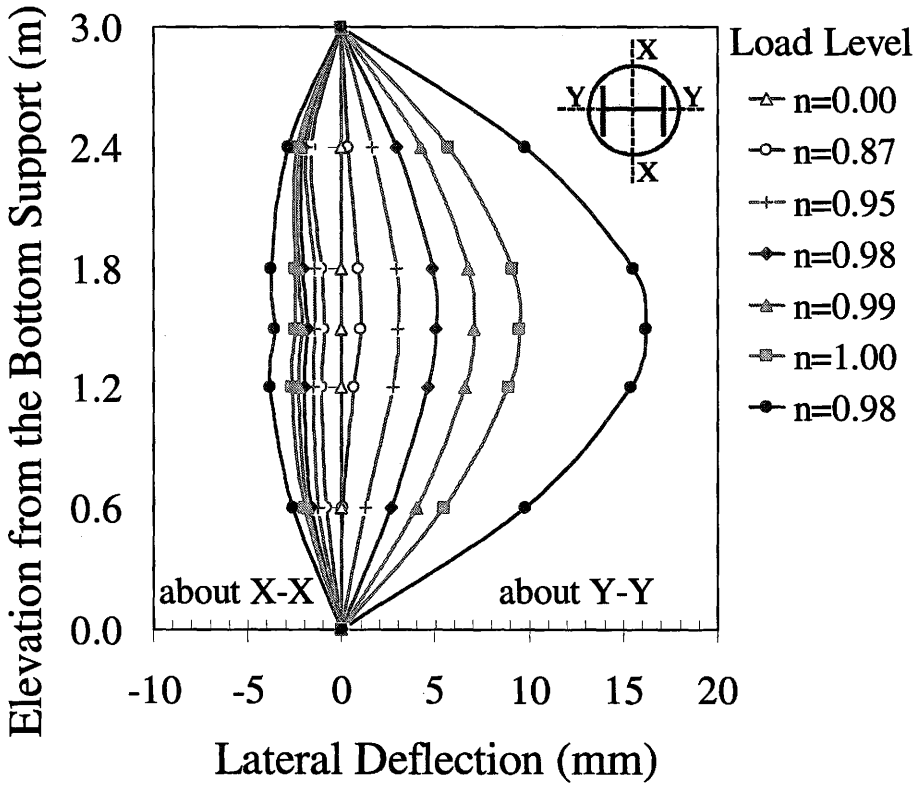

Figure 5.14. Lateral deflection along the height at the different axial load levels in Specimens *R-3.0*

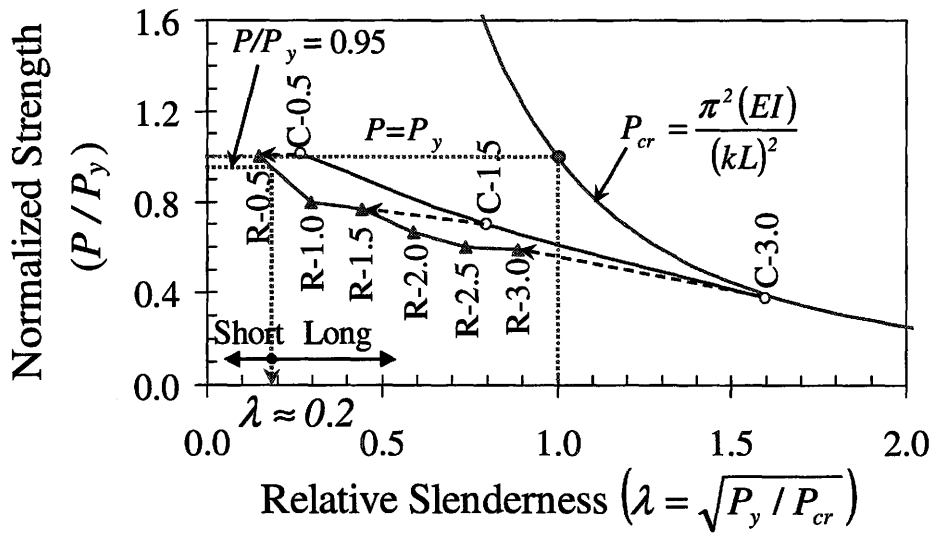

Figure 5.15. Normalized buckling strength curve for the columns specimens

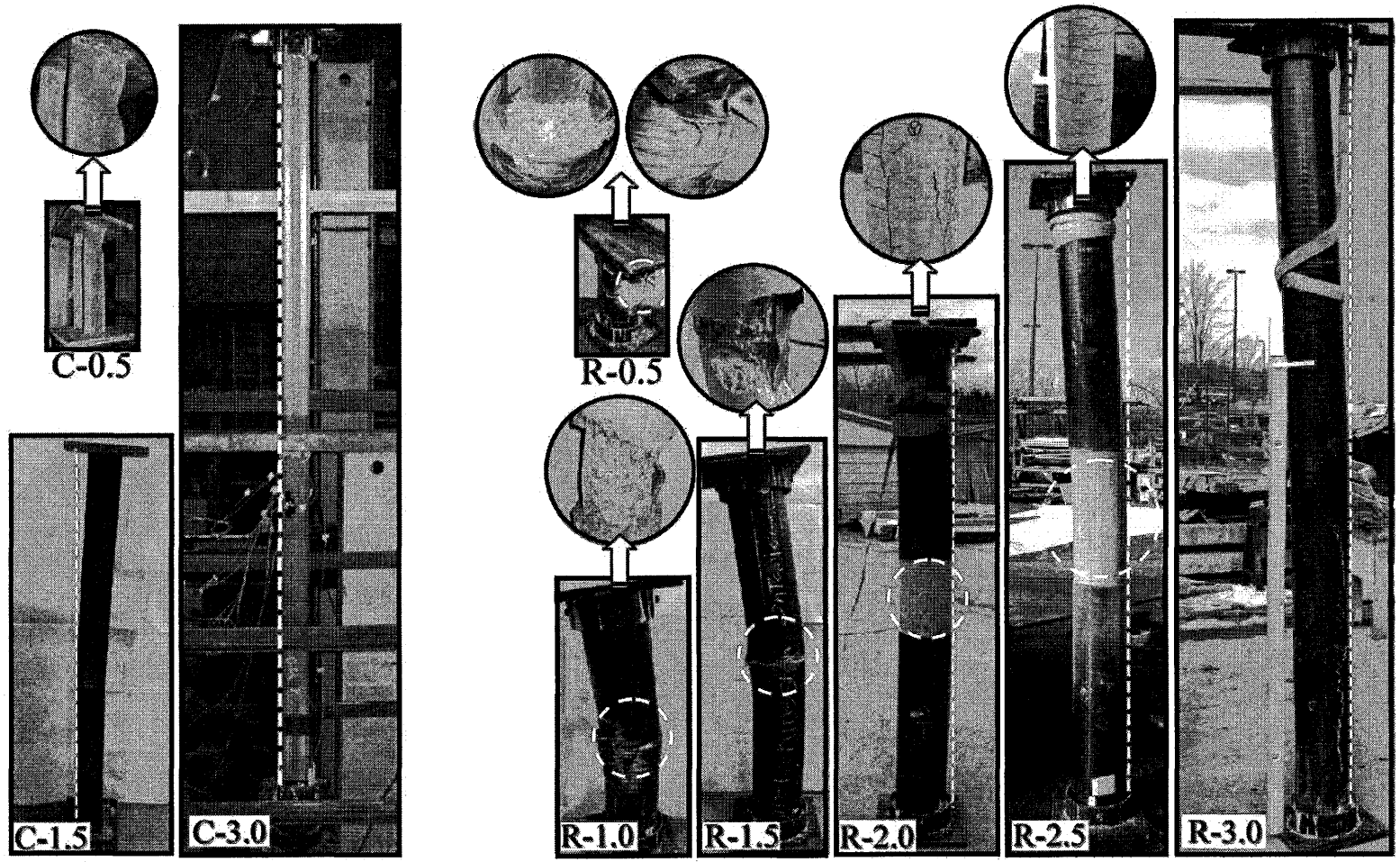

Figure 5.16. Photographs of the tested specimens after unloading

Chapter 6: Analytical Modeling and Design of a Novel FRP-encased Steel-Concrete Composite Column with Various Slenderness Ratios

6.1. Summary

A composite column comprised of steel, concrete and fiber reinforced polymer (FRP) tube is presented. The confinement and composite action between the constituent materials results in the enhanced compressive strength, ductility and energy dissipation capacity of the proposed composite columns compared to traditional reinforced concrete (RC) columns. Due to the presence of the FRP tube, current design methods for concrete-filled steel tubes (CFST) or concrete-encased steel (CES) columns are not directly applicable. An analytical model is developed to predict the behavior of the proposed composite columns with various slenderness ratios. Model results are found to be in good agreement with the experimental results from test of six columns ranging between 500 mm and 3,000 mm in height. A parametric study is conducted to investigate influence of the column diameter, FRP tube thickness, axial compressive modulus of the FRP tube and steel-to-concrete ratio on the capacity relationships and slenderness limits of the proposed composite columns. A simple design equation is proposed to predict the compressive capacity of the columns.

Keywords: analytical techniques, buckling, composite columns, confinement, design, fiber reinforced polymer (FRP), guidelines, slenderness ratio, tubes

6.2. Introduction

Fiber Reinforced Polymer (FRP) tubes are increasingly being utilized in the construction of structural elements due to their high strength to weight ratio and corrosion resistance. In construction of columns, FRP is primarily used as an external jacket to provide confinement to the concrete core (Teng et al. 2007; Ozbakkaloglu and Oehlers 2008; Mohamed and Masmoudi 2010). Confinement enhances the compressive strength of the concrete-filled FRP tubular (CFFT) columns, which reduces the required column cross-section compared to that of conventional reinforced concrete (RC) columns. Furthermore, replacing the external steel tube utilized in a concrete-filled steel tubular (CFST) column with a corrosion resistant FRP tube enhances column durability.

In an effort to integrate the advantages of various construction materials, Karimi et al. (2010a) proposed a novel composite column. The composite column consists of a steel section surrounded by a concrete-filled FRP tube, which eliminates the need for lateral ties. A schematic view of the composite column is shown in Fig. 6.1(a). The confinement and composite action between the constituent materials results in enhanced behavior. The FRP tube provides confinement to the concrete core and the concrete increases the buckling capacity of the steel column. Furthermore, the FRP protects the column and improves its durability. The proposed composite columns have higher ductility than CFFT columns due to the addition of steel.

A substantial amount of research focusing on modeling the behavior of short composite columns has been conducted (Safi et al. 1999; Therlault and Neale 2000; Binici and Mosalam 2007; Eid and Paultre 2008). However, few studies have concentrated on the development of analytical models for long composite columns where overall buckling governs the failure (Mirmiran et al. 2001; Liu and Nanni 2005; Shaat and Fam 2007). The primary objective of this study is to develop an analytical model to predict the behavior of the proposed FRP encased steel-concrete composite columns with various slenderness ratios. Analytical model predictions are subsequently compared with the experimental test

results conducted on six composite columns specimens. The analytical model is utilized in establishing slenderness limits and developing a design equation for the proposed composite columns.

6.3. Experimental Program

A total of six composite columns were tested during the experimental program. The columns ranged between the 500 mm and 3,000 mm in height. The specimens were constructed by placing a glass FRP (GFRP) tube around an I shaped steel column and the voids between the steel and the FRP tube were subsequently filled with concrete. Figure 6.1(b) shows a photograph and cross sectional dimensions of the tested columns.

The FRP tube was made of glass fibers. Table 6.1 shows the mechanical properties of the FRP tube. The average compressive strength of the confined concrete at the time of testing was 48.3 MPa. The yield and ultimate tensile strength of the steel were 411 MPa and 526 MPa, respectively.

The composite columns were tested in a compression test apparatus capable of applying 5,000 kN axial loading and the boundary condition were pin-pin. Results from the experiments are summarized in Table 6.2 in terms of the compressive strength and ultimate axial strain, which decreased with increased column height. The detailed experimental program is reported elsewhere (Karimi et al. 2010b).

6.4. Analytical Modeling

The analytical model is based on an incremental technique proposed by Mirmiran et al. (2001). In this technique the Euler buckling load is evaluated based on the stiffness of the column at each axial strain increment and compared with the corresponding cross-sectional compressive strength. If the Euler buckling load is greater than the cross-sectional compressive strength for all the strain increments, failure occurs due to loss of cross-section capacity and the column is consequently classified as a short column. In

longer composite columns, the stability and cross-sectional strength diagrams intersect (also referred to as the intersection point). Stability diagrams show the Euler buckling load at each strain increment. The specimen fails due to overall buckling beyond the strain limit corresponding to the intersection point and is consequently classified as a long column. If the two diagrams intersect in the elastic limit (corresponding axial strain of less than 0.002) the column is classified as a slender composite column which fails due to elastic overall buckling. If the intersection point is located in the inelastic range, the column fails due to inelastic buckling and is classified as an intermediate long column.

The methodology used to develop the cross-sectional strength and stability relationships is explained in the following sections in detail.

6.4.1. Cross-Sectional Strength

Figure 6.2 shows a free body diagram of the composite column components. The compressive load corresponding to an axial strain increment is calculated by superimposing the separate contributions of the steel, the confined concrete and the FRP tube in the load carrying capacity given by:

$$P = \sigma_s A_s + \sigma_c A_c + \sigma_f A_f \tag{6.1}$$

where, σ_s, σ_c and σ_f are the axial stress in the steel, concrete and the FRP tube, respectively, and A_s, A_c and A_f are their corresponding areas.

In this model, the steel is assumed to be an elastic-plastic material with a strain-hardening behavior from the yield to the ultimate stress. In the proposed composite column, the FRP tube is under a bi-axial state of stress as shown in Fig. 6.2(b). The FRP is assumed to remain elastic in the axial and lateral directions for all the strain increments. The stresses in the FRP tube can be evaluated based on the mechanics of composite materials as (Bank 2006):

$$\sigma_f = \frac{E_f}{1-\nu_{al}\nu_{la}}\varepsilon_a + \frac{\nu_{al}E_f}{1-\nu_{al}\nu_{la}}\varepsilon_l \tag{6.2}$$

$$\sigma_l = \frac{\nu_{la}E_{f,l}}{1-\nu_{al}\nu_{la}}\varepsilon_a + \frac{E_{f,l}}{1-\nu_{al}\nu_{la}}\varepsilon_l \tag{6.3}$$

where, σ_f and σ_l are the axial and lateral stresses in the FRP tube, respectively, and ε_f and ε_l are the corresponding strains. $E_{f,l}$ is the lateral tensile modulus of the FRP tube material.

In evaluating the cross-section capacity, it is assumed that failure occurs due to rupture of the FRP tube, resulting in a loss of confinement. Rupture of the FRP tube can be assessed using the Tsai-Wu criterion, which is commonly used in evaluating the failure of composite materials (Daniel and Ishai 2006):

$$\left(\frac{1}{S_{l,t}} - \frac{1}{S_{l,c}}\right)\sigma_{lu} + \left(\frac{1}{S_{a,t}} - \frac{1}{S_{a,c}}\right)\sigma_{fu} + \frac{1}{S_{l,t}S_{l,c}}\sigma_{lu}^2 + \frac{1}{S_{a,t}S_{a,c}}\sigma_{fu}^2 - \frac{1}{\sqrt{S_{a,c}S_{a,t}S_{l,c}S_{l,t}}}\sigma_{lu}\sigma_{fu} = 1 \tag{6.4}$$

where, $S_{a,c}$ and $S_{l,c}$ are the axial and lateral compressive strength of the FRP tube, respectively, and $S_{a,t}$ and $S_{l,t}$ are the axial and lateral tensile strength values, respectively.

Axial strain of the FRP tube at rupture can be evaluated by assuming strain compatibility between the FRP and the concrete and utilizing the expression proposed by Lam and Teng (2003) for the ultimate axial strain of FRP-confined concrete given by:

$$\varepsilon_{au} = \varepsilon_{co}\left[1.75 + 12.0\left(\frac{f_{lu}}{f'_{co}}\right)\left(\frac{\varepsilon_{lu}}{\varepsilon_{co}}\right)^{0.45}\right] \tag{6.5}$$

where, f'_{co} is the peak strength and ε_{co} is the corresponding axial strain (commonly taken as 0.002) of the unconfined concrete. f_{lu} is the ultimate lateral confining pressure which can be evaluated considering the equilibrium of the FRP tube (see Fig. 6.2(b)) as:

$$f_{lu} = \frac{2\sigma_{lu} t_f}{D} \tag{6.6}$$

The ultimate state of stress in the FRP tube (σ_{fu}, σ_{lu}) and the corresponding ultimate strain values (ε_{au}, ε_{lu}) can be evaluated by substituting Eq. (6.6) into Eq. (6.5) and solving Eqs. (6.2), (6.3), (6.4) and (6.5).

The constitutive relationship proposed by Lam and Teng (2003) was used in evaluating the concrete behavior in the proposed composite columns. The model assumes a parabolic stress-stain relationship for the confined concrete up to an axial strain level of ε_t followed by a linear branch until failure, as shown in Fig.6.3. The proposed axial stress-strain relationship is defined as:

$$\sigma_c = \begin{cases} E_c\varepsilon_c - \dfrac{(E_c - E_2)^2}{4f'_{co}}\varepsilon_c^2 & (0 \le \varepsilon_c \le \varepsilon_t) \\ f'_{co} + E_2\varepsilon_c & (\varepsilon_t \le \varepsilon_c \le \varepsilon_{au}) \end{cases} \tag{6.7}$$

where, ε_c and ε_t are the axial strain and the strain at the transition point in the stress-strain relationship of confined concrete, respectively. E_c and E_2 are the elastic moduli of the unconfined concrete and the slope of the linear branch in the stress-strain relationship of the confined concrete shown in Fig. 6.3, respectively.

Based on a comprehensive database of experimental tests, Lam and Teng (2003) expressed the compressive strength of confined concrete as a function of the lateral confining pressure using the following relationship:

$$f_{cc}^{'} = f_{co}^{'} + 3.3 f_{lu} \tag{6.8}$$

The above model was utilized in developing the cross-sectional strength curve for the composite columns tested in this study.

6.4.2. Stability Relationships

The buckling capacity of the composite columns is estimated using the Euler buckling formula expressed as:

$$P_E = \pi^2 \frac{EI}{(kL)^2} \tag{6.9}$$

where, k is the effective length factor taken as 1.0 for the pin-pin boundary conditions and L is the unbraced column length. EI is the equivalent tangent stiffness of the composite columns which is obtained from superimposing the stiffness of its components as:

$$EI = E_s I_s + E_c I_c + E_f I_f \tag{6.10}$$

where, I_c and I_f are the moment of inertia of the concrete and the FRP tube, respectively. The concrete modulus of elasticity varies with the strain increments and is evaluated from the first derivative of Eq. (6.7) calculated as:

$$E_c = \frac{d\sigma_c}{d\varepsilon_c} = \begin{cases} E_c - \dfrac{(E_c - E_2)^2}{2 f_{co}^{'}} \varepsilon_c & (0 \le \varepsilon_c \le \varepsilon_t) \\ E_2 & (\varepsilon_t \le \varepsilon_c \le \varepsilon_{au}) \end{cases} \tag{6.11}$$

The modulus of elasticity of the steel after yielding is taken as the slope of the strain-hardening branch in the stress-strain relationship. The FRP elastic modulus is assumed constant at all the strain increments.

6.4.3. *Definition of Slenderness Ratio*

The slenderness ratio (*kL/r*) of the proposed composite columns was estimated based on an equivalent radius of gyration calculated as:

$$r = \sqrt{\frac{I_{eq}}{A_{eq}}} \tag{6.12}$$

where, I_{eq} and A_{eq} are the moment of inertia and cross-sectional area of an equivalent concrete cross-section obtained by transforming the area of the steel and FRP to concrete as shown in Fig. 6.4. I_{eq} and A_{eq} are given by:

$$I_{eq} = \left(\frac{E_s}{E_c} - 1\right) I_{s,yy} + \frac{\pi}{64}\left(D + 2t_f \frac{E_f}{E_c}\right)^4 \tag{6.13}$$

$$A_{eq} = \left(\frac{E_s}{E_c} - 1\right) A_s + \frac{\pi}{4}\left(D + 2t_f \frac{E_f}{E_c}\right)^2 \tag{6.14}$$

where, E_s, E_c and E_f are moduli of elasticity of the steel, concrete and the FRP tube in compression, respectively; D and t_f are the inside diameter and thickness of the FRP tube and $I_{s,yy}$ and A_s are the moment of inertia with respect to the weak axis and cross-sectional area of the steel section, respectively. The estimated slenderness ratios for the tested composite column specimens are presented in Table 6.2.

Figure 6.5 shows the stability and cross-sectional strength curves for the tested composite columns. The axial load and strain are normalized with respect to the cross-sectional compressive strength and ultimate axial strain of short composite columns (P_{cs} and ε_{au}), respectively. As can be seen from Fig. 6.5, the short composite specimen *R-0.5* (*kL/r=10*) would fail due to loss of the cross-section capacity, whereas the remaining specimens would fail as a result of overall buckling. These predicted failure modes correspond to the failure modes observed in the experimental testing program.

Slenderness limit is defined as the slenderness ratio below which the composite columns are classified as short columns. It corresponds to the slenderness ratio of a column whose stability and cross-sectional strength curves intersect at the strain increment equal to ε_{au}. A slenderness limit of 19.8 was obtained for the tested composite columns as shown in Fig. 6.6. A slenderness ratio of 55.3, corresponding to a composite column whose stability and cross-sectional strength curves intersect at an axial strain of 0.002, separates the intermediate long and slender composite column specimens (see Fig.6.6).

6.5. Comparison of Analytical and Experimental Results

Results from the analytical model are summarized in Table 6.2 in term of the compressive strength and ultimate axial strain of the composite columns along with the ratio of analytical predictions to experimental results. From the table, it can be seen that overall the analytical predictions comply favorably with the experimental results. The axial load versus axial strain relationships for the six tested composite columns obtained from the analytical model are shown in Fig. 6.7 in comparison with the experimental results. From this figure, it can be seen that the analytical model predictions are in good agreement with the overall load-deformation behavior of the tested columns. The lower compressive strength values predicted by the analytical model are partially attributed to the effects of the shrinkage reducing admixture in the concrete mix utilized in the tested specimens (Karimi et al. 2010a).

6.6. Capacity Curve

The capacity curve indicates compressive capacity of the columns versus the slenderness ratio. Figure 6.8 shows the theoretical capacity curve for the tested columns obtained from the proposed analytical model versus the experimental data. The capacity predictions were within 11% of the experimental results. Based on Fig. 6.8, specimens *R-1.0* to *R-2.5* are classified as intermediate long and the specimen *R-3.0* as a slender composite column, respectively.

The capacity curve approach can be utilized as a design tool in predicting the compressive resistance of columns. However, the analytical model shows that the capacity curve developed in this study can be influenced by the cross-sectional dimensions and mechanical properties of the constituent materials. Consequently, in the following section a study is carried out to investigate the effect of various design parameters on the capacity curve and slenderness limit previously developed for the composite columns tested in this study.

6.7. Influence of Column Parameters on the Capacity Curve, Cross-Sectional Strength and Slenderness Limit

A study was conducted using the proposed analytical model to investigate effect of cross sectional dimension and mechanical properties of the constituent materials on the capacity curve and the slenderness limit. These parameters included the columns diameter (D), thickness of the FRP tube (t), axial compressive modulus of the FRP tube (E_f) and the steel-to-concrete ratio. Four different cases were examined for each of the parameters.

Figure 6.9 shows influence of the columns diameter on the capacity curve, cross-sectional strength and slenderness limit. The selected range for D is between one to four times the diameter of the tested columns. Other cross-sectional dimensions and materials properties were held constant. Increasing the columns diameter results in reduced confinement, which affects the cross sectional strength (P_{cs}). However, stability of the composite column is enhanced with increased diameter, which results in a higher normalized compressive capacity (P_u/P_{cs}) and slenderness limit, although the effect on the slenderness limit is not as significant. The slenderness limit increased from 19.8 to 25.6 with the increased column diameter.

A similar trend was observed in Fig. 6.10(a) with the reduced thickness of the FRP tube for t/t_0 ratios varying between 1.00 and 0.25, while keeping all remaining parameters constant. The slenderness limit increased from 19.8 to 24.7 with the reduced FRP

thickness as shown in Fig. 6.10(b). From Eq. (6.6) it can be seen that the ultimate lateral confining pressure is proportional to the thickness of the FRP tube. Consequently, increasing thickness of the FRP tube enhances cross-sectional strength (see Fig. 6.10(b)).

Figure 6.11 shows effect of the axial compressive modulus of the FRP tube (E_f) on the composite columns capacity curve, cross-sectional strength and slenderness limit. E_f/E_{f0} ratios were selected between 0 (corresponding to a tube with no axial stiffness) and 3, where E_{f0} is the axial modulus of the FRP tube in the tested composite columns. The normalized compressive capacity was found to increase with increased FRP axial modulus, however, the difference between the capacity curves reduced for slender columns. Figure 6.11 show the pronounced effect of the axial stiffness of the FRP tube on the slenderness limit. The slenderness limit increased from 14.8 to 36.5 with the increased axial modulus of the FRP from 0.0 to 30.9 GPa. Eq. (6.2) shows that E_f influences the bi-axial state of stress in the FRP tube. Maximum cross-sectional strength was obtained for E_f/E_{f0} equal to 1 (see Fig. 6.11(b)).

The effect of steel-to-concrete ratio on the capacity curves are shown in Fig. 6.12(a). The capacity curves were obtained for the steel-to-concrete ratios of 0.0%, 2.5%, 5.0% and 10.0%. As can be seen from Fig. 6.12(a), steel-to-concrete ratio had minor influence on the capacity curves for short or slender composite columns (kL/r greater than 80), which also resulted in negligible influence on the slenderness limit (see Fig. 6.12(b)). However, the normalized compressive capacity increased with increased steel-to-concrete ratio for intermediate long columns. Figure 6.12(b) shows enhancement in the cross-sectional strength with increased steel-to-concrete ratio however, it results in a less economical composite column due to the higher cost of the steel compared to concrete. A minimum amount of steel is recommended in the proposed composite column to satisfy ductility requirements.

The analytical model showed that the additional steel inside the composite section increased the buckling and cross-sectional compressive capacity of the composite columns. The enhancement was more significant in terms of the buckling capacity compared to the cross-sectional strength for the steel-to-concrete ratios of less than 2.5%, which resulted in a greater slenderness limit for such columns compared to a concrete-filled FRP tube without steel. The slenderness limit decreased with increased steel-to-concrete ratios greater than 2.5%.

6.8. Proposed Preliminary Design Equation

The design equation for evaluation of compressive strength in concrete-filled steel tubular columns provided in the Canadian steel code, CAN/CSA-S16-09 (CSA 2009) is modified and utilized in design of the composite columns in this study. The unfactored compressive strength of the columns is expressed as:

$$P_u = P_{cs}\left(1+\lambda^{2n}\right)^{-1/n} \tag{6.15}$$

where, n is a constant and λ is defined as:

$$\lambda = \sqrt{\frac{P_{cs}}{P_E}} \tag{6.16}$$

where, P_E is evaluated from Eq. (6.9) at the stage of initial loading. P_{cs} can be found from the analytical model.

The coefficient n in Eq. (6.15) was obtained as 0.97 through regression analysis using the capacity curve developed from the analytical model in Fig.6.8. Eq. (6.15) can be simplified by approximating n equal to unity as:

$$\frac{P_u}{P_{cs}} = 1 + \lambda^2 \tag{6.17}$$

The normalized compressive capacity predicted using the above equation was plotted against λ for composite columns with various slenderness ratios and compared favorably with the experimental data as shown in Fig. 6.13. Finally, by introducing resistance factors corresponding to each constituent material into Eq. (6.1) the factored compressive strength of the proposed composite column is given as follows in compliance with the expression provided in CSA-S806-02 (CSA 2002) for the factored cross-sectional strength of FRP-confined reinforced concrete columns:

$$P_r = \beta\left[\alpha_1 \phi_c f'_{cc} A_c + \phi_s f_y A_s\right]\left(1 + \lambda^2\right) \tag{6.18}$$

where, $\alpha_1 = 0.85 - 0.0015 f'_c \geq 0.39$, $\phi_c = 0.60$ for concrete and $\phi_s = 0.90$ for the steel section. f_y is the steel yield strength. The factor β is introduced to account for the strength reduction due to unexpected eccentricities. The load-carrying capacity of the FRP tube is conservatively ignored.

6.9. Conclusions

An analytical model was developed to predict the behavior of a novel composite column consisting of steel, concrete and FRP. The model utilized an incremental technique, which compares the stability and cross-sectional strength curves at each strain increment. The stability curves were evaluated using the Euler buckling formula accounting for the strain softening of the composite columns. The cross-sectional strength curve was obtained by superposing separate contributions of the constituent materials in carrying the axial load. The compressive behavior of the concrete was simulated using a FRP-confined concrete model.

To verify the analytical model, six composite columns ranged between 500 mm and 3,000 mm in height were constructed and tested under axial loading. The analytical model yielded good predictions of the experimental results. Over the wide range of *kL/r* values investigated, less than 11% error was observed between the normalized compressive strength predictions from the analytical model and the experimental results.

Based on the analytical model, a slenderness limit of 19.8 was established for the tested composite columns below which the slenderness effects are negligible and the columns are classified as short composite columns.

A study was carried out to investigate effect of the column design parameters such as the column diameter, FRP tube thickness, FRP tube axial stiffness and the steel-to-concrete ratio on the capacity curve and slenderness limit of the proposed composite columns. The study showed an increase in the normalized compressive strength of the columns with the increased column diameter to FRP thickness ratio, FRP tube axial stiffness and the steel-to-concrete ratio. The slenderness limit also increased significantly with the increased FRP tube axial stiffness.

A design equation was proposed based on the capacity curve obtained for the composite columns from the analytical model. The expression can be simply utilized by structural engineering in predicting compressive strength of the proposed composite columns.

Appendix 6.1. Notation

A_c = cross-sectional area of the concrete;

A_f = cross-sectional area of the FRP tube;

A_s = cross-sectional area of the steel section;

A_{eq} = cross-sectional area of the equivalent reinforced concrete column;

D = inside diameter of the FRP tube;

ε_a = axial strain;

ε_{au} = ultimate axial strain of short composite columns;

ε_{co} = axial strain in the concrete;

ε_{co} = axial strain corresponding to peak strength of the unconfined concrete;

ε_l = lateral strain in the FRP tube;

ε_{lu} = ultimate lateral strain in the FRP tube;

E_c = elastic modulus of concrete;

E_2 = slope of the linear branch in the axial stress-strain relationship of confined concrete;

E_f = axial compressive modulus of the FRP tube;

$E_{f,l}$ = lateral tensile modulus of the FRP tube;

E_s = elastic modulus of the steel;

f'_{co} = compressive strength of the unconfined concrete;

f_{lu} = ultimate lateral confining pressure;

f_y = yield strength of the steel;

I_c = moment of inertia of the concrete;

I_{eq} = moment of inertia of the equivalent reinforced concrete column;

I_f = moment of inertia of the FRP tube;

$I_{s,yy}$ = moment of inertia of the steel section with respect to the weak axis;

k = effective length factor

L = unbraced length of the column;

ν_{la} = Poisson's ratio of the FRP tube when the load is applied in the axial direction and contraction occurs in the lateral direction;

ν_{al} = Poisson's ratio of the FRP tube when the load is applied in the lateral direction and contraction occurs in the axial direction;

r = radius of gyration;

σ_c = axial stress in the concrete;

σ_l = lateral stress in the FRP tube;

$\sigma_{l,u}$ = lateral stress in the FRP tube at failure;

σ_f = axial stress in the FRP tube;

$\sigma_{f,u}$ = axial stress in the FRP tube at failure;

σ_s = axial stress in the steel;

$S_{a,c}$= axial compressive strength of the FRP tube;

$S_{a,t}$ = axial tensile strength of the FRP tube;

$S_{l,c}$ = lateral compressive strength of the FRP tube;

$S_{l,t}$ = lateral tensile strength of the FRP tube;

t_f = thickness of the FRP tube;

P = axial load;

P_{cs} = compressive cross-sectional strength;

P_r = factored compressive strength;

P_u = unfactored compressive strength;

Appendix 6.2. References

Bank, L. C. (2006) "Composites for construction." *John Wiley & Sons*, Hoboken, New Jersey.

Binici, B., and Mosalam, K. M. (2007) "Analysis of reinforced concrete columns retrofitted with fiber reinforced polymer lamina." *J. Compos. Part B-Eng.*, 38: 265-276.

CSA. (2002) "Design and construction of building components with fibre-reinforced polymers. CAN/CSA-806-02." *Rexdale BD*, Toronto.

CSA. (2009) "Limit states design of steel structures. Standard CAN/CSA S16-09." *Canadian Standards Association*, Mississauga, Ont.

Daniel, I. M., and Ishai, O. (2006) "Engineering mechanics of composite materials." 2nd ed., *Oxford University Press*, New York, NY.

Eid, R., and Paultre, P. (2008) "Analytical model for FRP-confined circular reinforced concrete columns." *J. Compos. for Constr.*, 12(5): 541-552.

Karimi, K., Tait, M. J., and El-Dakhakhni, W. W. (2010a) "Testing and modeling of a novel FRP-encased steel-concrete composite column." *J. of Compos. Struct.*, DOI: 10.1016/j.compstruct.2010.11.017.

Karimi, K., Tait, M. J., and El-Dakhakhni, W. W. (2010b) "Influence of slenderness on the behavior of a FRP-encased steel concrete composite column." *J. Compos. for Constr.*, submitted manuscript number CCENG-428.

Lam, L., and Teng, J. G. (2003) "Design-oriented stress-strain models for FRP-confined concrete." *J. Constr. and Build. Mat.*, 17: 471-489.

Liu, X., Nanni, A., and Silva, P. F. (2005) "Rehabilitation of compression steel members using FRP pipes filled with non-expansive and expansive light-weight concrete." *J. Adv. in Struct. Eng.*, 8(2): 129-142.

Mirmiran, A., Shahawy, M., and Beitleman, T. (2001) "Slenderness limit for hybrid FRP-concrete columns." *J. Compos. for Constr.*, 5(1): 26-34.

Mohamed, H. M., and Masmoudi, R. (2010) "Axial load capacity of concrete-filled FRP tube columns: experimental versus theoretical prediction." *J. Compos. for Constr.*, 14(2): 231-243.

Ozbakkaloglu, T., and Oehlers, D. J. (2008) "Manufacture and testing of a novel FRP tube confinement system." *Eng. Struct.*, 30(9): 2448-2459.

Saafi, M., Toutanji, H. A., and Zongjin, L. (1999) "Behavior of concrete columns confined with fiber reinforced polymner tubes." *ACI Mater. J.*, 96(4): 500-510.

Shaat, A., and Fam, A. (2007) "Fiber-element model for slender HSS columns retrofitted with bonded high-modulus composites." *J. Struct. Eng.*, 133(1): 85-95.

Teng, J. G., Yu, T., Wong, Y. L., and Dong, S. L. (2007) "Hybrid FRP-concrete-steel tubular columns: Concept and behavior." *J. Constr. and Build. Mat.*, 21: 846-854.

Therlault, M., and Neale, K. W. (2000) "Design equations for axially loaded reinforced concrete columns strengthened with fibre reinforced polymer wraps." *Can. J. Civ. Eng.*, (27): 1011-1020.

Table 6.1. Mechanical properties of FRP tube

Nominal Pipe Size		(mm)	200
Inside Diameter		(mm)	211
Structural Wall Thickness		(mm)	3.2
Lateral Tensile Strength		(MPa)	275
Lateral Tensile Modulus		(GPa)	15.9
Axial Compressive Strength		(MPa)	138
Axial Compressive Modulus		(GPa)	10.3
Axial Tensile Strength		(MPa)	138
Axial Tensile Modulus		(GPa)	10.3
Poisson's Ratio [(a)]	$\frac{\nu_{la}}{\nu_{al}}$		0.11 0.19

[(a)] The first subscript denotes the contraction direction and the second subscript denotes direction of the applied force. "*a*" and "*l*" denotes axial and lateral direction, respectively.

Table 6.2. Analytical model predictions versus experimental results

Specimen I.D.	Height (H) (mm)	Slenderness Ratio (kL/r)	Compressive Strength (P_u)			Ultimate Axial Strain (ε_{au})		
			Analytical (kN)	Experimental (kN)	Ana./ Exp.	Analytical (με)	Experimental (με)	Ana./ Exp.
R-0.5	500	10	3,440	3,821	0.90	11,865	11,700	1.01
R-1.0	1,000	21	3,179	3,040	1.04	9,160	9,388	0.98
R-1.5	1,500	31	2,387	2,935	0.81	2,330	3,277	0.71
R-2.0	2,000	41	2,372	2,545	0.93	2,208	2,840	0.78
R-2.5	2,500	51	2,264	2,295	0.99	2,059	2,369	0.87
R-3.0	3,000	62	2,020	2,251	0.90	1,751	1,903	0.92

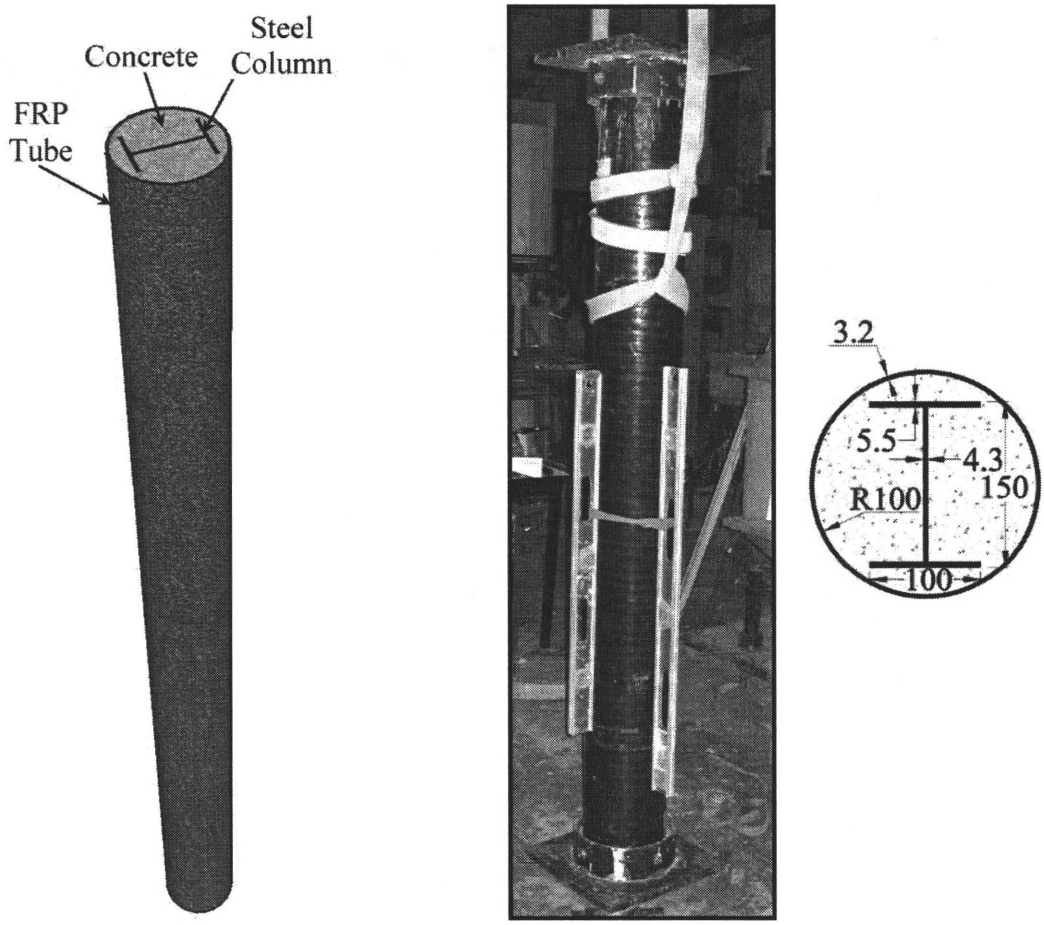

Figure 6.1. (a) Schematic view of the proposed composite columns (b) photograph and cross-sectional dimensions of the tested specimens in mm

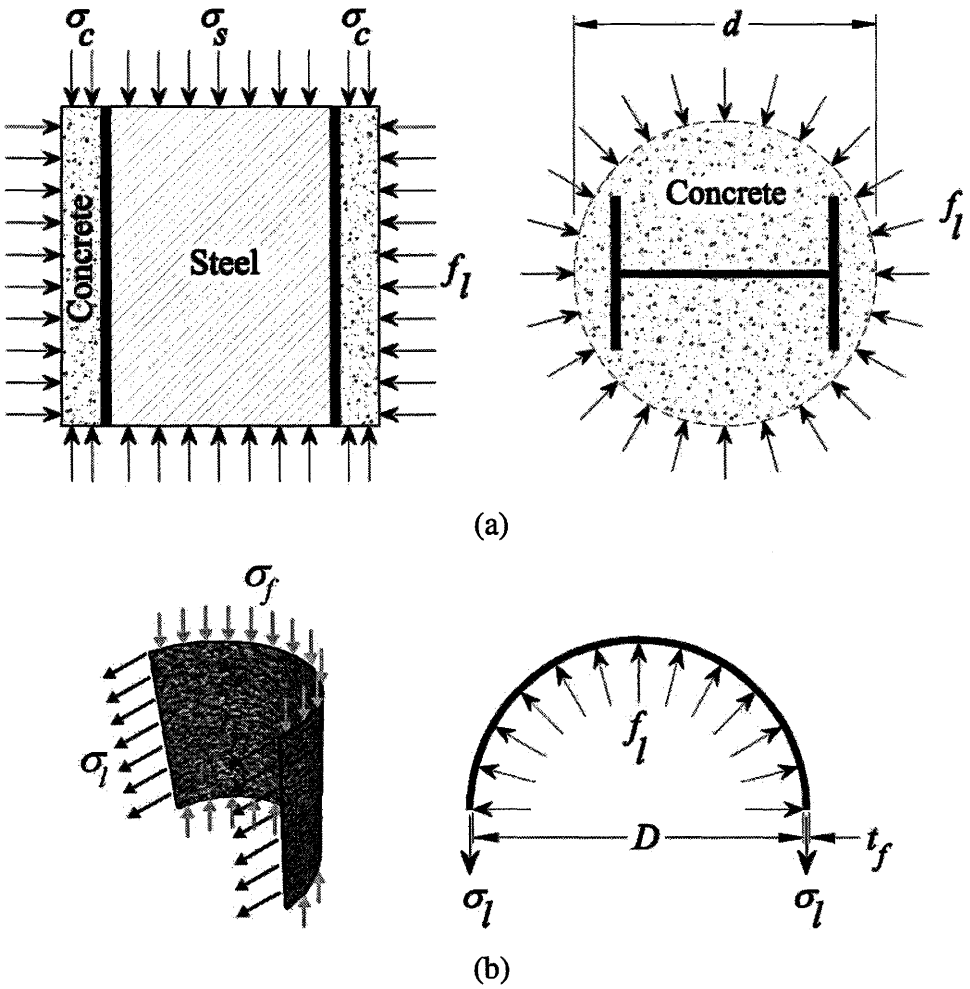

Figure 6.2. Free body diagram of the composite column components (a) concrete-encased steel section (b) FRP tube

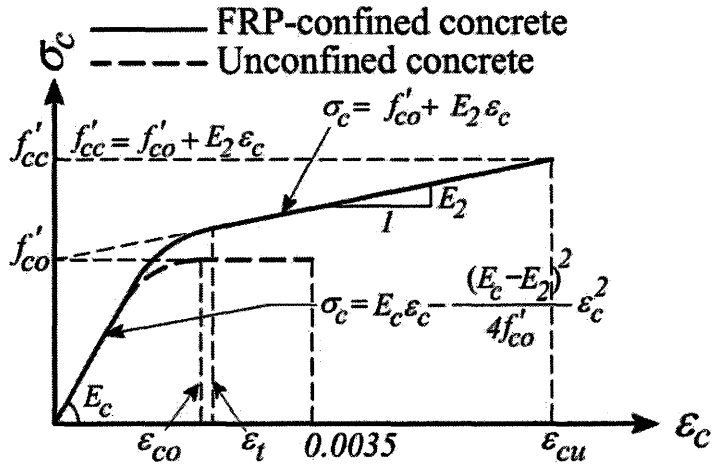

Figure 6.3. Constitutive model for FRP-confined concrete

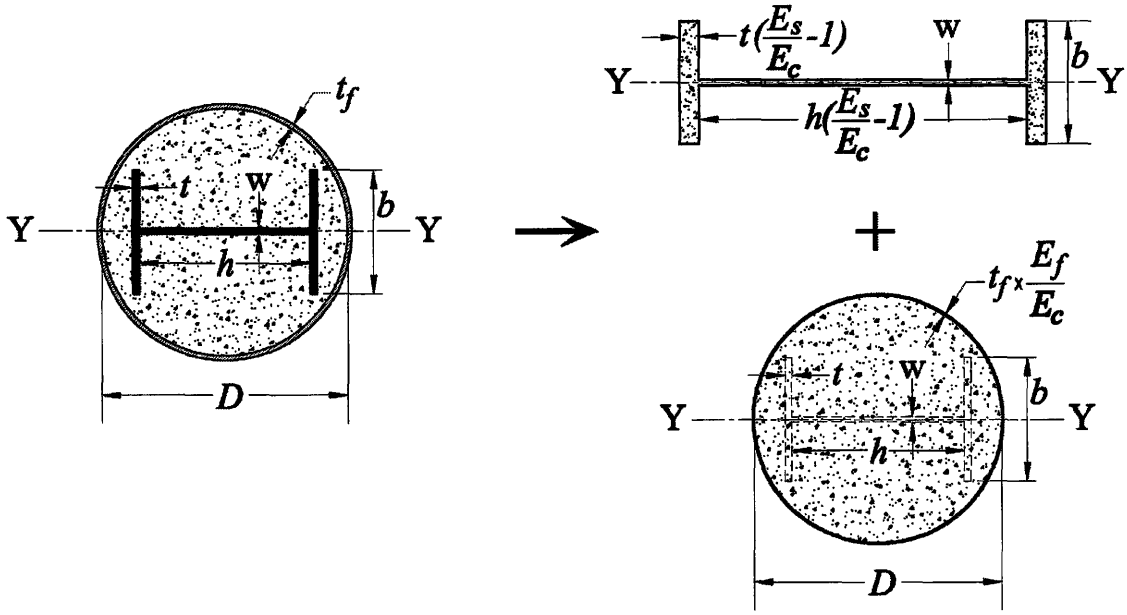

Figure 6.4. Transforming the composite cross section to an equivalent concrete section

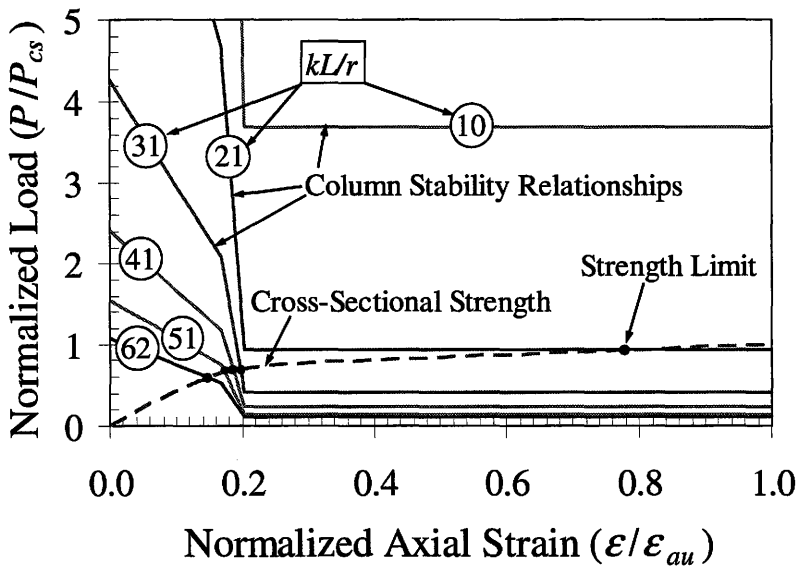

Figure 6.5. Normalized axial load versus normalized axial strain of the columns from the analytical model

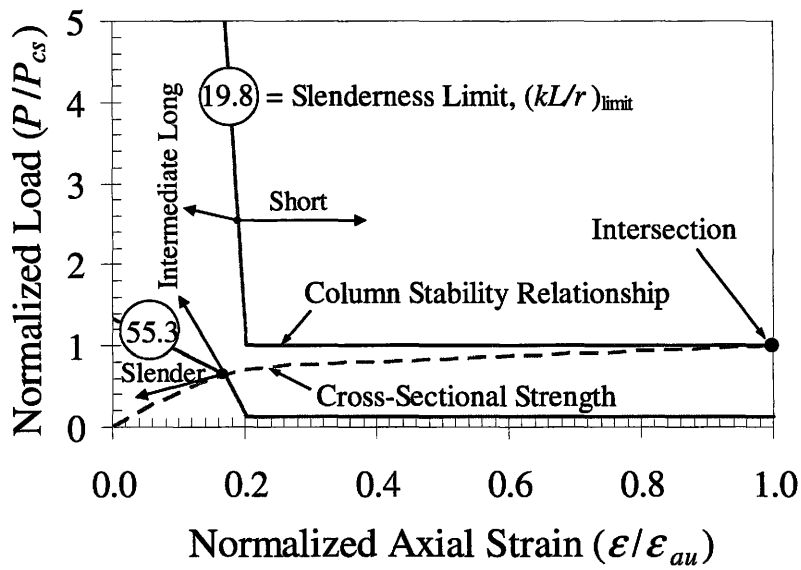

Figure 6.6. Evaluating slenderness limit for the composite columns using the analytical model

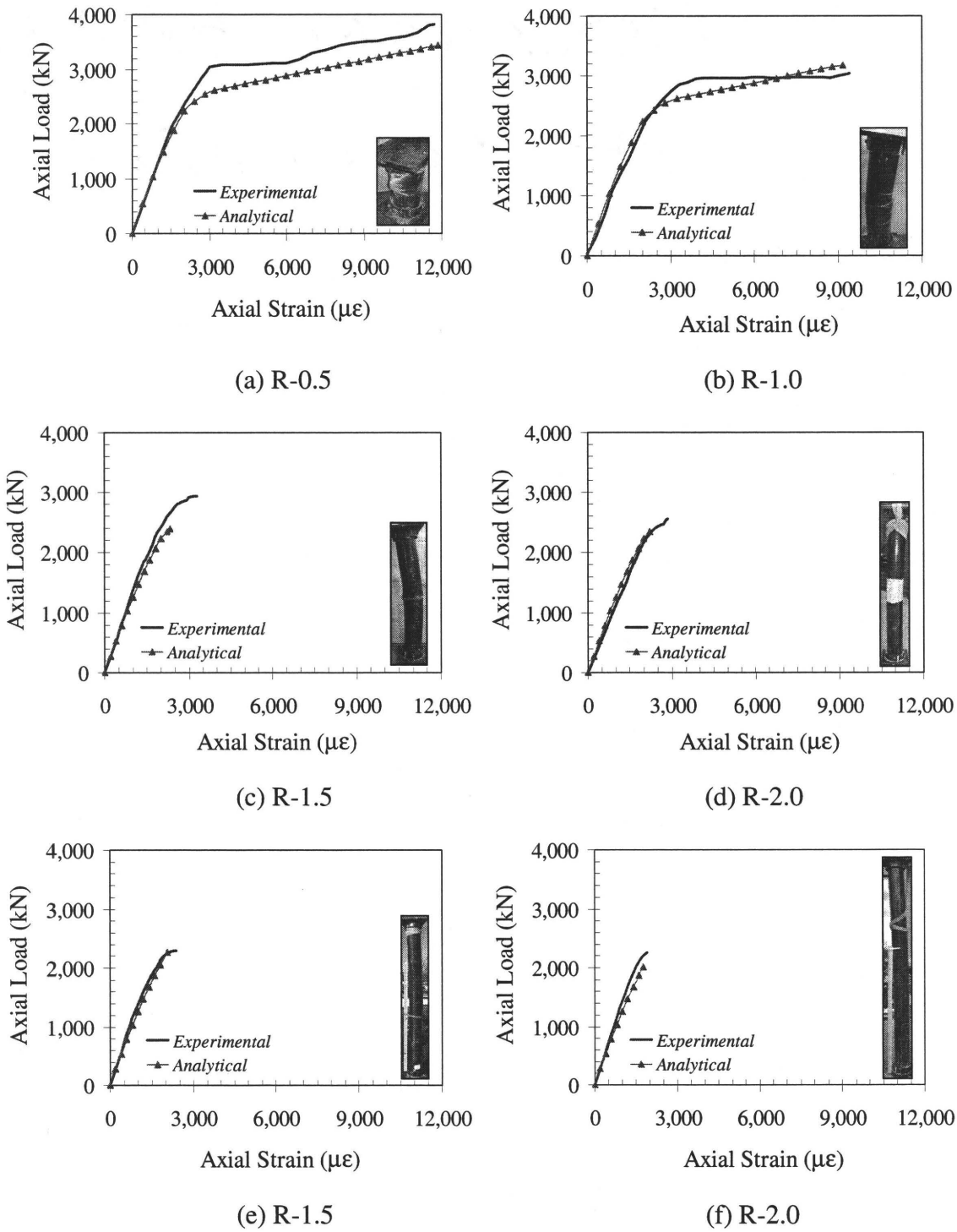

Figure 6.7. Analytically predicted axial load versus axial strain relationships for the composite columns in comparison with the test results

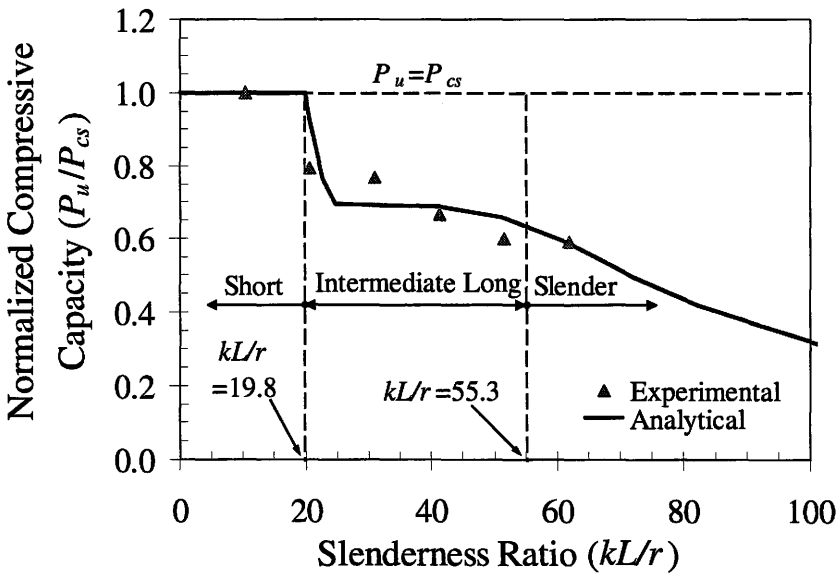

Figure 6.8. Predicted capacity curve versus experimental results

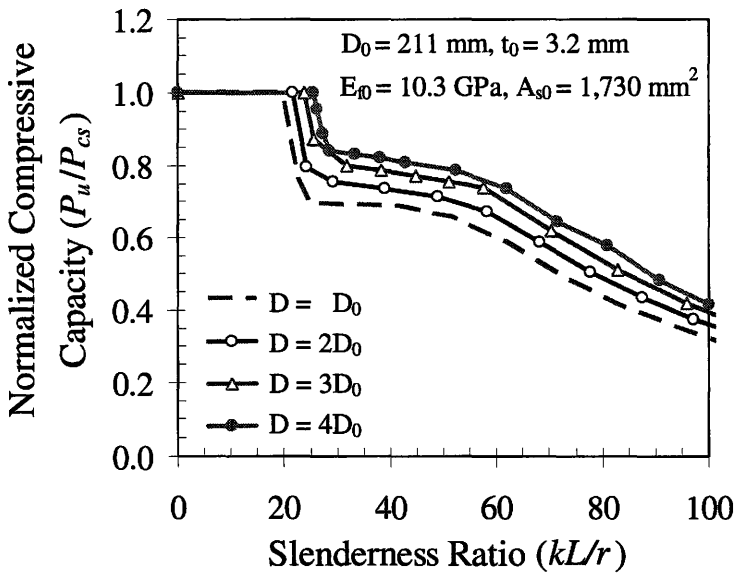

(a)

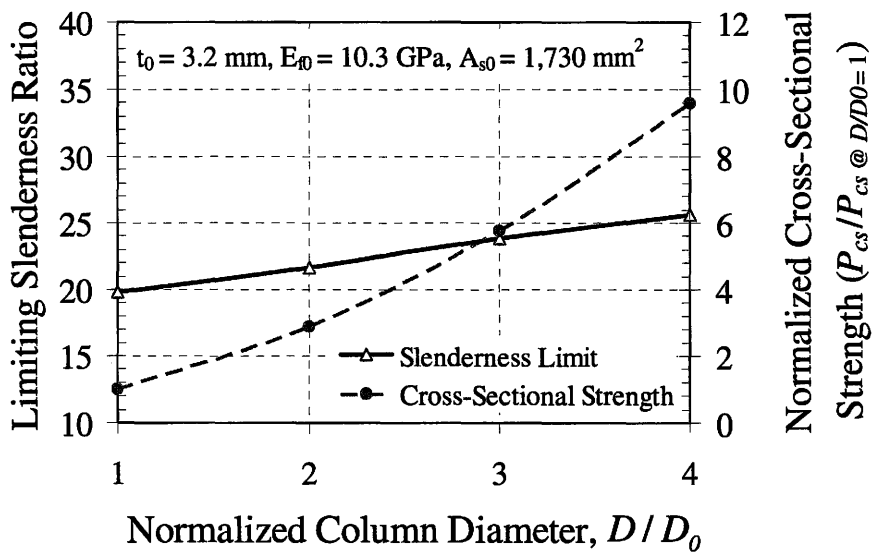

(b)

Figure 6.9. Effect of column diameter on the (a) capacity curve (b) cross sectional strength and slenderness limit

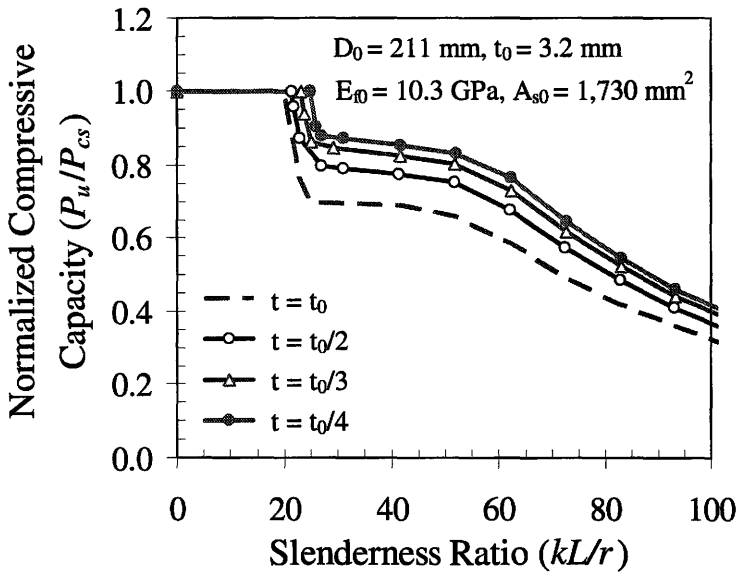

(a)

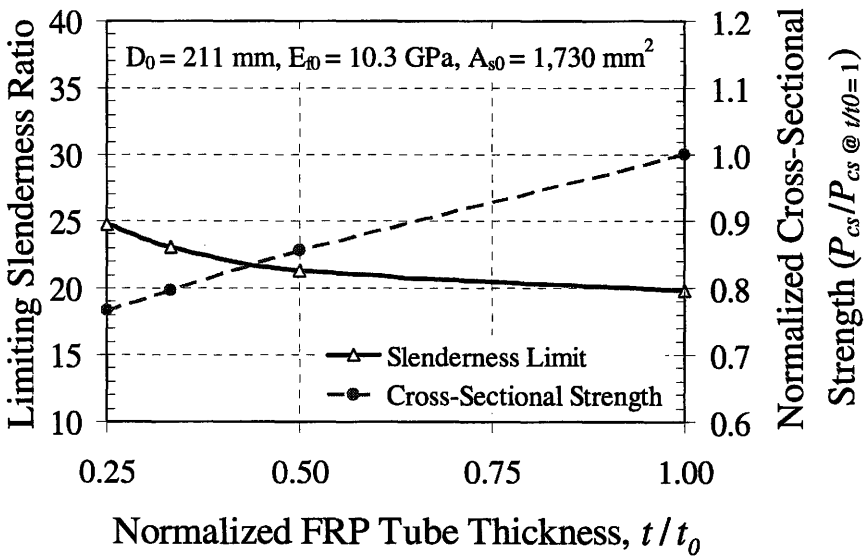

(b)

Figure 6.10. Effect of thickness of the FRP tube on the (a) capacity curve (b) cross-sectional strength and slenderness limit

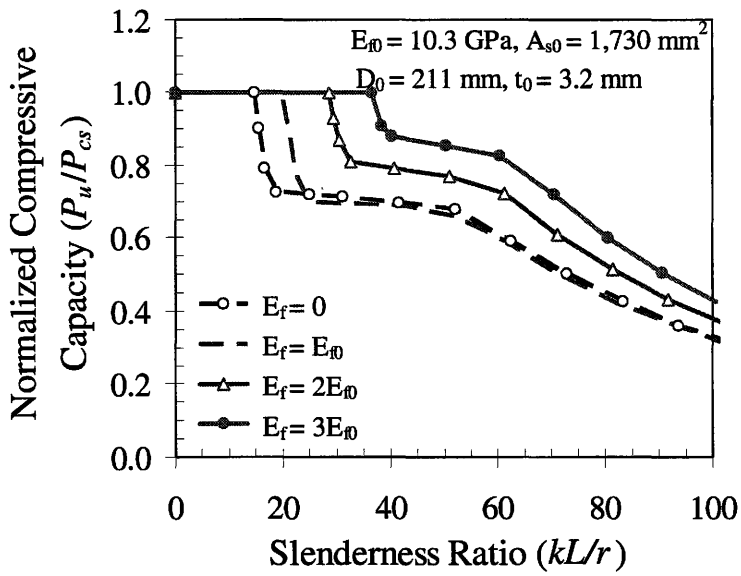

(a)

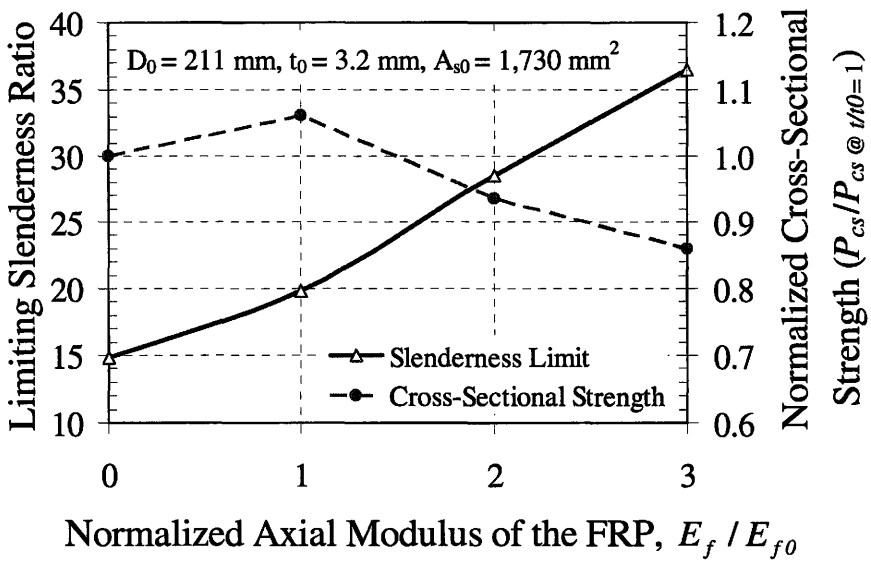

(b)

Figure 6.11. Effect of axial modulus of the FRP tube on the (a) capacity curve (b) cross-sectional strength and slenderness limit

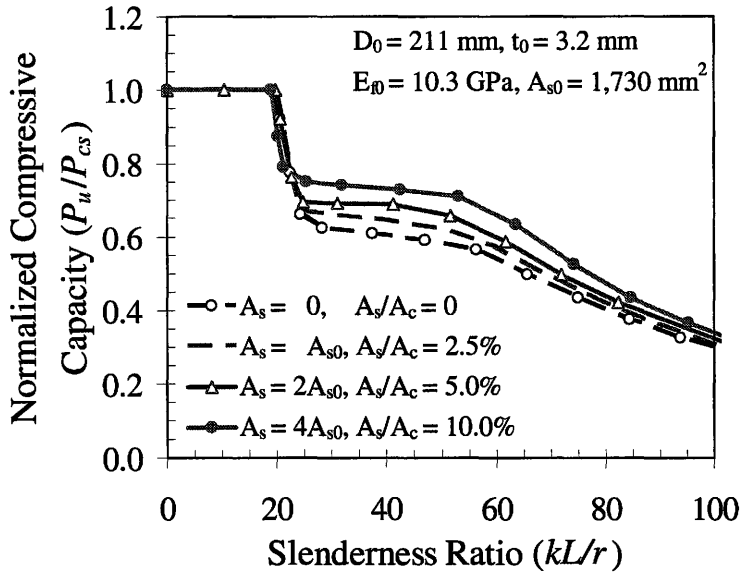

(a)

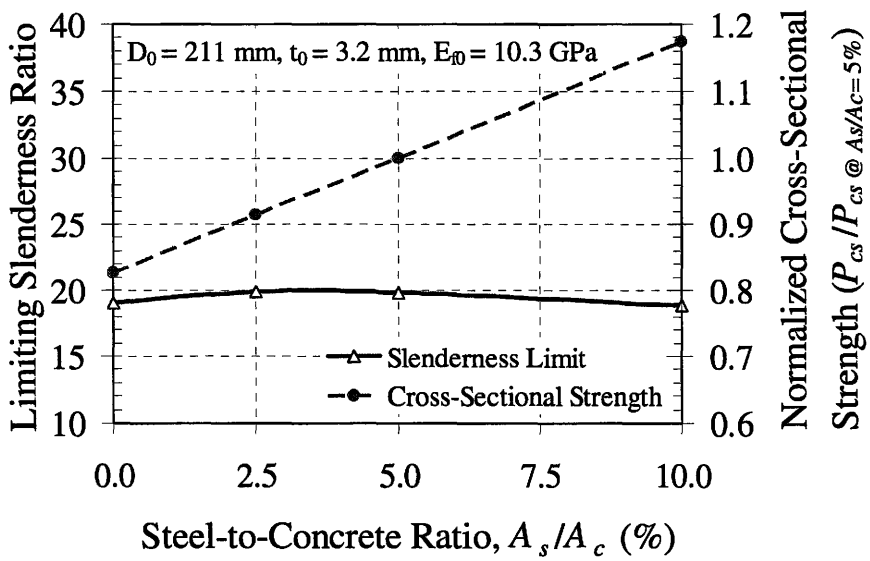

(b)

Figure 6.12. Effect of steel-to-concrete ratio on the (a) capacity curve (b) cross-sectional strength and slenderness limit

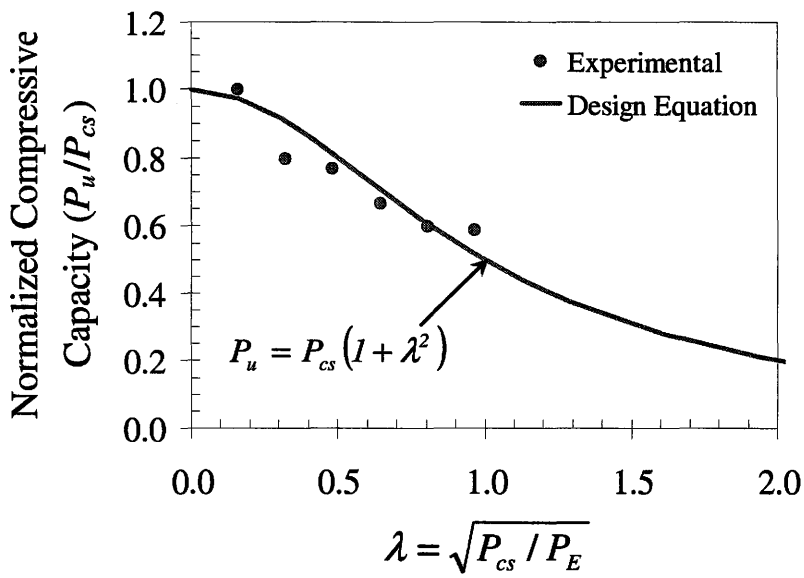

Figure 6.13. Predicted unfactored compressive capacity of the composite columns from the proposed design equation in comparison with the experimental results